NOVA SCHOOL OF SCIENCE & TECHNOLOGY

DEPARTAMENT OF CHEMISTRY

# ENGINEERING AN LTTM-POLYMERIC-DRUG FORMULATION FOR OSTEOARTHRITIS TREATMENT

ANA SOFIA MARTINS RODA

Master in Biochemistry for Health

DOCTORATE IN BIOTECHNOLOGY

NOVA University Lisbon

March, 2024

NOVA SCHOOL OF SCIENCE & TECHNOLOGY

DEPARTAMENT OF CHEMISTRY

# ENGINEERING AN LTTM-POLYMERIC-DRUG FORMULATION FOR OSTEOARTHRITIS TREATMENT

**ANA SOFIA MARTINS RODA**

Master in Biochemistry for Health

**Adviser:** Ana Rita Cruz Duarte
Associate Professor with habilitation, NOVA School of Science and Technology at NOVA University Lisbon

**Co-advisers:** Alexandre Babo de Almeida Paiva
Principal Investigator, NOVA School of Science and Technology at NOVA University Lisbon

Ana Alexandra Figueiredo Matias
Invited Researcher, iBET Oeiras

**Examination Committee:**

**Chair:** Ana Cecília Afonso Roque,
Full Professor, NOVA School of Science and Technology at NOVA University Lisbon

**Rapporteurs:** Ivana Radojčić Redovniković,
Full Professor, Faculty of Food Technology and Biotechnology at University of Zagreb

João Filipe Ramos da Silva Carvalho Borges,
Assistant Researcher, University of Aveiro

**Adviser:** Ana Rita Cruz Duarte,
Associate Professor with habilitation, NOVA School of Science and Technology at NOVA University Lisbon

**Members:** Hélder Miguel Duarte Pereira,
Medical Doctor & Professor of Orthopedics, University of Minho

Ana Cecília Afonso Roque,
Full Professor, NOVA School of Science and Technology at NOVA University Lisbon

Luísa Alexandra Graça Neves,
Assistant Professor, NOVA School of Science and Technology at NOVA University Lisbon

DOCTORATE IN BIOTECHNOLOGY

NOVA University Lisbon
March, 2024

Avó ☆

# ACKNOWLEDGMENTS

À minha supervisora, Professora Rita Duarte, enquanto profissional, com um empenho e science sparkle contagiante, como nunca antes vi. E à pessoa, humilde, generosa e com um coração tão grande quanto o seu amor pelo que faz. Obrigada pela inspiração, pela força, pela paciência, pela leveza e pelo sorriso. Acredito que foram estas as características que permitiram construir o nosso Des.Solve, uma equipa de entreajuda, complementaridade e bom desempenho, a par com um lado humano pouco comum, talvez inigualável, que permite trazer o melhor que cada um tem para dar à equipa.

Ao Dr. Alexandre, como co-orientador, pela contribuição nesta jornada.

À Drª Ana Matias um obrigada especialmente por ser parte do meu berço na ciência.

À equipa que acompanhou os meus primeiros passos na ciência, Drª Catarina Duarte, Dr. Arturo Bautista, Drª Teresa Serra, Vanessa Gonçalves, Agostinho, Liliana Rodrigues, Miguel, João Baixinho, Naiara, Melanie, Cátia Carmo, Daniel Deodato, e às minhas colegas e amigas Maria João e Ana Nunes. Maria, um modelo de ação e ponderação. Ana, uma luz e calma contagiantes. Obrigada às duas por caminharam comigo nesta jornada.

To all the science collaborators, Dr. Christoph Held, Dr. Ana Pereiro Estévez, Dr. Joana Silva, Dr. Alan Chan. Especially to Dr. Jaqueline and Professor Laura, a deep gratitude to you and all the professional enrichment. And of course, to all the Utrecht team, Remei, Carla, Kelly, Yeter, Shabaan, Saskia, Mattie, Katrin, Jie, Stijn and Oscar.

I also acknowledge my host institutions, NOVA School of Science and Technology and iBET (Instituto de Biologia Experimental e Tecnológica) as well as the financial support, which made this journey possible: the doctoral grant SFRH/BD/144424/2019 from FCT/MCTES, and the funds from the European Union under grant agreement number ERC-2016-CoG 725034 Des.Solve (ERC Consolidator Grant) from Horizon 2020, supported by the Associate Laboratory for Green Chemistry-LAQV financed by national funds from FCT/MCTES (UIDB/50006/2020).

E claro, à minha mais recente equipa, que me acompanhou durante estes 4 anos. Aos meus parceiros de gabinete, discussão científica e descompressão, Luísa Pereira, Silvia Rebocho, Duarte Rente, Hugo Monteiro, Cláudio, Célia e aos alunos e outros membros que foram passando, sempre com uma energia refrescante, Maria Miguel, Olga, Rafaella, Andreia, Carolina Vieira, Carolina Neca, Diogo. Um especial agradecimento à Joana Pereira que particularmente nesta fase final, assumiu muitas responsabilidades aliviando o processo aos colegas de doutoramento. E claro, aos meus companheiros Filipe e Filipa, pelo companheirismo dentro e fora da ciência que tornou o caminho mais fácil. Filipa, obrigada por me aturares, me motivares e me acompanhares. És um modelo de paciência e equilíbrio de vida pessoal e profissional.

E aos restantes colegas do Des.Solve, Inês Ferreira, Bruno Pedras, Ângelo, Mónica, Rita Craveiro, Rita Gameiro, Marta, Jelena, Gosia e Liane, também companheira nesta jornada. Reza, thank you for your motivational words.

Aos meus amigos 'da caixinha', André Miguel, Inês Marcelo pela vossa luz que me faz sempre querer ser melhor, num sítio de tranquilidade e acolhimento. André Miguel, obrigada por partilhares comigo um bocadinho do amor que cabe nesse grande coração, pela partilha, pela leveza e pelos sorrisos. Inês, trouxeste-me um lugar novo, de crescimento, amor, inspiração e equilíbrio. Ana Raquel Maia, uma das minhas amigas mais antigas, desde as bioquímicas de 2011. Espero que continues sempre a fazer parte da minha vida e a trazer contigo essa empatia e inspiração que tanto te caracteriza.

Catarina, não preciso de dizer nada, tu sabes. Miguel e afilhadas, estão também na bolha, onde mesmo sem palavras, estamos juntos.

Aos meus restantes amigos, colegas, familiares que de alguma forma fizeram parte desta caminhada. Kris, Diana, Inês Brito. Obrigada por estarem sempre aqui. Paulo, Rúben, Miguel Mataloto, Helena, Sofia, César, Sofia Vilar, Bruno, Cristina, Zé, Valdemar. Aos meus queridos NNtenses, em especial à Joana Lameira, Inês Baptista, Beatriz Nunes, Henrique, Cristiano Barata, Darian, Guilherme, Pedro, André, Luís, Paula Garcia, Sandra Hung e Chicó.

Zoe, Jonie, Francesca, Ivana, Steven, thank you for coming into my life, bringing light to new beginnings, joy, and growth!

E claro, um grande grande agradecimento ao Daniel, meu companheiro de vida há mais de 6 anos, em todos os momentos, bons e maus. É com a maior admiração e orgulho que caminho a teu lado. Obrigada pela paciência e sapiência, pelo amor, pela atenção, pelo crescimento, pelo acompanhamento, na vida e na ciência. E pela família que construímos juntos. Mitsuki, Cátia, Charlie, meus filhinhos, obrigada por me mostrarem que o amor não tem limites.

À minha avó, que me motivou com a partilha do seu orgulho e brilho nos olhos pela 'minha neta que está a fazer um doutoramento' e outras conquistas, que acompanhou de perto. Quantas saudades...Hoje estás aqui comigo, e esta conquista dedico-a a ti, estrelinha.

Mãe, Pai, a vocês a maior gratidão com todo o meu amor e coração.

Aos meus tios, Luís Martins e Carla Firmo, os meus grandes modelos de inspiração.

Rodinhaaaaaa, é genes, é amor, é cumplicidade, o melhor cocktail desta vida, meu grande (mas para sempre pequenino) amor!

E a mim, pela gestão emocional e profissional, pela superação e pela perseverança.

This was a challenging and enriching journey, which I am relieved it is coming to an end, while deeply grateful for the knowledge and opportunities I have experienced.

*I can and I will, watch me.*

# ABSTRACT

Osteoarthritis (OA) is a common degenerative joint disease, a major cause of disability globally, whose economic burden is substantial, thus requiring effective treatments to reduce its burden and improve patients' quality of life. In this context, the main strategy here followed was the use of Low Transition Temperature Mixtures (LTTMs) to incorporate drugs and biopolymer(s) already prescribed in OA therapeutics (e.g.: non-steroidal anti-inflammatory drugs (NSAIDs) and hyaluronic acid (HA), the main component of joints lubricant - synovial fluid), in such a way that it can improve their efficiency, overcome their limitations, and reduce the approval-time needed to reach the market.

LTTMs are particularly promising to enhance drugs' bioavailability and to be used as controlled delivery systems, especially upon combination with biomaterials, such as polymers. Hence, the main scope of this thesis was to provide an innovative therapeutic approach combining the following features:

**i. LTTM constituents with beneficial properties for OA therapy**. Different LTTM compositions were designed, developed, and characterized envisioning added synergetic action in OA therapy.

**ii. Increased NSAIDs bioavailability**. Selected LTTMs were studied to identify the most promising LTTM+NSAID combinations concerning this feature.

**iii. Compatibility towards the inclusion of selected biopolymers**. An injectable formulation was designed and characterized envisioning the inclusion of selected biopolymers in the same LTTM media used to enhance the bioavailability of NSAIDs.

**iv. Viability for intra-articular administration**. The designed formulation was studied aiming to validate proper features for the intended application.

**v. *In vivo* therapeutic potential for OA**. The developed injectable was evaluated in a post-traumatic OA rat model.

Briefly, glycerol:sorbitol (GS) emerged as a promising lubricant LTTM, improved celecoxib's (CEX) solubility and was compatible with HA, rendering an alternative to conventional physiologic solutions. GS+HA combination yielded a stable, injectable gel mimicking synovial fluid properties, further enhanced CEX bioavailability and modulated its release kinetics. *In vivo*, the HA+GS+CEX formulation effectively reduced pain and inflammation while distinctively inhibiting cartilage and bone degradation, contrarily to HA or HA+CEX alone.

Overall, this work allowed to develop a product prototype assembling two therapeutic agents individually approved for OA therapy in a unique formulation with improved therapeutic potential and convenience (2-in-1). An injectable formulation with the accomplished features is not yet available in the market and such a product is of high social and economic interest.

**Keywords:** Osteoarthritis, low transition temperature mixtures/deep eutectic systems, biopolymers, viscosupplementation, hyaluronic acid, non-steroidal anti-inflammatory drugs, celecoxib, intra-articular, injection, glycerol, sorbitol

# RESUMO

A artrose ou osteoartrose (OA) é uma doença articular degenerativa, uma das principais causas de incapacidade a nível mundial, e o seu encargo económico é considerável. Assim, é impreterível encontrar tratamentos eficientes que possam reduzir as limitações da doença e melhorar a qualidade de vida dos pacientes. Neste contexto, a principal estratégia delineada consistiu no uso de LTTMs (misturas de baixa temperatura de transição) para incorporar fármacos e biopolímeros(s) já aplicados na terapêutica da OA (ex: anti-inflamatórios não esteroides (AINEs) e ácido hialurónico (HA), o principal agente lubrificante das articulações - líquido sinovial), de forma a melhorar a sua eficiência, diminuir as suas limitações e reduzir o tempo necessário para chegar ao mercado.

Os LTTMs são particularmente promissores no aumento da biodisponibilidade dos fármacos e para sistemas de libertação controlada, especialmente quando combinados com biomateriais, como polímeros. Nesse sentido, o principal objetivo desta tese foi desenvolver uma abordagem terapêutica inovadora com as seguintes características:

**i) LTTMs com propriedades benéficas para a terapia de OA.** Diferentes composições de LTTMs foram delineadas, desenvolvidas e caracterizadas, visando uma ação sinérgica adicional na terapia da OA;

**ii) Aumento da biodisponibilidade dos AINEs.** LTTMs selecionados foram estudados em termos da combinação de LTTM+AINE mais promissora para essa funcionalidade;

**iii) Compatibilidade para inclusão de biopolímeros selecionados.** Uma formulação injetável foi desenvolvida e caracterizada visando a inclusão de biopolímeros selecionados no meio de LTTM usado para aumentar a biodisponibilidade dos AINEs;

**iv) Viabilidade para administração intra-articular.** A formulação desenvolvida foi estudada de forma a validar propriedades adequadas à aplicação pretendida;

**v) Potencial terapêutico *in vivo* para OA**. O injetável obtido foi avaliado num modelo de ratazana com OA pós-traumática.

Resumidamente, o LTTM de glicerol:sorbitol (GS) emergiu como lubrificante promissor, aumentou a solubilidade do celecoxibe (CEX), e foi compatível com HA, potenciando uma alternativa às soluções fisiológicas convencionais. A combinação GS+HA resultou num gel injetável estável, que mimetiza as propriedades do líquido sinovial, aumenta ainda mais a biodisponibilidade do CEX e modela a cinética de libertação. *In vivo*, a formulação HA+GS+CEX reduziu eficazmente a dor e inflamação, e distinguiu-se pela inibição da destruição óssea e de cartilagem, não alcançada pelo HA ou HA+CEX sem GS.

No geral, o trabalho desenvolvido permitiu obter um protótipo de produto reunindo dois agentes terapêuticos individualmente aprovados para o tratamento da OA, numa formulação única, com potencial terapêutico aprimorado e conveniência (2-em-1). Uma formulação injetável com estas características não está ainda disponível no mercado e é de elevado interesse social e económico.

**Palavras-chave:** Osteoartrite, misturas de baixa temperatura de transição/sistemas eutécticos, biopolímeros, viscosupplementação, ácido hialurónico, anti-inflamatórios, celecoxibe, intra-articular, injeção, glicerol, sorbitol

# LIST OF PUBLICATIONS

## Patent

PCT/IB2024/056817 patent application. Ana Roda, Ana Rita C. Duarte, Alexandre Paiva, Jaqueline Lourdes Rios and Laura B. Creemers. Injectable composition, methods and uses thereof, registered on 12/07/2024 (provisional patent since 19/12/2023)

## Papers published in international peer-reviewed scientific journals:

Ana Roda, Alexandre Paiva and Ana Rita C. Duarte. A Low Transition Temperature Mixture-based viscosupplementation complemented with celecoxib for osteoarthritis treatment, *International Journal of Pharmaceutics.* 2024, 656, 124088. doi: 10.1016/j.ijpharm.2024.124088

Ana Roda, Alexandre Paiva and Ana Rita C. Duarte. Therapeutic Liquid Formulations Based on Low Transition Temperature Mixtures for the Incorporation of Anti-Inflammatory Drugs, *Pharmaceutics.* 2021, 13, 1620. doi: 10.3390/pharmaceutics13101620

Ana Roda, Filipa Santos, Yeong Zen Chua, Aarti Kumar, Hoang Tam Do, Alexandre Paiva, Ana Rita C. Duarte and Christoph Held. Unravelling the nature of citric acid:L-arginine:water mixtures: The bifunctional role of water, *Physical Chemistry Chemical Physics*. 2021, 23, 1706. doi:10.1039/D0CP04992A

Ana Roda, Ana M. Matias, Alexandre Paiva and Ana Rita C. Duarte. Polymer Science and Engineering Using Deep Eutectic Solvents, *Polymers*. 2019, 11, 912; doi:10.3390/polym11050912

## Papers in preparation for publication in international peer-reviewed scientific journals:

Ana Roda, Jaqueline Lourdes Rios, Yeter Dilek, Kelly Warmink, Remei Escudero, Katrin A. Muenzebrock, Jie Du, Zhiming Wu, Alexandre Paiva, Ana Rita C. Duarte and Laura B. Creemers. A Low Transition Temperature Mixture-based viscosupplementation complemented with celecoxib for osteoarthritis treatment

## Oral presentations in international conferences:

Ana Roda, Jaqueline Lourdes Rios, Alexandre Paiva, Laura B. Creemers and Ana Rita C. Duarte. Green Solvents: New Horizons in Osteoarthritis Treatment. Accepted in the IMIL2024: 7th Edition of the Iberoamerican Meeting on Ionic Liquids, Coimbra, Portugal, 20-22 November 2024

Ana Roda, Alexandre Paiva and Ana Rita C. Duarte. Combining Low Transition Temperature Mixtures with hyaluronic acid and NSAID for osteoarthritis treatment. EPNOE2022: 5th International EPNOE Junior Scientist Meeting, Aveiro, Portugal, 8-9 September 2022

Ana Roda, Alexandre Paiva and Ana Rita C. Duarte. A two-in-one formulation for intra-articular injection in osteoarthritis. IMRC2022: XXIX International Materials Research Congress, Cancún, Mexico, 14-19 August 2022

Ana Roda, Ana A. Matias, Alexandre Paiva and Ana Rita C. Duarte. Exploring DES-like formulations to improve NSAIDs solubility. IMRC2021: XXIX International Materials Research Congress, Cancún, Mexico, 15-20 August 2021

Ana Roda, Filipa Santos, Yeong Zen Chua, Aarti Kumar, Hoang Tam Do, Alexandre Paiva, Ana Rita C. Duarte and Christoph Held. DES? Solutions? The Influence of Water on the phase behaviour of Ternary Liquid Mixtures. 2nd International Meeting on Deep Eutectic Systems, Lisbon, Portugal, 15-17 June 2021

Ana Roda, Alexandre Paiva, Ana Rita C. Duarte and Christoph Held. Insights into mixtures with water: DES or aqueous solutions? Flash oral presentation at IMIL2021: 6th Iberoamerican Meeting on Ionic Liquids, Chile, 24-26 May 2021

## Posters in international conferences:

Ana Roda, Jaqueline Lourdes Rios, Yeter Dilek, Kelly Warmink, Remei Escudero, Katrin A. Muenzebrock, Jie Du, Zhiming Wu, Alexandre Paiva, Ana Rita C. Duarte and Laura B. Creemers. The effect of a two in one viscosupplement delivering celecoxib in a rat model of osteoarthritis. 2024 OARSI World Congress on Osteoarthritis, Vienna, Austria, 18-21 April 2024

Ana Roda, Alexandre Paiva, Ana M. Matias and Ana Rita C. Duarte. Exploring NSAIDs bioavailability through THEDES-like liquid formulations. 12th World Meeting on Pharmaceutics, Biopharmaceutics and Pharmaceutical Technology, Vienna, Austria, 11-14 May 2021

Ana Roda, Ana M. Matias, Alexandre Paiva and Ana Rita C. Duarte. THEDES-like mixtures influence in the bioavailability of NSAIDs. 1st GREENERING International Conference, Costa da Caparica, Portugal, 15-16 February 2021

Ana Roda, Alexandre Paiva, Ana Rita C. Duarte and Christoph Held. DES? Solutions? Tools to characterize the effect of water in complex liquid mixtures. 1st GREENERING International Conference, Costa da Caparica, Portugal, 15-16 February 2021

Ana Roda, Ana M. Matias, Alexandre Paiva and Ana Rita C. Duarte. Biopolymeric-based THEDES for osteoarthritis treatment. 2nd International workshop on advanced materials for healthcare applications, Funchal, Madeira, 8-9 October 2019

Ana Roda, Ana M. Matias, Alexandre Paiva and Ana Rita C. Duarte. Glucosamine/Chondroitin-based THEDES for osteoarthritis treatment. 1st International Meeting on Deep Eutectic Solvents, Lisbon, 24-27 June 2019

# CONTENTS

# LIST OF FIGURES

# List of Tables

# ACRONYMS & ABBREVIATIONS

| | |
|---|---|
| **A** | |
| **ATDC5** | Chondrogenic cell line derived from mouse teratocarcinoma AT805 |
| **ACLt** | Anterior Cruciate Ligament transection |
| **B** | |
| **BV/TV** | Volume of mineralized bone per total volume, Bone volume fraction |
| **C** | |
| **CEX** | Celecoxib |
| **CAW** | Citric acid:L-arginine:water 1:1:7 (molar) |
| **Caco-2** | Epithelial cell line from human colorectal adenocarcinoma |
| **COX** | Cyclooxygenase |
| **ChCl** | Choline Chloride |
| **CRISPR-Cas9** | Clustered Regularly Interspaced Short Palindromic Repeats-associated protein 9 |
| **COSMO-RS** | Conductor-like Screening Model for Real Solvents |
| **D** | |
| **DES** | Deep Eutectic Systems, Deep Eutectic Solvents |

| | |
|---|---|
| **DSC** | Differential Scanning Calorimetry |
| **DMSO** | Dimethyl sulfoxide |
| **DMEM/F-12** | Dulbecco's Modified Eagle Medium/Nutrient Mixture F-12 |
| **DSMZ** | German Collection of Microorganisms and Cell Cultures |
| **DNA** | Deoxyribonucleic acid |
| **DWB** | Dynamic weight bearing |

**E**

| | |
|---|---|
| **ESCEO** | European Society for Clinical and Economic Aspects of Osteoporosis and Osteoarthritis |
| **EDTA** | Ethylenediaminetetraacetic |
| **EMA** | European Medicines Agency |

**F**

| | |
|---|---|
| **FDA** | Food and Drug Administration |
| **FBS** | Fetal Bovine Serum |
| **FTIR** | Fourier Transform Infrared |
| **$F_c$** | Crossover frequency |

**G**

| | |
|---|---|
| **GS** | Glycerol:sorbitol 2:1 (mol/mol) |
| **GBD** | Global Burden of Disease |
| **Glu** | Glucosamine |
| **GluS** | Glugosamine sulphate |
| **GHA** | Gel of hyaluronic acid in a mixture of GS:PBS (2:1 molar) |
| **GGluS** | Gel of hyaluronic acid and GluS in a mixture of GS:PBS (2:1 molar) |

| | |
|---|---|
| G' | Storage/elastic modulus |
| G'' | Loss/viscous modulus |
| H | |
| HA | Hyaluronic acid |
| HMW | High molecular weight |
| HSP | Hansen solubility parameters |
| HPLC | High-Performance Liquid Chromatography |
| HEK-293 | Human Embryonic Kidney cell line |
| I | |
| IA | Intra-articular |
| ISO | International Organization for Standardization |
| L | |
| LTTM | Low Transition Temperature Mixtures |
| LMW | Low Molecular Weight |
| L929 | Mouse fibroblasts cell line from connective tissue |
| LVR | Linear Viscoelastic Region |
| LOD | Limit of Detection |
| M | |
| MEM | Minimum Essential Medium |
| MTS | 3-(4,5-dimethylthiazol-2-yl)-5-(3-carboxymethoxyphenyl)-2-(4-sulfophenyl)-2H-tetrazolium |
| MW | Molecular weight |

| | |
|---|---|
| **µCT** | Micro-computed tomography |
| **N** | |
| **NMR** | Nuclear Magnetic Resonance |
| **NSAID** | Non-Steroidal Anti-Inflammatory Drugs |
| **NBF** | Neutral Buffered Formalin |
| **NOESY** | Nuclear Overhauser Effect Spectroscopy |
| **O** | |
| **OA** | Osteoarthritis |
| **OARSI** | Osteoarthritis Research Society International |
| **P** | |
| **PBS** | Phosphate Buffer Saline |
| **PDL** | Poly D,L-Lactide |
| **PEG** | Polyethylene glycol |
| **PEA** | Polyester-amide |
| **$PGE_2$** | Prostaglandin E2 |
| **POM** | Polarized Optical Microscopy |
| **PLGA** | Polylactic-co-glycolic acid |
| **PVP** | Polyvinyl pyrrolidone |
| **pMMx** | Partial medial meniscectomy |
| **R** | |
| **RA** | Rheumatoid Arthritis |

S

| | |
|---|---|
| **SYSADOA** | Symptomatic Slow Acting Drugs for Osteoarthritis |
| **SBP** | Subchondral Bone Plate |
| **SD** | Standard Deviation |

T

| | |
|---|---|
| **THEDES** | Therapeutic Deep Eutectic Systems |
| **$T_m$** | Melting temperature |
| **$T_f$** | Freezing temperature |
| **$T_g$** | Glass-transition temperature |
| **TGF** | Transforming Growth Factor |
| **TB** | Trabecular Bone |

# 1

# Introduction

This chapter, namely sections 1.5 and 1.6, contain part of the review manuscript: Ana Roda, Ana M. Matias, Alexandre Paiva and Ana Rita C. Duarte. Polymer Science and Engineering Using Deep Eutectic Solvents, Polymers. 2019, 11, 912; doi:10.3390/polym11050912
The publication content was here adapted, shortened, and complemented to present the most relevant information for the context of the work developed.

Section 1.5.2 was adapted from the introduction of the author's manuscript: Ana Roda, Alexandre Paiva and Ana Rita C. Duarte. Therapeutic Liquid Formulations Based on Low Transition Temperature Mixtures for the Incorporation of Anti-Inflammatory Drugs, Pharmaceutics. 2021, 13, 1620. doi: 10.3390/pharmaceutics13101620

The author was involved in the conceptualization, literature research and full preparation of the original manuscripts.

## 1.1 Motivation, Objective and Framework

Osteoarthritis (OA) is a musculoskeletal inflammatory disease affecting almost 7% of the world population [1]. It is characterized by cartilage loss between junctions, causing inflammation, pain and loss of joint function [2]. Common treatments focus on the symptomatic control by the administration of analgesic, anti-inflammatory drugs, oral supplements such as chondroitin and glucosamine, and intra-articular (IA) injections of corticosteroids and/or hyaluronic acid. The limitations of these therapies are mostly related to short-term efficiency, adverse effects and restricted bioavailability. In this context, Low Transition Temperature Mixtures (LTTMs) have emerged as a platform with potential solutions for those limitations. LTTMs are liquids formed by the combination of two or more compounds, that liquify at certain temperature and ratios. Including but not restricted to deep eutectic systems (DES), LTTMs can be designed as non-toxic, biodegradable and biocompatible liquids, normally characterized by its high and tunable viscosity [3,4]. The LTTMs versatility in terms of composition and rheologic properties can be highly promising in the design of tailored formulations, while carrying therapeutic components. A biocompatible formulation that enhances the bioavailability of marketed drugs is of great importance for oral and intra-articular OA treatments, improving their efficiency and safety, while avoiding the long-term development of new drugs associated to the length of the regulatory path. In the last years, LTTMs have shown promising prospects to increase drugs bioavailability [5], and to achieve controlled delivery through their viscosity, or by combination with other materials, such as polymers [6–11]. Moreover, the use of polymeric materials is widely described for tissue engineering of scaffolds for bone, cartilage and other tissues [12]. The combination of LTTMs and polymers has resulted in recent developments for both drug delivery applications [6–11] and the formation of biopolymer-matrices [13,14].

The *in situ* administration of drugs or supplements and its incorporation in a biocompatible liquid can also improve their bioavailability, potentiating their therapeutic effect. Moreover, biopolymer inclusion in a liquid for intra-articular injection could serve as a matrix to carry and mediate drug delivery. In sum, an IA injectable formulation for OA containing LTTMs, drugs and polymer(s) can promote: i) increased drugs' bioavailability and mediated delivery, ii) physical-elastic barrier in the synovial cavity to allow shock absorption and prevent bone friction,

iii) joint lubrication, iv) decreased inflammatory response and eventually, v) retard OA progression.

To the best of our knowledge, a system combining the described features is not yet reported. Herein, we propose the design of an LTTM-based system, incorporating a NSAID with enhanced bioavailability, while carrying biopolymer(s) to restore the rheologic properties of synovial fluids and promote a mediated drug delivery.

In this context, this document is divided into five main chapters, each comprehending a different stage of the work, as represented in Figure 1.1. Chapter 1 consists in a state-of-the-art of the several topics important for the work development. Chapter 2 explores the design and characterization of LTTMs, and their influence on the solubility and thus, bioavailability of different NSAIDs. The LTTM+NSAID with higher potential for intra-articular injection was selected and further explored in chapter 3, where the inclusion of cartilage biopolymers on the LTTM matrix was tested and characterized in terms of suitability for viscosupplementation. The LTTM-polymeric-drug formulations were also explored in terms of cytocompatibility, stability, and influence in the *in vitro* drug release. Finally, in chapter 4, the *in vivo* performance of a preselected formulation combining LTTM, hyaluronic acid and celecoxib, was studied in an OA-rat model. The last chapter – Chapter 5 – comprehends a general perspective of the major achievements regarding the developed work, and future challenges and prospects.

Considering that this PhD thesis was structured based on scientific articles published, submitted or under preparation, the respective chapters, namely, chapter 2 to 4, were presented in manuscript format.

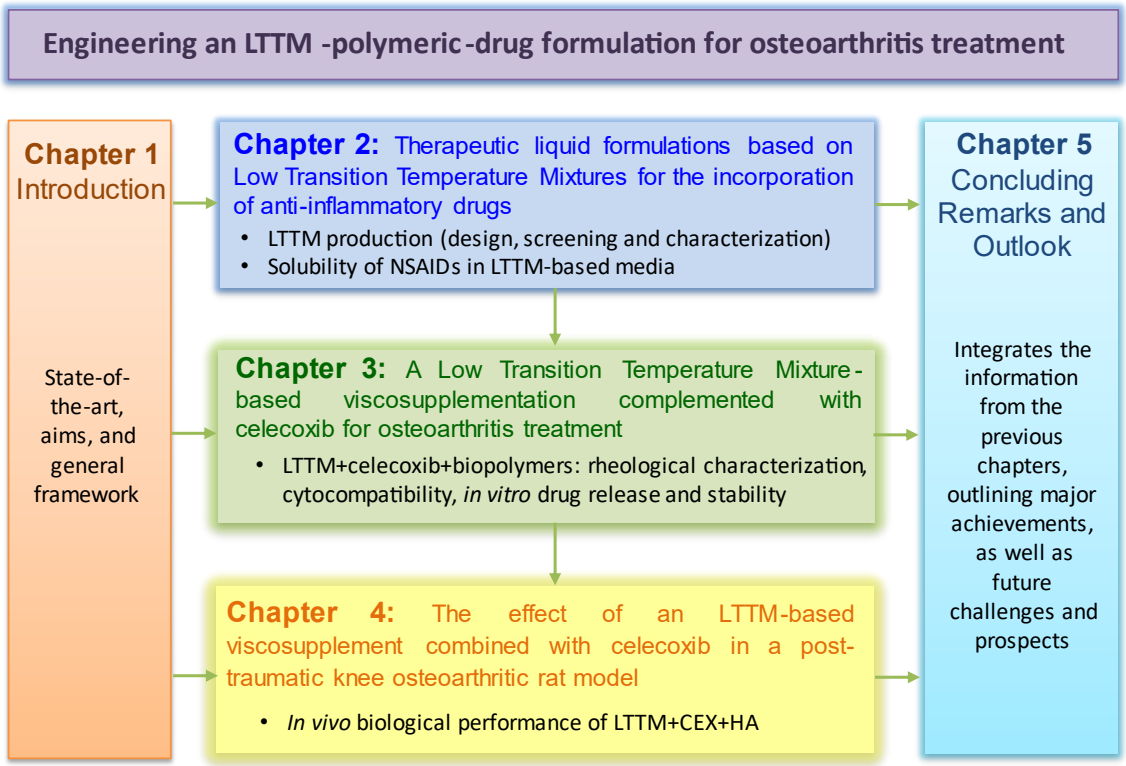


**Figure 1.1** – Schematic representation of the thesis framework.

## 1.2 Osteoarthritis

*...a burden to worldwide population*

Osteoarthritis (OA) is a musculoskeletal inflammatory disease affecting joints. Joints are composed by three main components: joint capsule, articular cartilage and synovial fluid (Figure 1.2). The outer part of a synovial joint is formed by the joint capsule, a component that comprehends the synovial membrane as inner layer and a fibrous capsule as external layer. The fibrous capsule, also called capsular ligament, supports the synovial membrane and the articulating bones; whereas the synovial membrane or synovium is a highly vascularized connective tissue that mediates the nutritional exchanges between blood and joint, and secretes or absorbs the synovial fluid. Internally, there is articular cartilage, a non-vascularized tissue covering the articulating bones surface that functions as shock absorber and prevents bone friction. Lastly, the core of a synovial joint is the synovial fluid, a highly viscous liquid that lubricates the

joints, provides nutrients for the cartilage surrounding cells and smoothens movement shocks and bone friction [15,16].

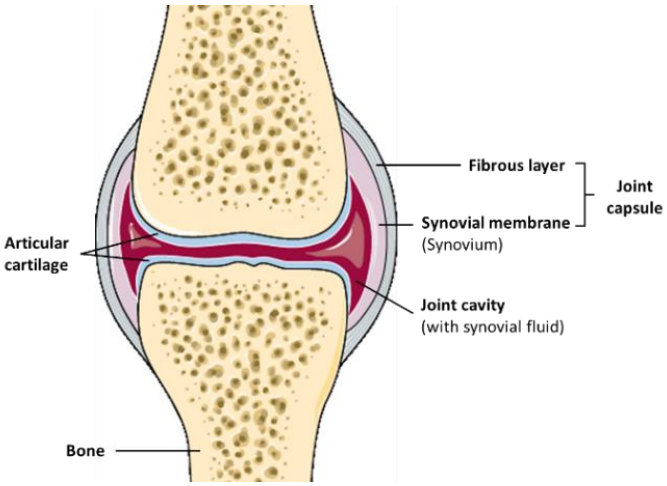


**Figure 1.2** – Illustration of a healthy synovial joint, adapted from SMART (Servier Medical Art, licensed under a Creative Commons Attribution 3.0 Unported License: http://smart.servier.com/).

In OA, both the articular cartilage and synovial fluid are compromised, losing their protective function which accelerates OA progression. This condition is characterized by cartilage loss, inflammation, bone changes or outgrowth (e.g: sclerosis, cysts, osteophytes), pain, stiffness and ultimately, loss of joint function [2,17,18]. Its incidence can be influenced or triggered by heterogeneous conditions such as ageing, genetics, trauma, physiological or anatomical abnormalities and others [17,19]. Being the most common form of arthritis, it affects about 7% of the world population [1,20], with an incidence (new cases) and prevalence (existing cases) rate rising with ageing in both sexes (Figure 1.3), and over the years, as the life expectancy increases. Moreover, it is more prevalent in women (60%) than man (40%) (Figure 1.3). In 2017, USA was the most affected country, with 10.5% of the people suffering from OA. In Europe, 6.7% of the population was affected by OA, with Portugal being the European leader of prevalence (8.5%) and the 3$^{rd}$ worldwide in terms of incidence and prevalence [20]. In terms of the joints affected, OA can occur at any joint, being most common in the knee, hands, hip, spine and foot [21].

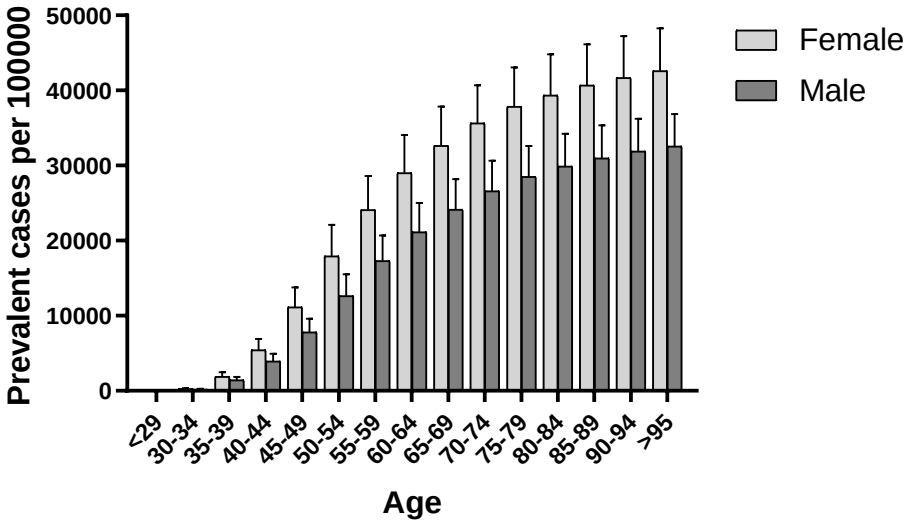


**Figure 1.3** – Global prevalence of osteoarthritis for age and sex in mean±SD (light grey: female; dark grey: male). Data from Global Burder of Disease (GBD) 2019 [20].

## 1.3 Conventional OA therapy

*…symptomatic management is still the only way*

The current approaches for OA management and therapy comprehend three main categories: non-pharmaceutical, pharmaceutical and surgical. The most common strategy applied for OA treatment is schematized in Figure 1.4.

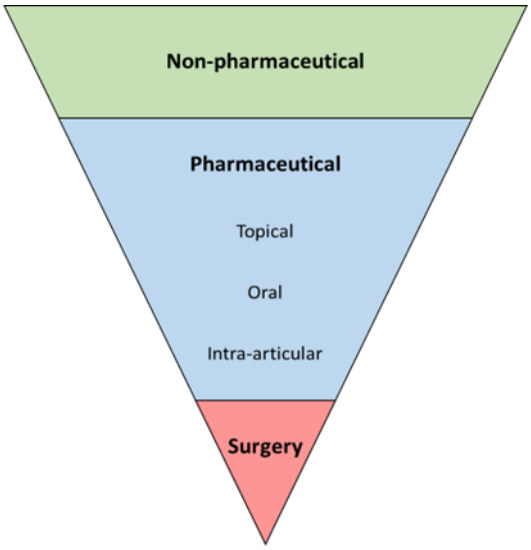


**Figure 1.4** - Schematic representation of the common lines of treatment currently applied to OA.

### 1.3.1 Non-pharmaceutical

*…a lifestyle medicine*

As soon as OA is diagnosed, non-pharmaceutical approaches are commonly recommended or prescribed, and personalized to the patient needs to retard OA progression. This category is considered the core of long-term OA management. Arthritis education, exercise, physiotherapy and weight control are crucial for the symptomatic control, function maintenance and patients' quality of life [22,23]. In some cases, biomechanical support (e.g insoles, canes, orthoses, braces or slaves) can also be beneficial for reducing weight overload in joints and/or to correct or compensate deformities, which have shown to decrease the degenerative progression of OA [23,24]. Moreover, the Osteoarthritis Research Society International (OARSI) organization recognized the importance of the holistic wellbeing of OA patients, recommending for the first time the practice of mind-body exercises (as Yoga or Tai Chi). These non-pharmaceutical approaches are often combined with pharmaceutic therapy for OA symptomatic relief.

### 1.3.2 Pharmaceutical

*…active agents towards symptomatologic relief*

The most common pharmaceutical approaches can be divided in 4 main categories: analgesics, non-steroidal anti-inflammatory drugs (NSAIDs), symptomatic slow acting drugs for OA (SYSADOA) and intra-articular injectables (Figure 1.5). The first line pharmaceutical option for OA therapy depend on the disease stage, patient co-morbidities, regional guidelines and medical opinion [25], but usually starts or includes OA symptomatic control with the administration of topical and/or oral analgesics and NSAIDs, such as celecoxib, diclofenac and ibuprofen [26]. The topical NSAIDs are preferably recommended by the OARSI 2019 guidelines in respect to oral analgesics, due to the lower effective dose needed, in comparison to the oral dose of the same drug [25]. Despite the safety and efficiency observed for NSAID treatments, these drugs can cause potentially severe gastrointestinal and cardiovascular adverse effects. For this reason, the intake of NSAIDs, especially oral, must be restricted to the shortest time needed, and to its minimal effective dose [22,23,27].

Paracetamol is also commonly prescribed as analgesic for OA [23–25]. However, its administration was conditionally not recommended for the first time by the OARSI 2019 guidelines, due to evidence of low or no efficiency in OA treatment, and to the imminent possibility of hepatotoxicity [25].

Other analgesics have also been conditionally administered. Capsaicin is an analgesic chili pepper extract, used in topical formulations for local pain relieve of some OA phenotypes, by reducing the sensorial nerve transmission. Despite being commonly recommended, its long-term application has been questioned, due to the possibility of partial or irreversible skin desensitization [24]. In the OARSI 2019 guidelines, the use of capsaicin is not recommended, given the inadequate efficacy and safety balance [25]. Duloxetine is a serotonin-norepinephrine reuptake inhibitor, commonly associated with the treatment of depression and anxiety [24]. However, this drug can also be used as analgesic for cases of chronic pain caused by dysfunction of the central nervous system, as it occurs to some OA patients, to whom other therapies may be inefficient [24,28]. Its adverse effects (nausea, constipation, hyperhidrosis, dry mouth, somnolence, fatigue and decreased appetite) [28] were considered acceptable [23], and its administration conditionally recommended by the 2014 OARSI guidelines for knee or multiple-joint OA [28]. Further pharmacotherapies for OA include oral or transdermal opioids. They cause several adverse effects as sedation, constipation, urinary retention, nausea, vomiting, respiratory depression, confusion [24], and most importantly, extreme chemical dependence. For these reasons, this class of drugs has been restrictedly administered when the remaining pharmaceutical and non-pharmaceutical options are inadequate [23]. Moreover, they have been reported to have limited effect in OA therapy [23,25] which, in addition to the international concern about opioids dependency, led OARSI (2019 guidelines) to strongly recommend against their administration [25].

The above-mentioned medications are considered rapid-acting drugs for OA. Complementary or optional therapies based on SYSADOA can be administered. Diacerein is a SYSADOA with anti-inflammatory, anti-catabolic and pro-anabolic effect on the cartilage and synovial membrane. Additionally, it has shown to reduce or retard subchondral bone remodeling. Its efficiency is comparable to NSAIDs in terms of pain and joint function, presenting a slower but prolonged action [29], with possible additive effect if combined [24]. Although it may cause

gastrointestinal adverse effects, skin reactions or less commonly, hepatobiliary disorders, it presents a general safety profile [24,29]. For these reasons, diacerein oral administration was considered as suitable for supplementation to other drugs, or even as an alternative first-line pharmaceutical therapy (by ESCEO – European Society for Clinical and Economic Aspects of Osteoporosis and Osteoarthritis, in 2016) [29].

In addition, chondroitin and glucosamine are natural cartilage constituents, usually used as oral SYSADOA supplements, associated with pain reduction and retarded osteoarthritis progression [23,30,31]. However, several studies question their efficiency [32,33]. The oral administration of these supplements may impair their bioavailability, whereas in topical administration the size of these biopolymers hinders their permeation through the skin barriers (transdermal permeation). Either way, the doses reaching the inflamed joints are probably insufficient to reach the therapeutic effect [34].

Additional pharmaceutical therapies for OA include intra-articular (IA) injections of corticosteroids and/or hyaluronic acid. Corticosteroid injections, namely, glucocorticoids, have short-term anti-inflammatory effect against pain and time-limited number of applications [22,35]. Despite some studies defend that corticosteroids protect the cartilage, retarding OA progression, their continued administration is associated to several adverse effects, such as tendon rupture and joint deterioration, Cushing syndrome, hyperglycemia, ophthalmic complications, osteoporosis, avascular necrosis and even accelerated OA progression [35,36]. Moreover, the intra-articular injection of corticosteroids often causes local infection [24].

In turn, hyaluronic acid injections are used as viscosupplementation, since it is the main component of the synovial fluid, responsible for its rheologic and lubricant properties. However, its benefits are controverse, especially in advanced stages of OA, most probably due to the accelerated clear rates of hyaluronic acid caused by the disease [37,38].

Despite these general lines of treatment, the therapeutics applied always depends on the clinician and on the patient needs in terms of OA type, stage and other health conditions.

Further detailed description and recent advances on celecoxib and hyaluronic acid viscosupplementation are available in the subsections 1.3.2.1 and 1.3.2.2, as those are the pharmaceutical approaches more comprehensively explored in the scope of this thesis.

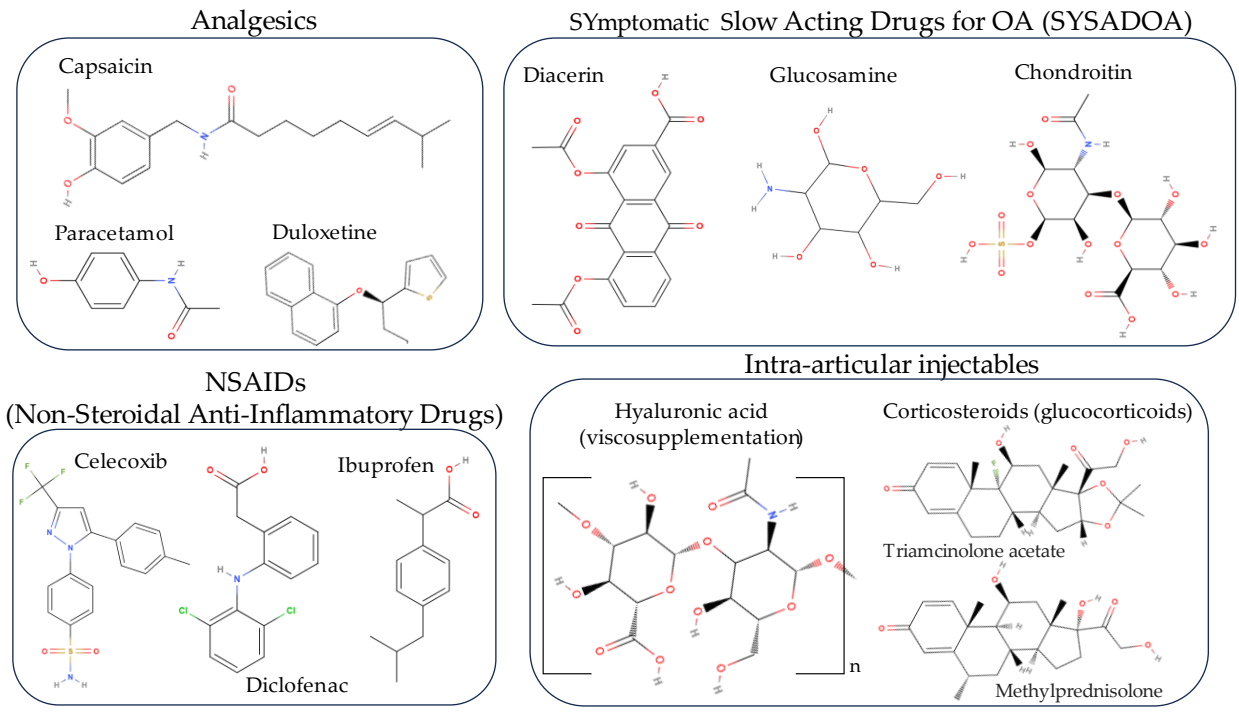


**Figure 1.5** - Schematic representation of pharmaceutic approaches used for OA treatment, including some examples and respective chemical structures (retrieved from molview.org).

#### 1.3.2.1 Celecoxib

Celecoxib is a first-line treatment option for OA pain. It is a NSAID with therapeutic benefits by the selective inhibition of cyclooxygenase-2 (COX-2). In OA, COX-2 levels are upregulated, leading to inflammatory chain reactions that cause a multitude of responses at different levels, such as synovium inflammation, pain sensitization, and cartilage degeneration due to the activation of degradation enzymes [39–41]. The selective inhibition of COX-2 reduces inflammation and pain, while avoiding the side effects associated to the non-selective COX-1 inhibition. Thus, it has an improved safety profile in respect to non-specific NSAIDs [42–45].

Regarding the clinical performance of orally administered CEX, most studies indicate improvements in pain and function, even though some effects are reported as minor or inconsistent throughout literature [33,46–49]. Moreover, preclinical studies defend some additional positive outcomes, that support a disease-modifying effect conferred by CEX [48]. Panahifar and co-workers studied the effect of daily oral doses of CEX in a post-traumatic OA rat model, equivalent to recommended human doses. The 3 month follow-up supported that CEX inhibited osteophytes enlargement, which may retard OA progression, even though no

chondroprotective effect was observed [50]. Despite the benefits of oral CEX uptake for OA, the effective amount of CEX reaching the joints is limited, and its continuous oral administration is associated to systemic adverse effects [47,51], albeit minor in comparison to other NSAIDs [43,44]. To overcome those limitations, preclinical studies have explored the *in situ* delivery of CEX, through intra-articular injection. For instance, Jiang and collaborators reported the effect of weekly IA injections of CEX (0.4% w/v) in a rabbit OA model. CEX successfully suppressed inflammatory promotors, and inhibited cartilage degeneration in comparison to the control group [52]. Furthermore, Hurtig and colleagues described a polymeric mixture (PDL-PEG) combined with CEX, that showed minimized systemic exposure and reduced inflammatory response (less effusion and $PGE_2$ levels), upon IA injection in a chronic inflammatory sheep model [53]. In a different study, Janssen et al. developed polyester-amide (PEA) microspheres for the sustained IA delivery of CEX (0.06% w/v). Early assessments in a OA rat model confirmed the anti-inflammatory action of CEX by the decreased levels of prostaglandin E2 ($PGE_2$), an inflammatory mediator [54]. Subsequent studies using this CEX-delivery system were conducted: Tellegen and the co-authors observed that the IA controlled delivery of CEX in a rat OA model decreased local joint inflammation, subchondral bone sclerosis, and reduced the formation of cysts, osteophytes and calcified loose bodies. Even though some effects were dose dependent, effective therapeutic action was achieved from 0.06 to 0.78% (w/v) of injected CEX [40]. Its safety and efficiency was further evaluated in dog patients (0.93% w/v), showing improvement in pain and limb function, while reducing medication dependency over 2 months [55]. Other works about IA injections for OA therapy reported different polymer-CEX combinations that minimized systemic CEX exposure [56,57], and were tolerable in healthy animal models, but not yet tested towards their effect in OA [56–58]. Overall, the developments on the IA delivery of CEX reported biocompatible and/or beneficial therapeutic outcomes for OA, however, the number of studies *in vivo* is still scarce. Up to date and to the best of our knowledge, no IA-injectable containing CEX is yet available for human therapy.

OA progression rate is highly accelerated for more advanced stages, leading to exponential disease development. Thus, all contributions towards OA therapy, even minor, might have a large impact on OA prognosis and patient quality of life. The translation of preclinical studies, variability between OA models, OA types, and severity, keep challenging the possible

conclusions towards the efficiency of CEX. Thus, it is crucial to increase the number of studies in order to standardize, optimize or personalize the relation of CEX with OA control and progression.

#### 1.3.2.2 Hyaluronic acid

*…perhaps there isn't a rule, but personalized approaches might be the answer.*

Hyaluronic acid is a naturally occurring polysaccharide and one of the main constituents of articular cartilage and synovial fluids [59]. Therefore, it is one of the most administered therapies for OA via intra-articular injection - viscosupplementation, even though its efficacy is controversial [26,60,61]. Efficiency tends to be higher in early-stage OA, where the retention time of HA is longer in comparison to advanced OA-phenotypes. The residence time and properties of HA in the synovial fluid and the inflammatory process are intrinsically correlated in a cyclic manner. As the inflammatory response increases, so does the HA degradation and/or clearance rate. Lower HA content impairs joint lubrication, cartilage and bone destruction. Worse OA symptoms trigger more inflammatory chain reactions, thus increasing HA depletion from the synovial fluid [16]. Therefore, it is of utmost importance to restore the viscoelastic and chondroprotective properties of the synovial fluid. Up to date, several viscosupplementations are commercially available, containing HA between 0.8 and 2.2%, with a molecular weight (MW) varying from 0.5 to >10 MDa [62,63]. Although viscosupplementations can provide prolonged relief of OA symptoms and retard its progression, it depends on several internal and external factors, thus rendering controverse outcomes [63–67]. Most studies evaluating the efficiency of viscosupplementations, consider them as a unique category, not accounting for the HA content in terms of MW and concentration. However, these parameters highly influence the effectiveness of those injectables. In 2020 and 2021, a systematic review and meta-analysis on this topic reported significant positive differences for treatments with high molecular weight (HMW) HA versus low molecular weight (LMW) HA for knee and hip OA [63,67,68]. Even though there is no standard categorization of the high to low MW range [63,67,69], in general, MW ≥ 1.2 MDa showed better improvement trends in comparison to inferior MW. Also, there was a higher therapeutic trend for increasing MW, especially noticeable for MW > 3 MDa [63,70] or ≥ 6 MDa [67]. MW > 10 MDa were an exception since their efficiency trend and safety

decreased in comparison to other HMW HA [63]. A study from 2017 also suggests that the combination of LMW and HMW HA may synergistically contribute to enhanced therapeutic efficacy. However, its efficiency was postulated by comparing the hybrid LMW-HMW HA at 3.2% with a HMW HA at 2% [71]. Despite a synergetic action cannot be ruled out, it can also be an effect of concentration, thus emphasizing the need to explore and account for the HA multifactorial influence. The intensity and duration of the therapeutic action is also important when discussing efficiency outcomes. Again, this analysis is not linear but generally, HMW have higher and longer symptomatic relief than LMW, especially when comparing extreme MW ranges (eg: 6-7 vs 0.5-0.73 MDa) [72,73]. In addition to the HA MW weight, its origin, concentration, and form, (e.g: linear or crosslinked) are also important features to be considered, and most often ignored [72,74,75]. For example, Larsen's team compared the same HA-derived product in its natural linear (non-crosslinked) structure versus the crosslinked form. The crosslinked HA had an apparent half-life (8.8 days) about 6-times higher than the linear form (1.5 days) in the knees of a healthy rabbit model [76,77]. Higher HA retention time Is expected to increase or prolong the therapeutic action, however, this is not straightforward. Whereas viscosupplements with MW > 10 MDa present the highest retention time reported (1 month) [78], their efficiency and safety seem to be lower than other HMW (MW 3.6 to 10 MDa) [63]. The biologic processes behind this or the action mechanisms that dictate the relation between their properties and therapeutic action are not yet well understood. Still, it is known that their action is much longer than their retention times, thus suggesting that physical-mediated changes are not the only nor the most important mechanism of action [37,63].

Even though the therapeutic effect of HA is not straightforward as it depends on multiple variables such as OA stage, HA type, external influences, and even intrinsic patient-variability, there is a clear tendency towards literature indicating that HMW HA have higher and longer efficiency in OA symptom relief. However, further studies are needed to understand the extent of those benefits and the maximum MW threshold from which the therapeutic effects decrease and why.

The positive therapeutic trend, indicated by most studies about viscosupplementations in OA, sustains its continuous while conservative use in OA therapy. Most health organizations have restrained recommendations due to the limited and debatable outcomes available. The

current field developments point to an expanding tendency to reach personalized therapeutic approaches rather than generic administration guidelines. The potential of HA viscosupplementations is pending on more advanced studies to comprehensively understand and evidence the relation between their properties (intrinsic and extrinsic), action mechanisms and efficiency.

### 1.3.3 Surgical

*…the last resource*

Surgical intervention is considered in severe OA stages, for which the remaining medical approaches are inefficient. Different types of surgery can be applied according to the patient clinic profile, such as: osteotomy (bone realignments), arthrodesis (joint immobilization by bone fusion) or arthroplasty (joint realignment or prosthetic reconstruction) [79]. These procedures are highly invasive, with long recovery times and permanently limit patients' quality of life. Therefore, surgery is a last resource approach, often still requiring complementary pharmaceutical medicine for symptomatic management.

Given the complexity and heterogeneous character of OA, human variability, and the different types and symptoms presented by OA, it is highly challenging to properly evaluate therapeutic outcomes. However, the current therapies focus mainly on OA symptomatic relief, which is not enough to prevent the trend of increased surgery incidence [80,81]. In this regard, it is essential to optimize the existing therapies in terms of efficiency and adverse effects, while developing therapies aiming to control or retard OA progression, thus reducing the need of surgical interventions.

## 1.4 Emerging therapies

*… aiming at disease modifying approaches*

Even though the general lines of OA treatment are still highly restricted to the above mentioned, there is a continuous effort from the clinicians and the scientific community to improve the existing therapies and to innovate, aiming to provide the patients more efficient, long-term, and less invasive care.

Whereas some of the research is focusing on symptom management and relief as first priority, there is also a growing investment on approaches to delay disease progression and even to restore joints, envisioning the ideal concept of disease-modifying therapies [82]. Most of the ongoing developments and emerging therapies focus on IA injections, given the advantages of this type of delivery. IA injections allow to target and easily access the affected joint(s), decreasing potential systemic adverse effects, while increasing the bioavailability of the therapeutics delivered, and thus, their efficiency. The major drawback of IA approaches is the rapid clearance upon injection, as it occurs with the conventional IA injections of corticosteroids or hyaluronic acid. For this reason, the design of new IA injectable therapies focusses on the achievement of extended bioavailability, sustained therapeutic delivery and prolonged joint retention [83]. In this scope, natural and synthetic delivery systems have been explored and can be divided in four major categories: 1. particulated or micellar delivery systems; 2. gene-based therapies; 3. cell-based therapies, and 4. scaffolds. Further combinations between these categories are often engineered for an improved performance.

Particulated or micellar delivery systems are designed as drugs recipients to achieve extended articular retention time, protect drugs from clearance and degradation, and to promote sustained drug delivery. Polymeric based-delivery systems are the most studied for this therapeutic approach, mostly because of the easier match with regulatory approved materials [38]. In 2017, the first polymeric particulated formulation was approved by the US Food and Drug Administration (FDA) for knee OA treatment [84]. Marketed as Zilretta™, it is composed by polylactic-co-glycolic acid (PLGA) microspheres containing a corticosteroid (triamcinolone acetonide) with extended-release for OA pain relief [38,85,86]. This IA delivery system accomplished improved, faster, and prolonged pain relief in comparison to the commonly administered shorted-acting IA of triamcinolone acetonide [86]. Given its recent approval, the outcomes of Zilretta™ repeated administration were not yet determined [85].

Gene therapy approaches envision the synthesis of therapeutic components within the joints, promoted by DNA inserted in chondrocyte cells by viral-based vectors or non-viral formulations. These treatments are designed for local administration, most commonly via intra-articular injection, targeting only the affected joints, maximizing its efficiency, and decreasing potential systemic adverse effects. The major progression in comparison to the conventional

therapies, is the intrinsic and continuous production of the therapeutic agents that overpasses the common limitations in achieving sustained and therapeutic doses [87]. In 2017, the first cell and gene therapy for knee OA treatment was approved and marketed in Korea: INVOSSA™, the pioneer gene treatment for OA and the fifth gene therapy approved worldwide. INVOSSA™ is an injectable formulation of human allogeneic chondrocytes expressing an anti-inflammatory cytokine, the TGF-β1 [87,88], with demonstrated efficacy for pain and function improvement [89,90]. Moreover, it showed to potentially delay OA progression, mainly at the level of cartilage damage and inflammatory profile [89,91]. Its approval was revoked due to composition mislabeling issues that were corrected, and further phase III clinical trials were authorized by the FDA in the US (listed as NCT03203330 in clinicaltrials.gov). This new clinical trial was initiated in 2018 and aims to increase the number of patients, and extend the monitoring period from 12 to 24 months, envisioning to be classified as a disease-modifying osteoarthritis drug (DMOAD). As mentioned, INVOSSA™ is considered both a gene and cell-based therapy, since it uses cells as genetic expressing vehicles.

The use of cells for the delivery and synthesis of therapeutics is one of the most explored subclasses within cell-based therapies, either by cellular transduction using genetic vectors or by direct DNA cellular edition using CRISPR-Cas9 (Clustered regularly interspaced short palindromic repeats-associated protein 9). Despite being highly promising, this approach raises several ethical questions since the long-term effects of DNA edition are not known yet [92,93]. Other subclass of cell-based therapies is the delivery or implantation of chondrocyte or stem cells, aiming to repair and regenerate damaged tissues [94]. The major challenge of these approaches is the rapid cell clearance as they do not have a proper surface to adhere and proliferate [38].

Further strategies involving tissue engineering are being explored to overcome or complement the current therapeutic limitations. Namely, scaffold engineering is emerging as a promising option for OA therapy [95,96]. Scaffolds are three-dimensional network structures that may be designed to increase physical stability in the joints, as well as to deliver therapeutic components such as biopolymers or drugs while conferring them higher chemical stability and longer retention time in the joints. Moreover, they can also retain cells, increase their adherence, enhance their proliferation, promote the production of extracellular matrix, and

ultimately cartilage regeneration [95–97]. Such scaffolds may be produced from synthetic, natural polymers, or a combination of both. Natural polymers, such as hyaluronic acid, collagen and chondroitin sulfate are ideal and widely explored for scaffold development, given their similarity to native tissues, and therefore, high biocompatibility and bioactivity [96,97]. For non-surgical approaches, injectable hydrogels are the most explored matrices within the scaffold's category since they are less invasive [96]. Moreover, they are composed by hydrophilic polymers which confer higher biocompatibility and a flexible but stable 3D matrix, by swelling in aqueous media [98]. In this context, hyaluronic acid (HA)-based hydrogels have been explored for OA, to overcome the limitations of HA viscosuplementation in terms of rapid clearance and chemical instability. By modifying and/or crosslinking HA, it is possible to maintain or enhance its properties and achieve stronger but flexible 3D structures. Theoretically, these HA-hydrogels would restore the protective function of the synovial fluid, while carrying the potential for tissue regeneration [99–101]. There are at least 3 marketed viscosupplements using crosslinked HA. As mentioned in section 1.3.2.2, although they are generally considered as safe and positive for OA symptomatic management, there is no evidence of regenerative effect. Additionally, there are some safety concerns, especially for the crosslinked-HA with higher MW [63]. Therefore, and given the potential of HA-hydrogels, research has focused on further exploring HA modifications and/or combinations with other biomaterials, aiming to tune the required physicochemical properties, such as mechanical strength and chondrogenic potential [101–103]. These modifications often result in products with residual chemicals or new properties, that can trigger unforeseen side-effects, limiting their safety and delaying their approval from the regulatory and commercialization entities. Thus, even though there has been a significant progress in the development of HA-hydrogels, these advances are still inadequate for clinical translation [99–101].

Some of the limitations encountered for cell therapies and tissue engineering could be overcome by combining them [104,105]. Based on this combinatory approach, a 4$^{th}$ generation surgical option was developed: the autologous matrix-induced chondrogenesis (AMIC®) [106,107]. It consists of microfracturing a region of the lesioned cartilage and placing a collagen-scaffold that resurfaces that area, thereby allowing the mesenchymal cells to differentiate into chondrocytes and proliferate. Additional products combining hydrogels and cells are

currently under clinical trials, and some were already approved for clinical use [96]: Cartipatch®, an agarose and alginate hydrogel with expanded cartilage cells [98,108,109]; CaReS®, a collagen gel with isolated autologous chondrocytes [98,109–111]; and CARTISTEM®, an HA hydrogel with mesenchymal stem cells [112–114]. However, all of these are invasive approaches as the materials are surgically inserted, and thus, only administered to certain advanced phenotypes of OA or other severe joint injuries [96,98,106]. Still, scaffold-tissue engineering for OA is a growing field, with high research engagement and thriving potential, especially for combination with other therapies, such as cell-based or drug delivery strategies.

## 1.5 Formulation with LTTMs for pharmaceutical and biomedical applications

*…on the path to improved therapies*

Current OA medical approaches and emerging therapies are still not enough for OA management, much less for slowing down disease progression, given their limitations or long-evaluation path before reaching the market. Therefore, it is of utmost importance to find therapies that can complement or improve treatments' outcome. A possible strategy to achieve this is to mitigate the drawbacks of current lines of treatment and/or enhance their therapeutic power. In this context, Low Transition Temperature Mixtures (LTTMs), including Deep Eutectic Systems (DES), are a contemporary platform with promising potential in the pharmaceutical and biomedical fields, for instance to increase drugs bioavailability and to incorporate biomaterials, topics further explored in the following subsections.

### 1.5.1 Deep eutectic systems and Low Transition Temperature Mixtures (LTTMs)

*…to be or not to be, DES is the question*

In a world where science uncertainty is the only constant, the scientific community has faced a non-consensual challenge on the nomenclature of deep eutectic systems (DES), and what should or should not be considered as such [115–120].

The term 'eutectic' was first introduced at the end of the 19th century (1884). By definition, it refers to the minimum freezing/melting temperature achieved by a mixture of two or more compounds at a particular molar ratio (Figure 1.6, left) [121]. The term deep eutectic solvents, also known as deep eutectic systems (DES) was later introduced by Abbott, in 2003, by referring to liquids formed just by mixing two solids: quaternary ammonium salts with metal salts, through the decrease of the freezing/melting point of the system [122].

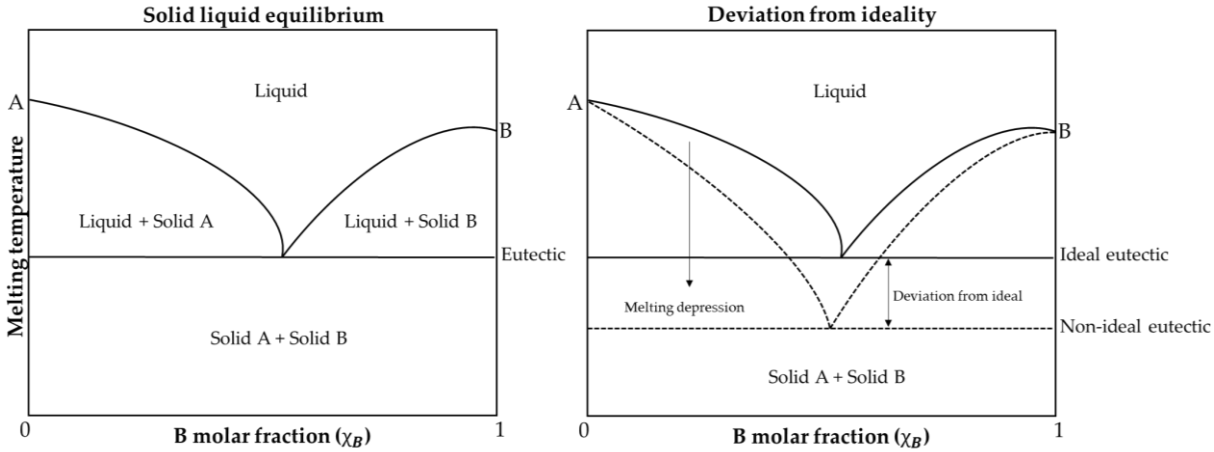


**Figure 1.6** - Phase diagram representation for A+B mixtures: melting temperature at different molar fractions of A+B (0, pure A; 1, pure B).

The concept of DES was further explored in the literature to understand their nature and liquefaction mechanism [118,120,123,124]. Even though DES are commonly referred to as a mixture of two or more compounds with a melting/freezing temperature ($T_m$/$T_f$) lower than the pure components, several authors attempted to define DES as a result of a deep melting depression caused by a deviation from ideality (Figure 1.6, right) [115,117,125–128]. This concept is often not restricted to a unique ratio of compounds, but rather to all the ratios above the liquidus line (Figure 1.6, left), which opens a larger spectrum of DES options with tunable properties [115]. The mechanism of DES formation is not yet fully understood, but consensual scientific evidence indicates that it occurs through hydrogen bonding, electrostatic interactions and/or Van der Waals interactions [129–133]. Nonetheless, up until now, there is no consensus on what should or not be considered as DES, especially for mixtures with liquid components, such as water, alcohols and some terpenes, or others whose $T_m$/$T_f$ is not possible to determine [116,118,134–137]. Therefore, other terminologies, such as Low Transition Temperature Mixtures (LTTMs) were introduced, trying to mitigate divergent opinions [138]. Considering the $T_m$/$T_f$ as one of the main parameters used to identify DES, Martins and co-authors [138] reported, in 2013, the concept of LTTMs, that comprehends mixtures with similar features to DES,

but whose $T_m$/$T_f$ were not possible to determine. Thus, the LTTM platform includes, but is not restricted to DES. Accordingly, LTTM was here used as a global term to refer to DES and other systems whose nature as DES or eutectic might be controverse.

The exponential concern with environmental issues highly motivated the development of green technologies. LTTMs have emerged as green solvents due to their potential biodegradability, biocompatibility, easy production, high yields and purity, widely available components, low toxicity and reduced volatility [4,9]. This type of solvent can be designed to fulfill the principles of green chemistry [139,140] while being highly tunable for several distinct areas. Good examples of LTTMs that fully represent green chemistry principles are natural DES (NADES), a subclass of DES formed by compounds from natural origin [141–143].

Throughout the last 20-years, an exponential interest has been given to the research on LTTMs, especially DES, a rate expected to maintain if not to increase (Figure 1.7).

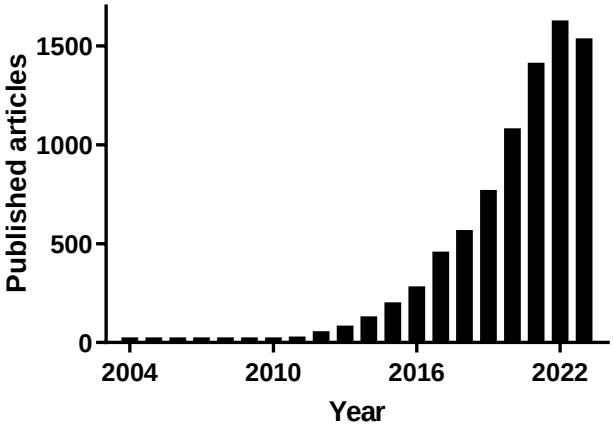


**Figure 1.7** - Number of published articles per year on LTTMs. Data from Web of Science ((ALL=(deep+eutectic+solvents)) OR ALL=(deep+eutectic+systems)) OR ALL=(Low+Transition+Temperature+Mixtures), accessed at 09 Jan 2024 [144].

Up until now, LTTMs have already been reported for several applications, primarily for electrochemistry, synthesis and extraction [142,145,146] and more recently, for pharma [5,147].

### 1.5.2 Therapeutic LTTMs for OA

*...a potential solution to overcome low drug bioavailability*

The potential of LTTMs for pharmaceutical applications was introduced by the concept of therapeutic deep eutectic systems (THEDES). By definition, THEDES are deep eutectic systems incorporating at least one active ingredient in the mixture [147]. Therefore, bioactive

compounds solubilized in DES are also considered as THEDES [5]. Either as starting material or solubilization, the inclusion of drugs in LTTMs showed to be particularly promising: the liquefaction of drugs enhanced their permeation, dissolution and absorption, thus increasing their bioavailability [5,148], which is often impaired, especially for drugs presenting low solubility in the physiological media. A biocompatible formulation that enhances the bioavailability of marketed drugs is of great importance for oral and intra-articular OA treatments, as it can improve the efficiency and safety of existing drugs, while avoiding the long-term development of new drugs associated to the regulatory entities.

To the best of our knowledge, few studies reported LTTMs to improve the bioavailability of drugs used for OA, with some significant improvements in drug solubility [149–152]. A work published by Lu and co-authors reported 17 salt-based LTTM formulations in which the solubility of several NSAIDs was increased 5 to 17-fold in respect to their solubility in aqueous media [152]. In a different study, Hyun et al. studied eutectic mixtures of celecoxib, with adipic acid or saccharin. In comparison to the aqueous media or the respective physical mixtures, the eutectics significantly improved the dissolution rate of celecoxib and its wettability [149]. Furthermore, Mokhtarpour and the co-workers published a study involving 4 NSAIDs and 2 other drugs, with a solubility enhancement of 127 to 136444-fold when dissolved in 5 different choline chloride-based DES instead of water. Their experimental results were in accordance with the empiric solubility predictions made using Hansen solubility parameters (HSP). The authors attributed the increased solubility of drugs in DES to the strong ionic-dipole interactions promoted by the DES, in addition to the common solubilization by hydrogen and dipole-dipole interactions. They also postulated that DES with weaker intermolecular interactions allow stronger interactions with the active principles. The results from this paper support the irrefutable DES potential for the solubilization of drugs. Additionally, it presents the HSP empiric model as predictive tool of DES solvation ability, that can be used to design and screen suitable THEDES [150].

An additional work, by Palmelund and colleagues, studied the solubility of 11 drugs, including anti-inflammatories (5 NSAIDs) and analgesics used for OA, in 6 LTTMs, 4 of which choline chloride-based and 2 of betaine:glycerol:water and lactic acid:glucose:water. The drugs solubility in these systems was compared with 4 conventional solvents, water, ethanol, glycerol and polyethylene glycol 300 (PEG300). In most cases, the LTTMs enhanced the solubility of the drugs in respect to water but not in comparison to the other conventional solvents. Moreover, using the computational Conductor-like Screening Model for Real Solvents (COSMO-RS) the

authors achieved good predictions of the experimental solubilities. This is also a powerful tool to screen several LTTM systems in regard to their solvation potential for certain drugs [151].

Despite few, the studies herein summarized are an important contribution to the state-of-the-art of therapeutic LTTMs, such as THEDES, as they made a very complete and comprehensive study of drug-LTTM combinations, being a starting point in terms of fundamentals, methods, and predictive tolls while representing the promising character of LTTMs to enhance OA-drugs bioavailability. However, few LTTM-drug combinations were studied, most of which based on choline chloride, that may be toxic systemically [153,154] as well as the betaine:glycerol DES [155]. Still, there is *'Plenty of room at the bottom'* (Richard P. Feynman), since there are more than $10^6$ possible LTTM combinations, whose progressive knowledge at a molecular and atomic level, will exponentially increase their potential and applicability, especially at the level of targeted design for certain applications, such as the improvement of drugs bioavailability for osteoarthritis therapy, further explored in chapter 2.

## 1.6 Formulation of LTTM–polymer products applied to pharma

*…combination brings innovation*

Within all the reported studies involving LTTMs, nearly 7% correspond to the use of LTTMs in polymeric applications [144]. The investigation on this field largely increased in the last decade (Figure 1.8 a), including solubilization, extraction, synthesis, or modification of polymers. More information on these topics is available in a comprehensive review on the literature developments regarding LTTMs applied to polymer science and engineering [156]. It comprises fundamental studies involving LTTMs and polymers, recent applications of LTTMs in polymer synthesis, extraction and modification, and the early developments on the formulation of LTTM–polymer products, the most important topic in the context of this thesis, and therefore, presented below. Despite being comparatively recent in the timeline of research connecting LTTMs and polymers, it already has a significant incidence in respect to the other areas reported, as represented in Figure 1.8b.

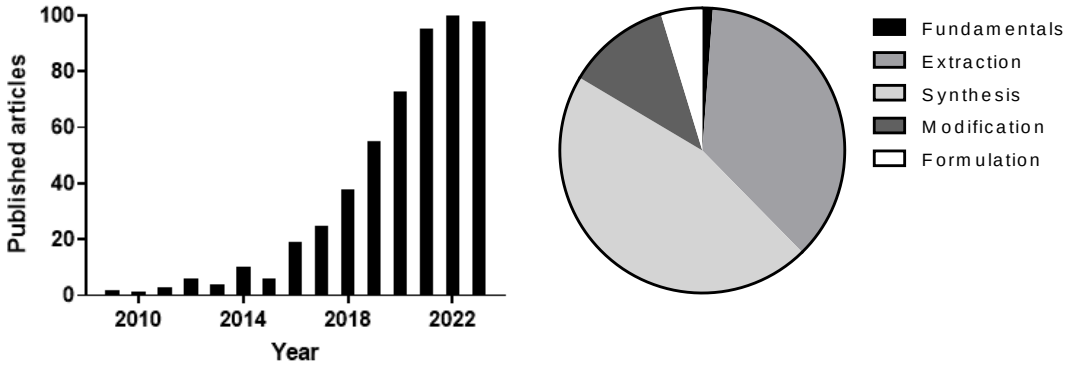


a) b)

**Figure 1.8** – a) Number of published articles per year on LTTMs and polymers: data from Web of Science (((ALL=(deep+eutectic+solvents)) OR ALL=(deep+eutectic+systems)) OR ALL=(Low+Transition+Temperature+Mixtures)) AND ALL=(polymer), accessed on 09 Jan 2024 [144]. b) Graphical representation of the relative incidence of the subareas explored within LTTM–polymer field [156].

Herein, the developments considered relevant for the formulation of LTTM–polymer products in the pharmaceutical field, especially for drug delivery, are summarized.

The developments presented in the literature, based on the combination of drugs, LTTMs and polymers, range a wide variety of applications, testing different active pharmaceutical ingredients and polymers. For instance, Mano et al. were the first reporting the encapsulation of THEDES (ChCl:mandelic acid 1:2 molar) in polymeric gelatin fibers by electrospinning, achieving a fast-dissolving delivery system [10]. A distinct approach was presented by Aroso et al., who developed polymeric delivery systems by impregnating THEDES of menthol:ibuprofen (3:1 molar) in a starch:poly-ε-caprolactone polymer blend. The produced 3D structures had larger porous and faster ibuprofen release than the polymeric matrix produced with ibuprofen powder [148]. A different study on polymeric delivery of DES was published by Silva et al. They designed a fatty acid antibacterial DES melting at physiologic temperature, thus allowing an efficient and stable load into a commercial polymeric gauze at that temperature, and easy diffusion from the gauze upon contact with body temperature. The tailored DES (lauric acid:myristic acid 1:1 molar) was efficiently loaded into the gauze through supercritical dispersion, and showed highly promising results for wound healing applications [11].

Further LTTM–polymeric products integrating LTTM as the main constituent can also be developed, as reported by Qin et al., who developed an LTTM gel supported with gelatin biopolymer for ionic skin applications. The gel produced from ChCl:ethylene glycol 1:2, with 22% gelatin presented a higher stretchability and toughness than the gels formed from the isolated

compounds (ChCl or ethylene glycol). The LTTM-based gels showed to be an advantageous nonvolatile alternative to common hydrogels for long-term performance in ionic skin devices [14], thus opening a new platform for the development of nonvolatile sensors based on LTTM materials. Moreover, the incorporation of pressure and strain sensors into the flexible ionic conductive LTTM gel allowed accurate monitoring of human finger bending and multitouch stimuli, potentially promising for healthcare devices with human skin-like sensory capabilities.

### 1.6.1 LTTM-polymeric gels for drug delivery

*…a route towards controlled delivery*

The combination of LTTMs and polymers can also be applied to develop formulations able to influence drug properties and mediate their delivery. The first authors to describe the use of polymeric eutectic systems for controlled delivery of active ingredients were Tuntarawongsa and Phaechamud [7,157]. They used a mixture of two therapeutic compounds—menthol and camphor—to form a therapeutic DES and designed two different delivery systems. The addition of eudragit® polymers to the eutectic liquid up to 40% w/w, increased its viscosity, allowing to form a gel product with potential for topic application, using as an advantage the menthol ability to increase skin penetration [157]. Moreover, an injectable formulation was developed: the same DES system incorporating 30% w/w of eudragit® was used for the solubilization and delivery of an additional active ingredient, ibuprofen. The hydrophobic properties of the DES prolonged the time of drug delivery in comparison to a pharmaceutical solvent commonly used for drug solubilization. Additionally, the viscosity enhancement conferred by polymer addition contributed to even higher delivery retardation [7]. The versatility of these polymeric eutectic systems has a high potential to design delivery systems with tailored sustained drug release.

In 2018, Liu et al. reported the use of mannose-dimethylurea-water 2:5:5 (molar) as a loading system for lipophilic (curcumin) molecules into a hydrophilic chitosan:alginate hydrogel. The amphiphilic nature of the produced LTTM could efficiently entrap curcumin in its hydrophobic core while being easily incorporated in the hydrogel due to the hydrophilic surrounding. Moreover, the external hydrophilic character of the LTTM promoted its spontaneous diffusion to the water phase during washing, maintaining the curcumin encapsulated in the hydrogel. The authors confirmed a similar behavior for a *Schisandra chinensis* fruit extract regarding the transfer of lipophilic molecules to the hydrogel. That extract was used as representative model of naturally existing LTTM-biopolymer matrices, which supports the prediction

that nature has such unique delivery systems, as a mechanism to improve the bioavailability of lipophilic metabolites [8].

In 2022, Xiao and colleagues reported their work on the use of LTTMs (arginine or lysine with citric acid 3:1 molar) as media for extraction of a Chinese herb medicine used for rheumatoid arthritis (RA). The LTTM-extract was then mixed with carbomer to form a hydrogel-delivery system for the medicinal extract. Based on their results on a collagen-induced arthritis rat model, they claim to have positive results on the local treatment of RA, through transdermic delivery [158]. In the same year, Pedro and co-authors contributed towards the transdermal administration of NSAIDs using an LTTM-polymer based product. The authors developed an alginate-based hydrogel incorporating an LTTM of arginine:glycerol (1:4 molar), able to improve the water solubility of ibuprofen up to 7917-fold. The combination between hydrogel and LTTM allowed to reach an 8.5-fold increase of ibuprofen's permeation across human skin, as opposed to the hydrogel without LTTM [159].

LTTM-based hydrogels impregnated with silica nanoparticles were also described by Li et al. for the topical delivery of encapsulated methotrexate, an immune-suppressor for rheumatoid arthritis. The strong affinity of the citric acid:arginine:$H_2O$ 1:3:16 (molar) LTTM to the skin, allowed a high and sustained penetration of the nanoparticle-matrix into the skin [160].

A last example, reported in 2023 by Panbachi and colleagues further emphasizes the power of polymer-embedded LTTM to mediate drug delivery. By incorporating indomethacin, a NSAID, in an LTTM of L-carnitine:ethylene glycol (1:4, molar ratio) with 15% w/w of polyvinyl pyrrolidone K30 (PVP), not only drug precipitation was inhibited, but also indomethacin's solubility was increased and its delivery sustained for a longer period than the LTTM without polymer [161].

Overall, LTTMs have shown several functionalities and advantages when combined with polymers. Particularly, the drug delivery from LTTM-polymeric matrices showed to be highly promising and especially relevant for the context of this thesis. Up to date, few polymeric-LTTM products for arthritis were reported. Still, the formulation of LTTM-polymer products is a growing field, with plenty of unexplored potential.

In chapter 3, the production of gels incorporating biopolymers, an LTTM and a NSAID for OA-joints administration, was explored and a product further selected for *in vivo* testing, reported in chapter 4.

## 1.7 Aims of the thesis

Osteoarthritis is a major social and economic burden globally, making it crucial to invest on the development of more effective treatments, which is the focus of this thesis. This work program aimed to develop an alternative osteoarthritis treatment by pursuing an integrational approach that takes advantage of the combined competences of LTTMs, biopolymers and drugs. The principal objectives of the project and respective approaches were:

1. **Produce LTTMs of interest.** 1st. Design different combinations of molecules of interest, such as sugars, polyols, organic acids, amino acids and other primary metabolites and therapeutic agents, namely cartilage constituents, vitamins and/or anti-inflammatory agents, considering their number of hydrogen bond donors (HBD) and acceptors (HBA); 2nd. Screen the viability of producing liquid systems (LTTMs) from the designed mixtures; 3rd. Characterize the stable LTTMs produced (e.g: physicochemical properties, bioactivity *in vitro*). This step allows to validate LTTMs with the required features for the purposed application;
2. **Obtain NSAID-LTTM combinations that enhance drug bioavailability.** 1st. Assess the solubility and thus, bioavailability of NSAIDs in physiological media upon incorporation in LTTM. 2nd. Select the promising combinations for further development.
3. **Produce and validate LTTM-biopolymer-drug mixture for intra-articular injection.** 1st. Test the compatibility of selected biopolymers, particularly natural components of synovial joints (e.g: glucosamine sulphate, hyaluronic acid) in the selected LTTM with and without drug; 2nd. Characterize rheological properties (injectability, temperature stability, viscoelasticity and adaptability to weight-bearing behavior), biocompatibility *in vitro*, chemical stability and influence on the *in vitro* drug release. 3rd. Select stable and injectable formulations with properties validated towards osteoarthritis treatment.
4. ***In vivo* performance.** Evaluate the effect of the produced LTTM-biopolymer-drug injectable in an animal model of osteoarthritis.

In a holistic perspective, the final goal was to obtain an intra-articular injectable product with innovative properties towards localized OA therapy, including: a biocompatible LTTM-biopolymeric-NSAID composition, with viscoelastic properties able to protect and lubricate the joints while delivering a NSAID with enhanced bioavailability and thus, improved therapeutic potential.

# 2

# THERAPEUTIC LIQUID FORMULATIONS BASED ON LOW TRANSITION TEMPERATURE MIXTURES FOR THE INCORPORATION OF ANTI-INFLAMMATORY DRUGS

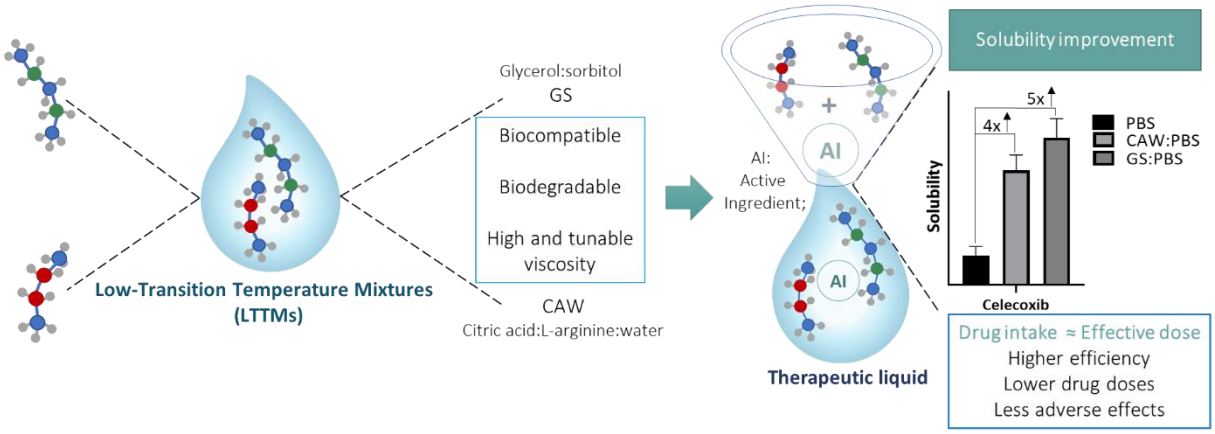

This chapter was adapted from the author's manuscripts:

Ana Roda, Alexandre Paiva and Ana Rita C. Duarte. Therapeutic Liquid Formulations Based on Low Transition Temperature Mixtures for the Incorporation of Anti-Inflammatory Drugs, Pharmaceutics. 2021, 13, 1620. doi: 10.3390/pharmaceutics13101620

Ana Roda, Filipa Santos, Yeong Zen Chua, Aarti Kumar, Hoang Tam Do, Alexandre Paiva, Ana Rita C. Duarte and Christoph Held. Unravelling the nature of citric acid:L-arginine:water mixtures: The bifunctional role of water, Physical Chemistry Chemical Physics. 2021, 23, 1706. doi:10.1039/D0CP04992A. In the context of this thesis, only the physicochemical characterization of citric acid:L-arginine:water was used, namely the results from spectroscopic analysis by NMR and FTIR.

The author was involved in the conceptualization and design of all the developed research and performed all the experimental work herein presented as well as data processing, interpretation, and full preparation of the original manuscripts; except the cytotoxicity analysis of CAW (non-published data) which was kindly provided by Filipa Santos.

## 2.1 Abstract

Most nonsteroidal anti-inflammatory drugs (NSAIDs) present poor aqueous solubility, impairing their efficiency in physiological media. In this context, Low Transition Temperature Mixtures (LTTMs) are a promising platform to overcome drugs' poor solubility, forming therapeutic liquid formulations. In this chapter, the LTTMs of citric acid:L-arginine:water (CAW) and glycerol:sorbitol (GS) were studied. The physicochemical properties of LTTMs were characterized by state-of-art techniques commonly used for these systems, namely differential scanning calorimetry (DSC), nuclear magnetic resonance (NMR) and Fourier transform infrared (FTIR). The cytotoxicity of GS was also evaluated in L929 mouse fibroblasts, and compared to the one of CAW, previously reported. The LTTMs were further assessed in terms of their ability to increase the solubility of 6 NSAIDs in physiological media. The viscosity, polarity and pH properties of the studied mixtures were related to the solubility of NSAIDs. pH and polarity were the parameters that most influenced the drugs solubility. Ibuprofen, naproxen, ketoprofen, indomethacin and flurbiprofen did not present any solubility improvement in the formulations tested. However, concentrated mixtures of CAW or GS in the physiologic-mimicked media (PBS) rendered a celecoxib solubility 4 and 5-times higher than PBS, respectively. These therapeutic liquid formulations of celecoxib in CAW or GS can be a promising tool to increase celecoxib's therapeutic efficiency in local applications.

**Keywords:** Low Transition Temperature Mixtures, nonsteroidal anti-inflammatory drugs, therapeutic liquid formulations, solubility, celecoxib

## 2.2 Introduction

Nonsteroidal anti-inflammatory drugs (NSAIDs) are anti-inflammatory, antipyretic and analgesic medicines commonly used worldwide for the symptomatic relief of headaches, strains, sprains, viral infections as the flu or corona, arthritis and other cases of pain, fever and/or inflammation [162]. Despite being regarded as generally safe, most NSAIDs require the intake of higher amounts than the therapeutic dose due to their general low solubility in the physiological media [163]. Further, these drugs are associated to gastrointestinal, cardiovascular and other adverse effects potentiated by high doses and prolonged consumption [162]. In the case of chronic diseases like osteoarthritis, this is specially concerning as this is the most administered treatment for the persistent symptoms of pain and inflammation [22,25,164]. In this

context, biocompatible formulations that improve the efficiency and safety of marketed drugs are of great importance.

Recently, the platform of LTTMs, including deep eutectic systems (DES) and therapeutic DES (THEDES) has been presented as a promising alternative strategy for drug delivery by increasing their solubility [147,148,165–170] and/or their biological activity [170–172]. As expressed by the name, LTTMs present low temperature transitions, which are commonly liquid at room temperature [138]. Their liquefaction is solely promoted by interactions between their components, not involving any chemical reaction and rendering 100% atom economy, which complies with several green metrics. Moreover, their constituents can be chosen from non-toxic, biodegradable and biocompatible molecules, as required for pharmaceutical products [173]. Envisaging therapeutic applications, drugs can be incorporated in LTTMs, either as a starting material or by solubilization. This type of therapeutic formulations have been described as propitious to improve drugs bioavailability by facilitating their permeation, dissolution and absorption [5,147,165–169,174,175]. Formulations with increased drug solubility post-administration are highly promising as drug dosage can be minimized up to the effective amount, reaching therapeutic efficiency with lower drug intakes and reducing adverse effects.

Regarding NSAIDs, some studies already reported their improved solubility in LTTMs comparatively to aqueous media and other conventional solvents [149–152], as previously introduced in chapter 1, section 1.6, as representative of the progress on the topic. Despite the positive outputs of LTTMs in improving NSAIDs solubility, up to date, few therapeutic combinations were studied, most of which using potentially toxic LTTMs [153–155]. Therefore, different and diverse therapeutic formulations must be designed, studied and tailored for the required application(s). This was the main purpose of this chapter, in which LTTMs, mainly of glycerol:sorbitol (GS) and citric acid:L-arginine:$H_2O$ (CAW) were explored, namely in terms of their properties and influence in the solubilization of NSAIDs in physiological media.

## 2.3 Experimental section

### 2.3.1 Materials

Citric acid monohydrate (≥99.5%, ref. 131018) was purchased from PanReac AppliChem (Spain), glycerol (99.5%, ref. GL0026) and malonic acid (≥99%, ref. AC14300250) from Scharlau (Spain), sorbitol (≥ 98%, ref. S1876) from Sigma Aldrich (France), oxalic acid (98%, ref. 186432500) from Acros Organics (Belgium), D-glucosamine sulphate (98%, ref. J66271) from Alfa Aesar (USA),

D-glucosamine hydrochloride (>98%, ref. A15532) from ThermoFisher Scientific (Germany), and polyethylene glycol 600 (PEG600, ref. 807486) from Merck (Germany). L-arginine (≥98%, ref. W381918), acetylsalicylic acid (aspirin, ≥99%, ref. A5376), ibuprofen sodium salt (≥98%, ref. I1892), Reichardt's dye (90%, ref. 272442), Nile red (≥98% ref. 19123) and phosphate buffer saline (PBS, ref. P4417) tables were acquired from Sigma Aldrich (USA). PBS solution was prepared in deionized water (0.01M phosphate buffer, 0.0027 M potassium chloride, 0.137 M sodium chloride, pH 7.4, 25°C) and stored at 4°C. Dimethyl sulfoxide-$d_6$ (DMSO-$d_6$, 99,96% D, ref. D031T) was bought to Eurisotop (France). The mouse fibroblast L929 cell line was provided by the DSMZ Catalogue of Human and Animal Cell Lines (ACC2, Germany) [176]. For the cell media: Minimum Essential Medium (MEM, with 1.5 g/L sodium bicarbonate, non-essential amino-acids, L-glutamine and sodium pyruvate, ref. 10-009-CV), Fetal Bovine Serum (FBS, ref. 35-079-CV), trypsin 0.25% (ref. 25-050-CI) and antibiotic-antimycotic solution (10000 U/mL penicillin, 10 mg/mL streptomycin and 0.025 mg/mL amphotericin, ref. 30-004-CI) were obtained from Corning (USA). The 3-(4,5-dimethylthiazol-2-yl)-5-(3-carboxymethoxyphenyl)-2-(4-sulfophenyl)-2H-tetrazolium (MTS, <2%, ref. G3581) solution was purchased from Promega (USA). The NSAIDs celecoxib (≥98%, ref. PZ0008, USA), naproxen (ref. N8280, USA), ketoprofen (≥98%, ref. K1751, India), and flurbiprofen (≥98.5%, ref. F8514, India) were purchased from Sigma Aldrich whereas ibuprofen (99%, ref. B20989) was bought from AlfaAesar (Germany), and indomethacin (>98%, ref. I0655) from TCI Chemicals (Japan). The acetonitrile (ref. 412042), phosphoric acid (85-90%, ref. 79606), and potassium dihydrogen phosphate (99%, ref. 011594) used for high-performance liquid chromatography (HPLC) were provided by Carlo Erba (France), Fluka (Switzerland), and AlfaAesar (Germany), respectively. The buffers of phosphoric acid 0.2% (50:50, v/v) and potassium dihydrogen phosphate 50 mM 50:50 (v/v), pH 4.2 were prepared in deionized water.

## 2.3.2 Screening and preparation of liquid formulations

Selected components were mixed in their respective ratios and submitted to heating and stirring (Table 2.1). Mixtures for which a translucid liquid was obtained were further assessed towards stability or mechanism of liquefaction.

### 2.3.2.1 Water content determination

The water weight was controlled for the selected LTTMs. Karl-Fisher was used for GS (831 KF Coulometer with a generator electrode without diaphragm - Metrohm, Switzerland, using hydranal Coulomat AG reagent (Honeywell, USA). Briefly, a small droplet of GS was placed in

hydranal and its water content determined by coulometric titration. For CAW, its water content was measured thermogravimetrically up to 150° C, using a moisture analyzer DAB 200–2 (Kern, Germany), since it is more accurate for water amounts > 25%. All measurements were done in triplicate, and the water content presented in weight percentage, as mean ± SD.

### 2.3.3 Differential Scanning Calorimetry (DSC)

Samples were pre-equilibrated at 40°C for 5 min and further submitted to a colling (40 to -90°C, isothermal 5 min) and heating cycle (-90 to 150°C), at a rate of 10 °C/min.

For GS and respective pure components, thermal events were acquired using a DSC Q200 from TA Instruments Inc. (USA), for samples sealed in aluminum hermetic pans/lids, with a nitrogen flow rate of 50 mL/min. The respective thermal events were determined using the TA Universal Analysis 2000 (4.7.0.2) software.

For PEG600, ibuprofen and mixtures of both (Figure A.1, Appendix A), DSC analysis was performed on a Linkam DSC 600 coupled to a T96-S temperature controller (Linkam Scientific Instruments Ltd, UK). Samples were placed in quartz pans and analyzed under a nitrogen flow rate of 80 mL/min. Scans were pre-calibrated with indium at the conditions of sample analysis.

### 2.3.4 Nuclear Magnetic Resonance

Nuclear magnetic resonance (NMR) spectra were obtained on a Bruker Avance III 400 spectrometer (USA), upon homogenizing about 400 µL of each sample with 50 µL of DMSO-$d_6$. Proton NMR ($^{1}$H NMR) and 2D NOESY spectra were recorded at 400 MHz. Samples suspected to suffer from esterification (Table 2.1) were analyzed by carbon NMR ($^{13}$C NMR), recorded at 100 MHz. Chemical shifts were expressed in ppm. MestReNova software (11.0.4-18998) was used for data analysis.

### 2.3.5 Attenuated total reflection-Fourier transform infrared (ATR-FTIR)

ATR-FTIR spectra with 4 $cm^{-1}$ resolution were acquired at room temperature from 16 scans on a PerkinElmer Spectrum Two (USA) in Transmittance mode (% T) and in a wavenumber range of 400-4000 $cm^{-1}$.

### 2.3.6 Cytotoxicity

The cytotoxicity was performed in a mouse fibroblast L929 cell line, according to the ISO/EN 10993 guideline [177]. Cells were cultured in MEM media supplemented with 10% FBS and 1% of antibiotic-antimycotic solution. Cultures were maintained in a humidified incubator with 5% of $CO_2$, at 37°C. Cell metabolic activity was determined through MTS colorimetric assay, for which non-supplemented MEM was used. Cell monolayers with an initial concentration of $1x10^4$ cells/100 µL were seeded in a 96-well plate for 24 hours. The cell media was then removed and 100 µL of the different sample concentrations were added. After an incubation period of 24h, samples were removed, and the cells washed with PBS. The MTS reagent, previously diluted 62.5-fold in non-supplemented MEM media, was then added. Upon 3h of incubation, the absorbance (Abs) was measured at 490 nm in a VICTOR Nivo™ microplate reader (PerkinElmer, USA). Three independent experiments were performed for each sample, analyzed in triplicate. The percentage of cell metabolic activity was calculated as follows:

$$\text{Metabolic activity (\%)} = \frac{\text{Abs (sample)}}{\text{Abs (control)}} \times 100 \qquad (1)$$

The 50% inhibitory concentration ($IC_{50}$) was estimated using GraphPad Prism 8.0.1 software and expressed as mean ± SD.

### 2.3.7 Viscosity

The viscosity of the liquid systems was measured using a rheometer (Anton Paar MCR102, Austria) with a 50 mm stainless steel parallel plate geometry. The samples were loaded to the plate, equilibrated at the initial analysis temperature for 5 minutes, and analyzed at a constant shear stress of 20 Pa, within a temperature range between 4 and 80°C, at a rate of 10°C/min. Measurements were made in triplicate and the results expressed as mean of dynamic viscosity ± SD.

### 2.3.8 Polarity

Polarity analysis was performed using nile red and Reichardt's dye as solvatochromic probes. Stock solutions of 1 mg/mL and 5 mg/mL were prepared in methanol, for nile red and Reichardt's dyes, respectively. 10 µL of nile red or 100 µL of Reichardt's dyes were added to about 1g of CAW, GS or $H_2O$. The polarity of $H_2O$ was measured for comparison, instead of PBS, as the salts of PBS interfere with the dyes used. Their maximum wavelength ($\lambda_{max}$) was

obtained from UV spectra, and used to calculate their energy transition ($E_T$) values and establish their relative polarities according to [178,179]. $E_T$ values were expressed as the mean ± SD of three replicates.

$$E_T = \frac{28591}{\lambda_{max}} \text{ kcal/mol} \quad (2)$$

### 2.3.9 pH measurements

The pH of liquid mixtures was measured at room temperature using an analogic pH meter (914 pH/Conductometer, 2.914.0220, Metrohm, Switzerland), with a glass electrode coupled to a temperature sensor (NTC, 6.0228.010, Metrohm, Switzerland).

### 2.3.10 NSAIDs solubility

NSAIDs were added in excess to GS and CAW and stirred at 100 rpm and 37°C for 24h. Different volumes of fresh PBS were then added to the GS and CAW to achieve a final ratio of LTTM:PBS (w/w) of 2:1, 1:1 or 1:10. These mixtures were stirred at the same conditions for another 24h. The solubility of the NSAIDs in each mixture was determined by high performance liquid chromatography (HPLC). For this, the mixtures were filtered (0.22 µm PTFE hydrophilic) and stored at 4°C until further analysis by HPLC. The solubility of the NSAIDs in PBS (physiologic mimic) was also tested as control. PBS was saturated with each NSAID and stirred for 48h at 37°C, 100 rpm. Upon filtering, the solubility was determined by HPLC. Each solubility assay was performed at least in triplicate, and data represented as mean ± SD.

#### *2.3.10.1* HPLC

The NSAIDs solubility was quantified by HPLC, according to methods adapted for indomethacin [180] and for ibuprofen, naproxen, ketoprofen, flurbiprofen and celecoxib [181]. Briefly, 10 µL of indomethacin samples were analyzed in an Agilent 1100 Series HPLC (Agilent, USA) using a ZORBAX SB-Phenyl column (250 x 4.6 mm 5 µm, Agilent, USA), with isocratic elution at a flow of 1 mL/min in acetonitrile:phosphoric acid 0.2% (50:50, v/v) and detection at 237 nm in a UV-vis detector (Agilent, USA). In turn, 20 µL of celecoxib, naproxen, ketoprofen, flurbiprofen or ibuprofen samples were analyzed in a Smartline HPLC Series (Knauer, Germany), eluted in a Keystone Kromasil C18 column (250 x 4.6 mm 5 µm, Thermo Scientific, USA) with acetonitrile:potassium dihydrogen phosphate 50 mM 50:50 (v/v), pH 4.2, at an isocratic flow of 0.6 mL/min and detected at 220 nm in a Smartline 2500 UV-detector (Knauer, Germany). All analyses were performed at 25°C.

The calibration curves were prepared by dilution of the drug in eluent at the following linear ranges: indomethacin 5.2-260 mg/L; celecoxib 0.14-142 mg/L; naproxen 0.31-31 mg/L; ketoprofen 0.12-58.5 mg/L; flurbiprofen: 11.4-114 mg/L; ibuprofen 12-60 mg/L. A known concentration of drug in PBS was tested as control to assure the method feasibility. The GS and CAW mixtures were also tested in the methods used. No interference of these mixtures was observed.

### 2.3.11 Statistical analysis

Statistical analysis was performed using GraphPad Prism 8.0.1 software. Normal distribution was evaluated by Shapiro-Wilk test. The metabolic activity profiles of GS and the respective physical mixture (G+S) did not follow a normal distribution. Thus, they were compared through the non-parametric Mann Whitney test. Regarding the solubility data, it followed a normal distribution, being submitted to one-way NOVA analysis. Statistically significant differences were considered for $p \leq 0.05$.

## 2.4 Results and Discussion

### 2.4.1 Preparation of LTTMs

Several mixtures of drugs, organic acids, sugar, alcohols, and biopolymers were designed and screened in terms of their nature as LTTMs (Table 2.1). The mixtures that did not form a liquid at room temperature, were not stable, or liquified upon chemical reaction instead of physical interactions were no further characterized. This was the case for ibuprofen sodium salt:glucosamine mixtures, that suffered from Maillard reaction, a chemical reaction occurring between amines and reducing sugars, and influenced by salts [182], which was visually detected by its characteristic non-enzymatic browning. Additionally, the mixtures between PEG600 and the tested organic acids suffered chemical changes detected by $^{13}C$ NMR, most probably due to esterification reaction, as product of the chemical combination of the alcohol groups (glycol) with the organic acids (Figure A.3 and Figure A.4, Appendix A). Therefore, those mixtures were also excluded from the study. In turn, PEG600:ibuprofen was an ideal mixture (Figure A.2, Appendix A) not considered for the scope of this work since it had a $T_m$ near room temperature, which could compromise the formulation's thermal stability, even at small amplitude of temperatures (Table A.2, Appendix A).

The GS and CAW systems were selected based on their favorable properties towards osteoarthritis (OA) treatment. In the case of CAW, it contains L-arginine that has been reported as anti-inflammatory adjuvant in human osteoarthritic cells [183]. Moreover it was also reported to increase the synthesis and deposition of collagen [184], an important component of cartilage whose wear is the main cause of OA symptoms. A molar ratio of CAW 1:1:7 was chosen based on the results from previous studies with this mixture [5]. Regarding GS, its content in glycerol confer lubricant properties [185,186] while sorbitol adds viscosity, an important feature in gel formulation. To the best of our knowledge, this is the first study reporting this mixture. Four molar ratios were tested (1:2, 1:1, 2:1 and 3:1) but only the 2:1 and 3:1 formed translucid liquids at room temperature. The GS 2:1 molar ratio was chosen as it was observed to gelify overtime when resting at room temperature. To guarantee consistent initial properties of GS 2:1, these samples were equilibrated prior to use at 80°C. Given that only one molar ratio of each system (CAW 1:1:7 and GS 2:1) was herein studied, these mixtures were identified as CAW and GS throughout the text. The water content of these LTTMs was controlled during the study and confirmed to be constant for both mixtures (GS = 0.15±0.06 %, CAW = 26.24±0.51 %).

The properties of the selected LTTMs are presented in the following sections. Their physicochemical properties were first studied by DSC, NMR and FTIR, and the biological properties, namely the cytotoxicity, was evaluated. Other properties such as viscosity, polarity and pH were explored and correlated with the NSAIDs solubility to provide insights on the mechanisms that influence drugs' solubility.

**Table 2.1** - Attempts to prepare LTTMs of mixtures of interest. Selection criteria: aspirin and ibuprofen screened as analgesics, glycerol and PEG600 as lubricants [185–187], and glucosamine as natural biopolymer, precursor of cartilage. Remaining organic acids, sugar or water used as hydrogen bond donors or acceptors of the respective combination, in the attempt to promote hydrogen-bonding interactions towards liquefaction.

| Mixtures | Molar ratios | Temperature (°C) | Visual aspect at room temperature | Observations |
|---|---|---|---|---|
| Aspirin:sorbitol | 1:1, 2:1, 3:1 | ≤ 80 | White powder | - |
| Aspirin:sorbitol:$H_2O$ | 1:1:1, 2:1:1, 3:1:1, 1:1:2, 2:1:2, 3:1:2 | ≤ 80 | White powder | - |
| Ibuprofen sodium salt:sorbitol | 3:1, 1:1, 1:5, 1:6 | 70-80 | Powder in suspension | - |
| | 1:2 | 70-80 | Translucid yellow liquid | Highly viscous, not miscible with water (phase separation) Difficult to scale-up (not stable at 10 g, lab scale) |
| | 1:3,1:4 | 70-80 | Translucid yellow liquid | Unstable (crystalize) |
| Ibuprofen sodium salt:sorbitol:$H_2O$ | 3:1:1, 1:1:1, 1:3:1, 1:4:1, 1:5:1, 1:6:1, 1:2:3, 1:2:5, 1:2:10, 1:2:20 | 70-80 | Paste or precipitate | - |
| Ibuprofen sodium salt:glucosamine sulphate | 3:1 | ≤ 80 | Gradually darker mixture | Maillord reaction |
| Ibuprofen sodium salt:glucosamine hydrochloride | 3.5:1 | ≤ 80 | Gradually darker mixture | Maillord reaction |
| Ibuprofen:sorbitol:$H_2O$ | 1:2, 2:1, 3:1 | 40-60 | White powder | - |
| Ibuprofen:glucosamine sulphate | 3:1 | ≤ 80 | White powder | - |
| Ibuprofen:glucosamine hydrochloride | 3.5:1 | ≤ 80 | White powder | - |

| | | | | |
|---|---|---|---|---|
| PEG600:ibuprofen | 1:1, 3:2, 2:1, 4:1, 7:1 | 50-65 | Translucid liquid | $T_m$ near room temperature (Figure A.1, Table A.2, Appendix A) |
| | 1:2, 2:3 | 50-60 | White paste or precipitate | - |
| PEG600:glucosamine sulphate | 4:1 | ≤ 70 | Yellow paste | - |
| PEG600:glucosamine hydrochloride | 4:1 | ≤ 70 | Yellow paste | - |
| PEG600:citric acid monohydrate | 8:1, 6:1, 4:1 | 50-60 | Translucid liquid | Esterification reaction (Figure A.3, Appendix A) |
| | 2:1, 1:1, 1:2, 1:3, 1:4 | 50-60 | Translucid liquid | Esterification reaction (Figure A.3, Appendix A) |
| PEG600:malonic acid | 2:1, 1:1, 1:2, 1:3, 1:4 | 50-60 | Translucid liquid | Esterification reaction (Figure A.4, Appendix A) |
| | 1:6, 1:8 | 50-60 | Solid in suspension | - |
| PEG600:oxalic acid | 2:1, 1:1, 1:2 | 50-70 | Translucid liquid | Oxalic acid may be associated to OA progression [188,189] Possible esterification |
| Glycerol:sorbitol | 2:1, 3:1 | ≤ 80 | Translucid liquid | Gelifies along time |
| | 1:1, 1:2 | ≤ 80 | Paste | - |

### 2.4.2 Thermal characterization

DSC is often used in the characterization of LTTMs, as they are commonly defined as mixtures with low temperature transitions, either glass transition temperatures ($T_g$) and/or melting temperatures ($T_m$). The DSC results for the CAW systems, as previously reported [118], depicted a melting peak around -13°C which was attributed to the free water component of the mixture; no other $T_m$ corresponding to the ternary mixture or the pure components was observed in the conditions tested. Regarding the system GS and its pure components, the thermal events are represented in Figure 2.1. As observed, pure sorbitol showed a $T_m$ around 98°C, in accordance to other values reported in the literature for its stable form [190–192]. In turn, no melting events were possible to acquire for pure glycerol or the GS system, only their $T_g$ of -81°C and -62°C, respectively, were detected. The $T_g$ measured for glycerol was concordant with reported elsewhere [193]. Although glycerol has a $T_m$ value around 17±4°C [194], it has been described to behave as a supercooled liquid due to its high viscosity [193], which is in accordance to the lack of crystallization and subsequent melting herein observed.

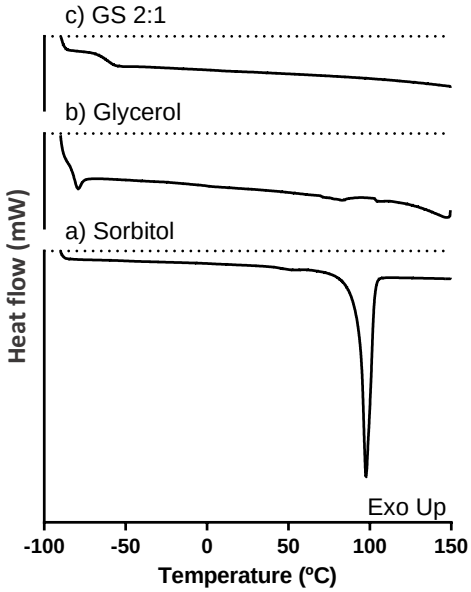


**Figure 2.1** - DSC thermogram of a) sorbitol, b) glycerol and c) GS 2:1 molar ratio.

### 2.4.3 Intermolecular interactions

The intermolecular interactions of LTTMs were here explored through spectroscopic techniques. FTIR spectroscopy is widely used for the identification of functional groups, whose

signal may shift when molecular interactions are established. Given the complex nature of CAW as a ternary mixture containing water, characterization was performed by comparison with the pure components and binary mixtures of citric acid or L-arginine with water, at the same ratio or pH of CAW. The mixtures prepared, their ratios, physical state, and pH are reported in Table A.3, Appendix A. Since the pH alone might be the reason for the solubility increase of L-arginine in water, a mixture of L-arginine:water (1:7) was prepared and acidified with HCl rather than citric acid, to identify the role of pH. It was observed that this mixture did not lead to the formation of a liquid at room temperature, neither before nor after acidification. The other way around was also evaluated: changing the pH of the binary citric acid:water 1:7 (translucid liquid at pH 0.5) to pH=3.5 using NaOH instead of L-arginine, caused the formation of a white solid paste at room temperature. These observations support that the liquid formation is not only a function of pH, but it is additionally influenced by the involving species. In this case, the mixture of L-arginine and citric acid in the presence of water seems to have unique properties in addition to pH that promote their liquefaction. One possibility could be complexation of the oppositely charged species $[H_2Cit]^-$ and $[Arg]^+$ (Figure A.5, Appendix A) in water, yielding a salt that might have higher water solubility than the non-charged precursor molecules. Hence, this hypothesis was addressed by FTIR. The functional groups of pure citric acid and L-arginine were identified, and the respective stretching and bending vibrations were assigned as summarized in Table A.5, Appendix A [195–199] and Table A.6, Appendix A [195,200–202]. The most important changes in the vibrations of the binary mixtures or CAW compared to the pure components are represented in the spectra of Figure 2.2, right. Furthermore, the chemical structure of the pure components and their variation with pH is represented in Figure A.6, Appendix A). In the spectra of all aqueous mixtures under investigation, the water contribution can be identified by the broadening of the band regions between 3000-3500, 1500-1800 and 500-900 $cm^{-1}$. Additionally, it is possible to identify the peaks of L-arginine and citric acid. In the L-arginine powder form, two sharp peaks corresponding to the guanidine and primary amine groups can be distinguished at 3302 $cm^{-1}$ and 3357 $cm^{-1}$, respectively. When water is added (L-arginine:water 1:7, Figure 2.2 right, b), a broader peak is observed for the guanidine amines due to their transition to the delocalized charge state. At pH 3.5 (Figure 2.2 right, c), the primary amine is also charged causing the amine peaks to overlap around 3323 $cm^{-1}$. Additionally, the O-H stretching of L-arginine in its pure form (3057 $cm^{-1}$, Figure 2.2 right, a) shifts to higher frequencies due to the establishment of hydrogen bonding interactions with the surrounding media (Figure 2.2 right, b-d). Regarding citric acid, the most important vibrations are from the O-H and C=O stretching of the carboxylic groups, centered at 3297 and 1719 $cm^{-}$

[1], respectively. When mixed with water at pH 3.5, the O-H vibrations are broadened and shifted, and the maximum is at 3340 $cm^{-1}$.

Comparing the citric acid:water and L-arginine:water mixtures at pH=3.5 with the ternary CAW, it is possible to observe a combined contribution of the same O-H and N-H stretching peaks (Figure 2.2 right, c-e). If the liquefaction of CAW was promoted by the ionic complexation of $[H_2Cit]^-$ and $[Arg]^+$, the dipole moments of those functional groups would be changed. However, different vibrations in the FTIR spectra were not observed, refuting the salt formation hypothesis. To sum up, the liquid is neither a case of salt formation nor exclusively induced by the acidic pH value. Thus, other L-arginine:citric acid interactions mediated by water must be the reason for the deep melting point depression of the ternary system, probably H-bonding interactions. This was further explored by NMR analysis.

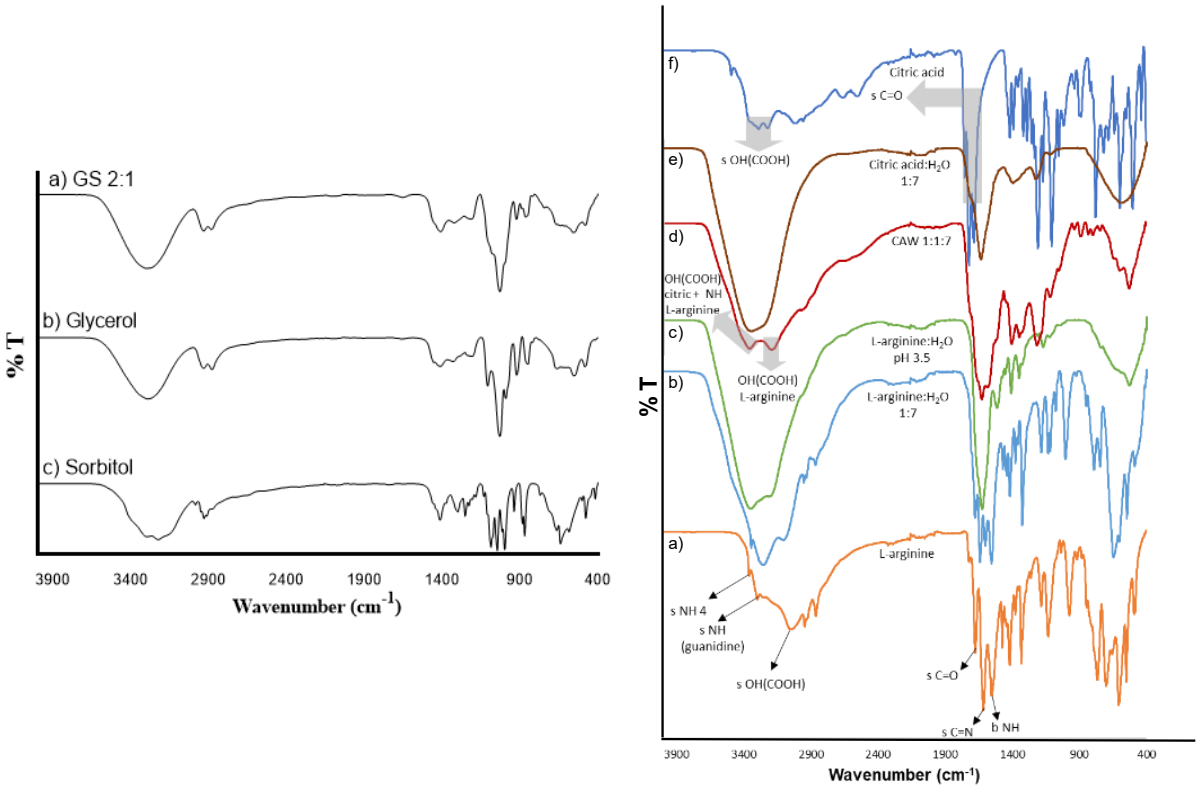


**Figure 2.2** - FTIR spectra of LTTMs and components. Left: a) pure sorbitol; b) pure glycerol and c) GS 2:1 molar ratio. Right: a) pure L-arginine; b) L-arginine:$H_2O$ 1:7 mol; c) L-arginine:$H_2O$ pH=3.5; d) citric acid:L-arginine: $H_2O$ 1:1:7 mol; e) citric acid: $H_2O$ 1:7 mol; f) pure citric acid. "s" and "b" refer to stretching and bending vibrations, respectively. Numbers attributed according to the chemical structures from Figure A.6, Appendix A.

Regarding GS, the spectra of the pure components and their mixture is presented in Figure 2.2, left. The bands between 3000 and 3500 $cm^{-1}$ correspond to O-H stretching, while the C-H stretching is comprehended between 2800 and 3000 $cm^{-1}$. Further, O-H bending vibrations can

be identified at 1411-1415 $cm^{-1}$, and C-OH stretching vibrations within 950 to 1150 $cm^{-1}$. These spectra and respective assignments [195] are concordant to others previously reported for glycerol [194,203,204] and sorbitol [191,194,205,206]. Given that glycerol and sorbitol are composed by the same functional groups (hydroxyls and alkyls), their pure spectra have overlapping bands (Figure 2.2 left, a and b). Thus, the GS spectra (Figure 2.2 left, c) has a combined profile of both molecules, predominantly glycerol since it is the main component. This confirmed that neither glycerol or sorbitol suffered chemical changes upon mixing and heating. Furthermore, the FTIR spectra do not evidence a hydrogen-network-change since no band shifts are observed for the GS systems with respect to the pure molecules. This probably occurs because the new hydrogen interactions between glycerol and sorbitol did not significantly alter the strength and dipolar moment of the pool of interactions, and thus, their vibration frequency did not change.

In addition to FTIR, NMR spectroscopy was performed for the identification of hydrogen-bonding interactions between the components of the LTTMs, the predominant type of interactions responsible for their formation.

Since CAW is a ternary mixture, it was compared with pure citric acid, L-arginine and with aqueous solutions of those compounds, in the same ratio or at the same pH (around 3.5) of CAW (Table A.3, Appendix A). Only citric acid:water 1:7 and the pure components solutions at pH=3.5 rendered liquid mixtures and therefore, only those were compared with CAW (Figure 2.3, right). For the mixture L-arginine:water at pH=3.5, it was possible to identify the protons from water and most of the protons of the L-arginine's amine and alkyl groups (Figure 2.3 right, d). In turn, for the citric acid:water 1:7 or pH=3.5, it was only possible to detect the alkyl groups and a contribution of the hydroxyl protons' overlapped with the protons from water. This influence of the hydroxyl group was attributed to the downfield shift of the concentrated solution of citric acid (1:7 molar) (Figure 2.3 right, b) in comparison to its diluted solution at pH 3.5 (Figure 2.3 right, a). Interestingly, the same peak of citric acid:water 1:7 appears for the ternary mixture 1:1:7 (Figure 2.3 right, c), but broader. This broadening-effect observed for the CAW in comparison to the binary solutions, might be related to its high viscosity. According to Stokes-Einstein-Debye law, high viscosity mixtures lead to slower rotational molecular diffusion [207–210] and longer T2 relaxation times [211,212]. These translate into broader NMR peaks, as previously reported for viscous LTTM mixtures [213].

Given that the only difference from the samples of Figure 2.3 right, b and c was the addition of L-arginine, the appearance of a new peak is most probably caused by hydrogen-bonding interactions with the L-arginine molecules, in addition to the ones between citric acid and

water. Moreover, in the NOESY spectra for CAW there are cross peaks between the protons from the citric acid alkyl groups and the protons of L-arginine chemical groups (Figure A.7, Appendix A) that may indicate spatial correlation. This supports that in addition to the expected interactions between $H_2O$-$H_2O$, citric acid-$H_2O$, citric acid-citric acid, L-arginine-$H_2O$ and L-arginine-L-arginine, further citric acid-L-arginine and/or mutual interactions between the three components might occur. Given that the cross peaks are in the same phase as the diagonal peaks (positive, red peaks), this might also be a case of spin diffusion due to the high viscosity. Still, since viscosity is a direct cause of mixing the three components, it is highly probable that they are spatially close and interacting. Combined with the evidence from $^1$H NMR analysis that there is a change in the hydrogen bonding network for CAW in comparison to the independent water solutions of citric acid or L-arginine, these findings might be compliable with the formation of a supramolecular network, which is characteristic of DES. In sum, it is noticeable that the interactions between the water molecules and the functional groups of citric acid and L-arginine, namely, amine, carboxyl and hydroxyl groups may play a major role in establishing those interactions.

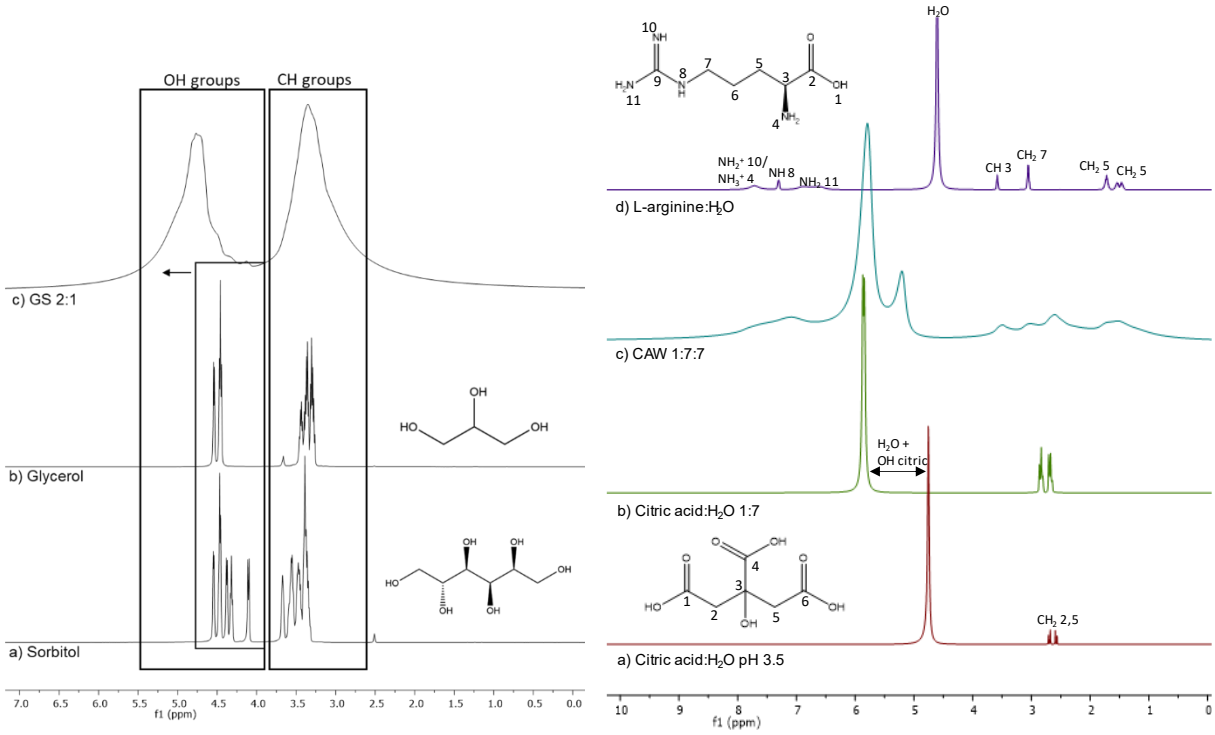


**Figure 2.3** - H[1] NMR spectra of LTTMs and components. Left a) sorbitol, b) glycerol and c) GS 2:1 molar ratio. Right: a) citric acid:$H_2O$ pH=3.5; b) citric acid:$H_2O$ 1:7; c) citric acid:L-arginine:$H_2O$ 1:1:7; d) L-arginine:$H_2O$ pH=3.5. The functional groups of the protons detected were identified and numbers attributed according to the respective chemical structures (see species distribution in Figure A.6, Appendix A).

Regarding GS and pure components, their $H^1$ NMR spectra were compared. The proton peaks corresponding to the hydroxyl and alkyl groups of glycerol, sorbitol and their mixture (GS) were identified and are presented in Figure 2.3. Since the pure components have similar functional groups, their representative peaks are overlapped (Figure 2.3 b and c). In the GS mixture (Figure 2.3 a), this translates into two broad peaks comprehending the groups of the pure components. Even though the alkyl peak of the mixture is aligned with the ones from the pure components, the hydroxyl band of GS shifted downfield in respect to the same groups of the individual compounds. This shift is an indicator of hydrogen-interactions established between the hydroxyl groups of glycerol and sorbitol.

To further address the interactions-network that allowed to form the LTTMs herein studied, dynamic molecular studies would have to be conducted. Additionally, magic-angle spinning (MAS) NMR has recently been described as a good technique to overcome some of the conventional NMR limitations in the characterization of viscous mixtures, like LTTMs [213]. This MAS NMR technique also allows to analyze and compare both liquid and solid mixtures, which, in the field of LTTMs, might be highly useful in understanding those interactions between the involved molecules that are responsible for the mixture liquefaction.

### 2.4.4 Cytotoxicity evaluation

The LTTMs cytotoxicity was assessed in an L929 cell line, as a model of normal cells, according to ISO 10993 [177].

**Table 2.2** - $IC_{50}$ determined for glycerol, sorbitol, GS 2:1, G+S 2:1, citric acid, L-arginine and CAW 1:1:7 (molar ratio), represented in mean ± SD.

| Sample | $IC_{50}$ (g/mL) |
|---|---|
| Glycerol | 0.2583 ± 0.0225 |
| Sorbitol | 0.0751 ± 0.0064 |
| GS 2:1 | 0.1564 ± 0.0113 |
| G+S 2:1 | 0.1656 ± 0.0154 |
| Citric acid | 0.0013 ± 0.0006 |
| L-arginine | 0.0176 ± 0.0011 |
| CAW 1:1:7 | 0.0044 ± 0.0002 |

As it is possible to observe in Table 2.2, the pure glycerol and sorbitol presented a higher $IC_{50}$ than citric acid and L-arginine. In terms of the respective mixtures, this translated into an $IC_{50}$ for CAW about 35-fold lower than the one of GS. The values obtained for the CAW and respective components are in the same order of magnitude previously reported in a Caco-2

cell line [5], which supports a consistent *in vitro* effect. The low $IC_{50}$ of CAW indicates *in vitro* cytotoxicity at low concentrations, which could limit its use, even though its translation to *in vivo* is not straightforward, Regarding the glycerol and sorbitol components and respective mixtures, the lowest $IC_{50}$ was obtained for sorbitol which may be attributed to osmotic stress induced in cells [214]. Additionally, for GS and the physical mixture G+S, maximum cell metabolic activity was observed up to a concentration of 0.075 g/mL (Figure 2.4). Thus, its metabolic activity profile was further analyzed.

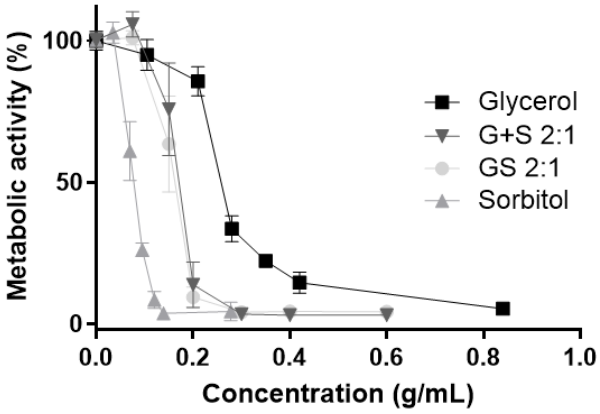


**Figure 2.4** - Cell metabolic activity (%) for different concentrations of glycerol, sorbitol, GS 2:1 and G+S 2:1. No significant differences between the metabolic activity profiles of GS and G+S (p-value > 0.8).

As previously reported, supramolecular complexes may have different results in regards to respective non-interacting pure components [153,154,170]. Hence, given the possibility of the GS system to have a supramolecular network, characteristic of some LTTMs, like DES, it is important to compare the system with the physical mixture of the individual components at the same proportion (G+S). Since upon dilution, both GS and the respective physical mixture G+S have equivalent influence in the cell metabolic activity (Figure 2.4), it can be postulated that if GS has a supramolecular complex organization, it is disrupted after aqueous dilution in the range of concentrations herein tested. Despite some DES can incorporate water up to certain amounts, it is commonly reported that above certain quantity, water dissolves the pure components, disrupting their supramolecular network [134,135,215], which might be the case and explain the observed results. Thus, despite the GS dilutions studied in the cytotoxicity assay are probably aqueous solutions, no further conclusions are possible to obtain in regard to the network arrangement of higher concentrations or non-diluted form of GS.

According to ISO 10993-5 [177], metabolic activities > 70% are considered non-cytotoxic. Thus, the results herein acquired support that *in vitro*, the GS system can be considered non-

cytotoxic for concentrations < 0.15 g/mL, which *in vivo* will depend on the type of administration and pharmacokinetics.

### 2.4.5 Viscosity assessment

The viscosity is a parameter known to highly influence the dissolution rate of a solute in a solvent. Therefore, the characterization of this parameter in new liquid systems is highly important for their choice as a delivery vehicle and suitable application. The dynamic viscosity of CAW and GS was studied as a function of temperature and the results are represented in Figure 2.5. While handling the GS system, it was observed that its viscosity depends on time and temperature. This suggests a reversible physical rearrangement of the structure, which is consistent with the observation of its gelification over time at low temperatures (<40 °C). However, at 80°C the influence of these factors is no longer observed, guaranteeing consistent initial properties. Thus, the viscosity profile of GS was performed from 80 to 4°C to ensure reproducibility. In turn, for CAW it was performed from 4 to 80°C, to avoid the influence of water evaporation.

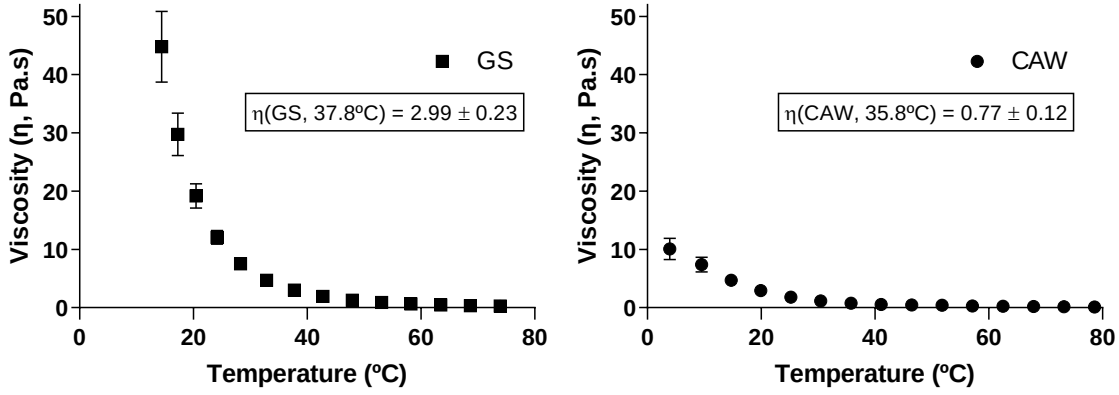


**Figure 2.5** - Dynamic viscosity for: a) GS from 80 to 4°C; b) CAW from 4 to 80°C.

As it is possible to observe, the viscosity decreases as the temperature increases, for both systems. Moreover, it can be observed that the GS (Figure 2.5 a) has a higher viscosity than CAW (Figure 2.5 b). At values close to the physiologic temperature, GS presented a viscosity value around 2.99 Pa.s (37.8°C), which is 3.9-times higher than the one of CAW (0.77 Pa.s, 35.8°C). Since the dissolution rate is slower for higher viscosities [216], this translates in diffusion rates slower for GS in comparison to CAW. Therefore, the use of CAW as delivery system would probably be more adequate for applications that require rapid dissolution rates, while GS may be more advantageous for sustained release applications.

### 2.4.6 Solubility insight

The goal of the present study was to evaluate if GS and CAW could be used as therapeutic liquid mixtures by carrying different NSAIDs and improving their solubility in respect to PBS. For this, the solubility of the drugs was determined in concentrated GS and CAW media, with a ratio of 2:1 (w/w) GS:PBS and CAW:PBS. This ratio was set to mimic formulations for localized administration (e.g.: intra-articular injection) and to screen whether the GS and CAW systems have potential to increase the NSAIDs solubility in physiological media. The results obtained for the 6 NSAIDs tested are summarized in Figure 2.6.

Reported solubility values for the different NSAIDs vary in some cases to a great extent. Nonetheless, according to our experiments, the solubility obtained for ibuprofen in PBS is lower than those reported in the literature (2000 to 7300 mg/L) [217–220]; for indomethacin the value obtained is concordant with Ivanova et al. (1150-3170 mg/L) [221] but much higher than the indicated by Cayman (50 mg/L) [222]; ketoprofen's solubility in PBS is within the range reported by Cayman (500 mg/L) [223] and Shohin et al. (3310 mg/L) [224] but lower than the one of Felton et al. [219]; for flurbiprofen, the determined PBS solubility is in accordance with Sadik et al. (130±40 mg/L) [225] and Daravath et al. (98±10 mg/L) [226], despite the heterogeneity of values reported (98 to 9000 mg/L) [219,225–228]; the value obtained for naproxen is in agreement with Cayman (1000 mg/L) and Kumar et al. (750±250) mg/L, being lower than the Felton and co-authors' value (4259 mg/L); in turn, celecoxib presented a PBS solubility equivalent to Abu-Diakes et al. (1.58±0.03 mg/L) but lower than Rawat and co-workers (47.15 mg/L).

While the experimental values of the NSAIDs solubility in PBS herein determined are in accordance with part of the literature, there are also visible discrepancies within the values reported. These differences might be due to several factors, such as drugs particle size, polymorphism, purity, precision of the quantification method, time and temperature of the assay and storage, phosphate concentration of the buffer, among others.

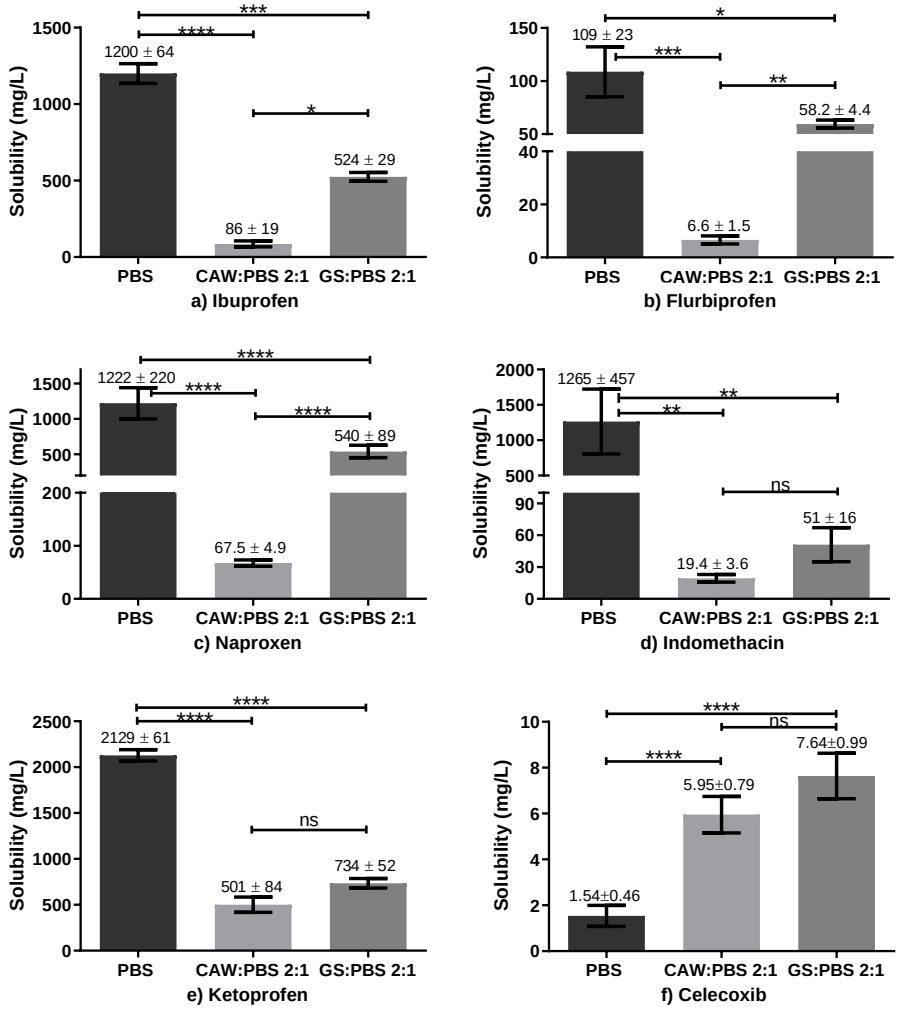


**Figure 2.6** - Solubility of NSAIDs in PBS, CAW:PBS 2:1 and GS:PBS 2:1 (w/w).****$p < 0.0001$; ***$p \leq 0.0007$; **$p \leq 0.01$; *$p \leq 0.03$; $^{ns}p > 0.1$.

Regarding the comparison of drugs solubility in the studied media, all NSAIDs presented a higher solubility in PBS than in the 2:1 GS:PBS or CAW:PBS, except for celecoxib. For those NSAIDs, the CAW seems to strongly act as antisolvent. On the contrary, the CAW:PBS 2:1 and particularly, the GS:PBS 2:1 increased the celecoxib solubility by 4-fold and 5-fold, respectively. To better understand these observations, polarity and pH measurements were carried out.

The polarity is one of the parameters considered when evaluating the capacity of a solvent to dissolve a solute, through the principle 'like dissolves like'. Thus, the polarity of GS and CAW was estimated and compared to water as standard solvent and equivalent of PBS. This was carried out using two solvatochromic probes whose absorption spectra shifts depending on the polarity of the solvent. The nile red dye was used as it is more appropriate for apolar solvents while the Reichardt's dye is better for polar solvents. According to the energy transition values ($E_T$) calculated from equation (2), it was possible to establish the relative polarity of the studied systems. Since water is extremely polar, it was only analyzed by the Reichardt's dye. Moreover, for the CAW only the nile red was suitable because the Reichardt's dye reacts with the carboxylic acid groups from citric acid and L-arginine [229,230]. The results obtained are summarized in Figure 2.7.

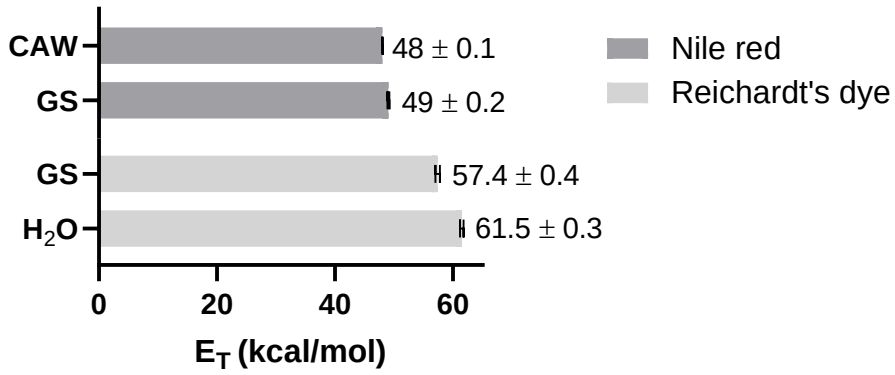


**Figure 2.7** - $E_T$ values obtained for CAW, GS and $H_2O$ using nile red and/or Reichardt's dye.

From the nile red analysis it can be stated that CAW is slightly more polar than GS whereas the Reichardt's dye data indicate that $H_2O$ is more polar than GS. Therefore, their relative polarity can be ordered from the highest to the lowest as follows: $H_2O$ > CAW > GS. Upon dilution in physiological media, their relative polarity will vary accordingly.

The pH is also an important parameter when evaluating the solubility of certain compounds because it influences their structure according to the pKa of the functional groups, which can dictate a higher or lower solubility. Therefore, the pH of PBS and the several ratios between GS:PBS and CAW:PBS tested in the solubility assay are summarized in Table 2.3. As observed, both PBS and GS:PBS mixtures present a neutral pH while the CAW:PBS systems have an acidic pH.

**Table 2.3** - pH values for PBS and mixtures of CAW:PBS and GS:PBS at different ratios (w/w).

| Media | pH |
|---|---|
| PBS | 7.4 |
| CAW:PBS 2:1 | 3.5 |
| GS:PBS 2:1 | 7.1 |
| CAW:PBS 1:1 | 3.5 |
| GS:PBS 1:1 | 7.2 |
| CAW:PBS 1:10 | 3.6 |
| GS:PBS 1:10 | 7.3 |

In terms of polarity, celecoxib had higher solubility in the less polar solvent (GS:PBS) while the other NSAIDs presented the highest solubility in the more polar solvent. This might be explained by their differences in terms of chemical composition (Figure 2.8).

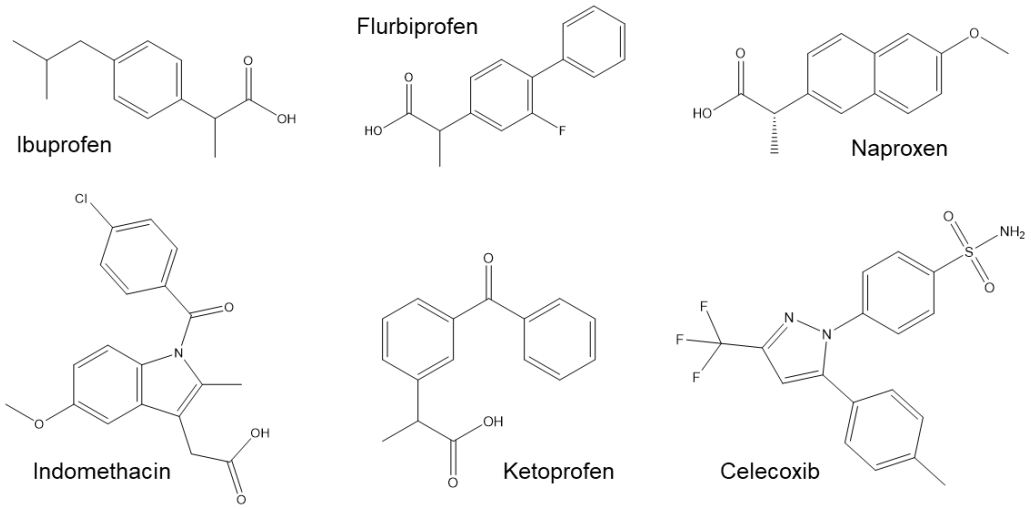


**Figure 2.8** - Chemical structure of ibuprofen, flurbiprofen, naproxen, indomethacin, ketoprofen and celecoxib.

Although celecoxib has some polar groups such as the fluorines, it has also 3 non-polar rings and thus the final polarity balance might be closer to the one of GS:PBS. In turn, a common feature between ibuprofen, indomethacin, ketoprofen, flurbiprofen and naproxen is their carboxylic acid group, which is not present in celecoxib. This functional group contributes to their higher polarity and clarifies the deep decrease in solubility observed for the CAW:PBS media, which is related to its pH. The pKa of the NSAIDs' carboxylic acids varies within 3.9 to 5.3 [231–233]. Therefore, at the acidic pH of CAW:PBS media (3.5), the COOH is mostly protonated (Figure A.6, Appendix A), decreasing the solubility of those drugs in the mixture. On the contrary, at the neutral pH of PBS and GS:PBS, the COOH group is deprotonated, increasing the drugs solubility in those media. Another interesting feature for this group of drugs is that,

while all of them present a mean solubility higher for GS:PBS than CAW:PBS, the difference was not statistically significant for indomethacin and ketoprofen. This is probably caused by their additional polar groups, mainly the carbonyl (C=O), which increases their polarity, decreasing the solubility in GS:PBS.

Regarding celecoxib, within the studied parameters, its solubility was mostly dependent on polarity since its pKa is about 11 [234] and thus, it was in the non-charged form at all pH's. Overall, celecoxib was the only NSAID that presented an increased solubility of about 4-fold for the CAW:PBS 2:1 and 5-fold for the GS:PBS 2:1, in comparison to PBS alone. This confirms that concentrated formulations of CAW and GS may be suitable for localized administration of celecoxib with improved efficiency.

Since it presented an improved solubility in those media, celecoxib was further tested in 1:1 and 1:10 (w/w) ratios of GS:PBS and CAW:PBS to mimic applications where the formulations are diluted in the physiological media (e.g.: oral or systemic). As observed in Figure 2.9, there were no statistically significant differences between the solubility determined in PBS, CAW:PBS 1:1, GS:PBS 1:1, CAW:PBS 1:10 and GS:PBS 1:10. Even though the 2:1 (w/w) formulations of CAW:PBS and GS:PBS increased celecoxib's solubility, upon dilution in PBS, the dissolution advantage conferred by CAW and GS is lost. Therefore, these systems could lose advantage for administration pathways such as oral, for which the delivery systems would be highly diluted in the physiological media.

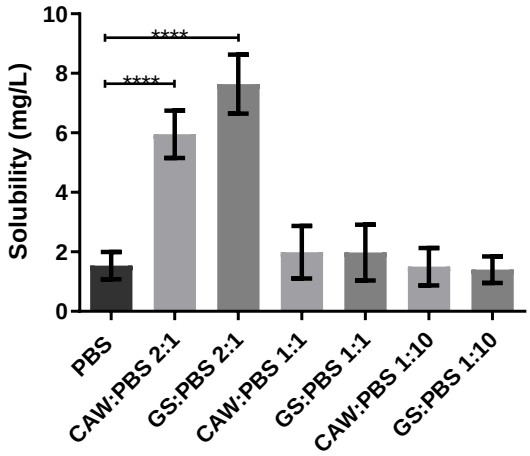


**Figure 2.9** - Solubility of celecoxib in PBS and different ratios of GS:PBS and CAW:PBS (2:1, 1:1 and 1:10, w/w). Statistical differences between PBS, CAW:PBS 2:1 and GS:PBS 2:1 (****$p < 0.0001$). The differences between CAW:PBS 1:1, GS:PBS 1:1, CAW:PBS 1:10, GS:PBS 1:10 and PBS were not significant ($p > 0.9999$).

Considering the global solubility results, it can be stated that from all the therapeutic liquid mixtures studied, the GS or CAW with celecoxib are the ones with prospect for further development towards localized administration. Envisioning intra-articular injection, the

administration pathway chosen to be explored in the scope of this thesis, GS would be preferential to CAW, since it has neutral pH as opposed to CAW, which depicted an acidic pH that could compromise the natural intra-articular features (neutral), and potentially contribute to local acidosis, one of the characteristics of chronic inflammation [235].

## 2.5 Conclusions

In this chapter, several mixtures were designed and screened towards their nature as LTTMs. GS and CAW mixtures were the selected LTTMs to be further explored in terms of their properties and ability to improve NSAIDs solubility in therapeutical applications. To the best of our knowledge, the GS LTTM and respective characterization was reported for the first time. Within the NSAIDs studied, CAW:PBS and GS:PBS 2:1 (w/w) formulations improved the solubility of celecoxib 4-fold and 5-fold in comparison to PBS, respectively. In general, this is a promising achievement for local applications, with concentrated therapeutic liquid systems, of which GS:PBS was selected specifically for the design of intra-articular injectable formulations, as further explored in chapter 3.

In sum, the developments herein achieved represent a starting point for the optimized production of a therapeutic formulation with increased celecoxib solubility, which potentially translates into higher efficiency and reduced adverse effects. For the pharmaceutical industry it also represents a valorization of the commercial drug. Moreover, the compounds used in the formulations are commonly used as excipients and thus, could avoid the time associated with the regulatory entities to reach the market.

# 3

# A Low Transition Temperature Mixture-based viscosupplementation complemented with celecoxib for osteoarthritis treatment

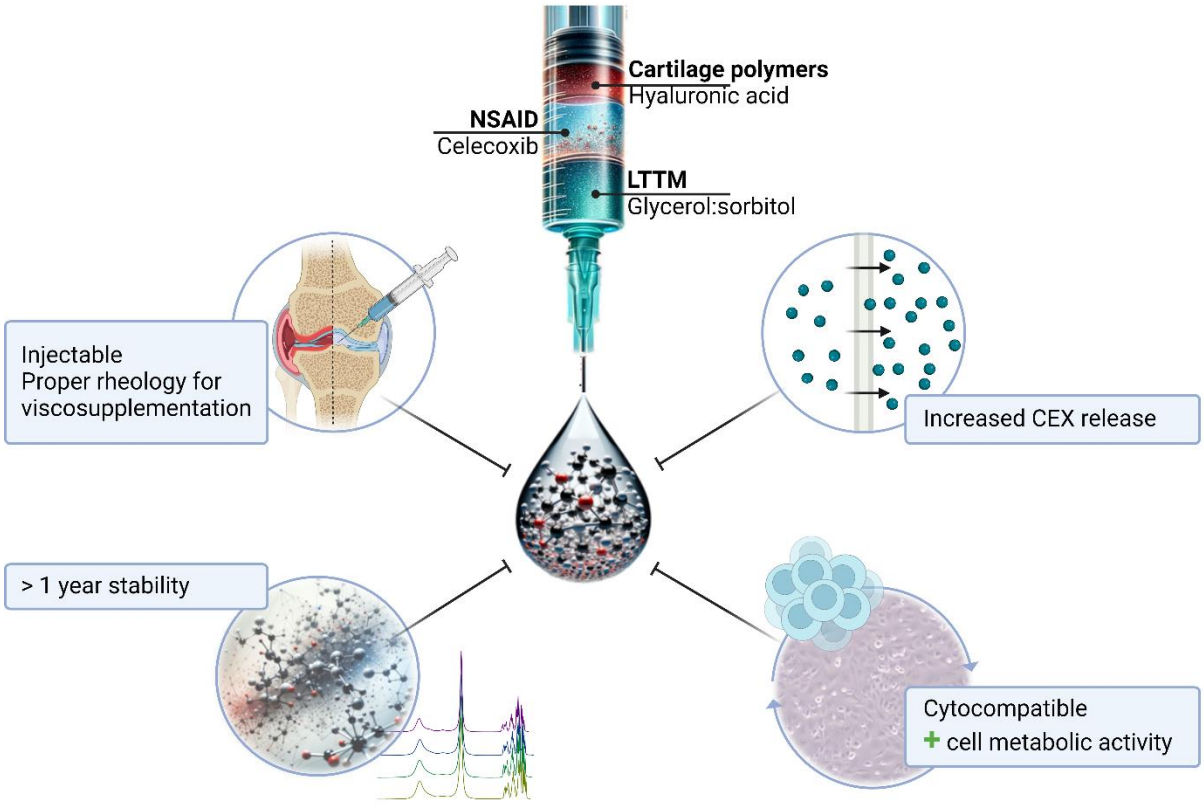

Adapted from the manuscript: Ana Roda, Alexandre Paiva and Ana Rita C. Duarte. A Low Transition Temperature Mixture-based viscosupplementation complemented with celecoxib for osteoarthritis treatment, International Journal of Pharmaceutics. 2024, 656, 124088. doi: 10.1016/j.ijpharm.2024.124088

The author was involved in the conceptualization and design of all the developed research and performed all experimental work, data processing, interpretation, and full preparation of the original manuscript.

## 3.1 Abstract

Viscosupplementation consist in hyaluronic acid (HA) intra-articular injections, commonly applied for osteoarthritis treatment. In parallel, non-steroidal anti-inflammatory drugs (NSAIDs) are widely administered for pain relief. Here, both HA and celecoxib (a NSAID) were combined in a formulation based on a low transition temperature mixture (LTTM) of glycerol:sorbitol (GS), a potential lubricant liquid that showed to increase celecoxib's solubility, thus rendering a potential alternative viscosupplement with enhanced therapeutic efficiency. The inclusion of glucosamine, a cartilage precursor, was also studied. Rheological properties, crucial for viscosupplementation were assessed: the parameters of crossover frequency, storage (G') and loss (G'') moduli profiles, their values at walking or running frequencies, zero-shear-rate viscosity, stable viscosity across temperatures and shear thinning behavior, support viscoelastic properties suitable for viscosupplementation. Biological tests on chondrogenic cells (ATDC5), confirmed the gels cytocompatibility. Regarding drug release from the gel, high and low clearance scenarios were studied. Both provided an increased celecoxib (CEX) release (6 to 73-fold) in comparison to the dissolution in PBS. The low clearance setup presented the highest CEX release for the longest period, emphasizing the importance of gel structure in CEX delivery. NMR stability studies over time favored the GS+HA+CEX (GHA+CEX) gel as a promising alternative viscosupplement, candidate for further *in vivo* evaluation.

**Keywords:** Low Transition Temperature Mixtures, anti-inflammatory, celecoxib, hyaluronic acid, viscosupplementation, osteoarthritis

## 3.2 Introduction

In Osteoarthritis (OA), both articular cartilage and synovial fluid are compromised, causing inflammation, pain and loss of joint function [2]. Cartilage and synovial fluid are the joint constituents that confer their main protection through shock absorption and bone-friction prevention. The synovial fluid also acts as joint lubricant and nutrient provider for the cartilage surrounding cells [15,16]. In this context, viscosupplementation is one of the most common treatment approaches, consisting on intra-articular (IA) injections of hyaluronic acid (HA), the main component of the synovial fluid, responsible for its rheologic and lubricant properties

[37]. Furthermore, chondroitin and glucosamine (Glu) are additional cartilage constituents and precursors, respectively, usually administered as oral supplements, associated with pain reduction and retarded OA progression [23], probably limited by their low bioavailability. Another treatment often applied for the symptomatic relieve in OA is the administration of non-steroidal anti-inflammatory drugs (NSAIDs) [25]. The therapeutic efficiency of orally administered NSAIDs is also compromised by their low bioavailability and restricted due to the associated side effects [162,163]. A local administration, such as intra-articular injection can prevent some of the limitations observed for current treatments and potentiate their efficacy.

The use of Low Transition Temperature Mixtures (LTTMs) is a promising strategy to increase the solubility and bioavailability of bioactive molecules, as reported by numerous studies [146,149, 227,150,173,174,222–226]. This potential was explored in chapter 2, where designed combination of molecules of interest were screened (e.g: organic acids, sugars, amino-acids, polyols, etc) and selected LTTMs further characterized and studied towards their capacity to improve the solubility of several NSAIDs in PBS, as physiological media. From those, glycerol:sorbitol (GS, 2:1 molar ratio) rendered a 5-fold increase of celecoxib's solubility in GS:PBS 2:1 (w/w) media, and it was further selected for the development of an IA injectable since it has a neutral pH, as characteristic of synovial fluids [235]. Moreover, GS presents beneficial properties for the development of IA injections for OA: while glycerol presents intrinsic lubricant properties [185,186], its combination with sorbitol forms an LTTM highly viscous, an important aspect in the design of liquid formulations to be injected in the synovial cavity, given the high viscosity of synovial fluids. Moreover, LTTMs can be combined with other materials, such as polymers to create or modify drug-delivery systems for controlled release [156]. The combination of LTTMs with cartilage biopolymers, such as HA and Glu (glycosaminoglycan constituent) can help to achieve that purpose, while providing potential building blocks for the cartilage matrix. In this context, HA is especially interesting since low amounts can easily produce gel-like formulations, depending on its molecular weight and other modifications, such as cross-linking [62,242]. High molecular weight (HMW) HA mixtures, create more complex and rigid networks, while improving the therapeutic efficiency of viscosupplements [63,67]. Therefore, in the work presented in this chapter, HMW HA was strategically used, in combination with GS and CEX, for the design of an IA viscosupplement with enhanced drug bioavailability. Moreover, this formulation is expected to provide improved therapeutic action in respect to conventional viscosupplements, as it comprises two active ingredients (CEX and HA) with proven efficiency in OA-management, and additional lubricant properties conferred by GS.

In sum, injectable formulations combining GS, CEX and HA, with and without Glu were developed. The main goal was to evaluate their viability to be used for viscosupplementation and to assess their performance as CEX-delivery system. For that, their rheological properties were characterized, their cytocompatibility was evaluated in a chondrogenic cell line and the *in vitro* release profile of CEX investigated.

## 3.3 Experimental section

### 3.3.1 Materials

Glycerol (99.5%, ref. GL0026) was purchased from Scharlau (Spain) and sorbitol (≥ 98%, ref. S1876) from Sigma Aldrich (France). Phosphate buffer saline tablets (PBS, ref. P4417) were acquired from Sigma Aldrich (USA) and reconstituted as described by the manufacturer (pH 7.4, at 25 °C). Celecoxib (≥ 98%, ref. PZ0008) was purchased from Sigma Aldrich (USA). Hyaluronic acid sodium salt (HA, high molecular weight: ≥ 1 MDa, ref. J66993) and glucosamine sulphate (98%, ref. J66271) were bought from AlfaAesar (China). Dimethyl sulfoxide-$d_6$ (DMSO-$d_6$, 99,96% D, ref. D031T) was acquired from Eurisotop (France). The chondrogenic cell line ATDC5, derived from mouse teratocarcinoma AT805, was obtained from the European Collection of Authenticated Cell Cultures (ECACC 99072806, UK). DMEM/F-12 (Dulbecco's Modified Eagle Medium/Nutrient Mixture F-12) with (ref. 11320074) and without phenol red (ref. 21041) were purchased from Gibco (UK). The solutions of 0.25% trypsin (ref. 25-050-CI), Fetal Bovine Serum (FBS, ref. 35-079-CV) and the antibiotic-antimycotic solution (10000 IU/mL penicillin, 10 mg/mL streptomycin and 25 µg/mL amphotericin, ref. 30-004-CI) were acquired from Corning (USA). The MTS solution (3-(4,5-dimethylthiazol-2-yl)-5-(3-carboxymethoxyphenyl)-2-(4-sulfophenyl)-2H-tetrazolium, <2%, ref. G3581) was obtained from Promega (USA). For the high-performance liquid chromatography (HPLC), acetonitrile (>99.9%, ref. 34967) from Honeywell, Riedel-de Haën (Germany) and potassium dihydrogen phosphate (98-102%, ref. 11591) from AlfaAesar (Germany) were used. The potassium dihydrogen phosphate 50 mM 50:50 (v/v) buffer was prepared in deionized water and the pH adjusted to 4.2, using phosphoric acid (85-90%, ref. 79606) from Honeywell, Fluka (Germany).

### 3.3.2 Gel preparation

The LTTM of glycerol:sorbitol 2:1 molar ratio (GS) was prepared by heating and stirring, until a translucid liquid was obtained. The liquid GS was mixed with PBS at a mass ratio of 2:1,

and used as media for gel preparation. Four types of gels were then produced. All gels were composed of 1% HA (w/w). Another group of gels was also supplemented with glucosamine sulphate (GluS), adding 10 mg of GluS per gram of gel. For the gels with CEX, this was incorporated by dispersing about 2 mg/ml of CEX (above saturation) in the GS:PBS mixture, which was stirred for 24h before the addition of HA and/or glucosamine. The composition and nomenclature of the gels is discriminated in Table 3.1.

**Table 3.1** - Composition and name given to the gel samples formulated.

| Composition | Gel name |
|---|---|
| GS:PBS+HA | GHA |
| GS:PBS+HA+GluS | GGluS |
| GS:PBS+HA+CEX | GHA+CEX |
| GS:PBS+HA+GluS+CEX | GGluS+CEX |

### 3.3.3 Rheology

The rheology of the gels was studied in a Modular Compact Rheometer MCR102 (Anton Parr, Austria) using a 2° angle cone-plate geometry (Cone CP25-2, 25 mm diameter, Anton Parr). All measurements were performed in the linear viscoelastic region (LVR) of the materials, determined by amplitude sweep at a frequency of 10 Hz, 37°C and within a shear strain ranging from 0.001 to 20 (LVR from 0.001 to 1). The real range was adjusted by the equipment, according to its ability to reach a stable reading. Frequency sweep analysis was performed at a shear strain of 0.1 and 37°C. The gels were equilibrated at 37°C for 5 min and the storage (G') and loss moduli (G'') were then determined as function of the frequency (100 to 0.01 Hz). The viscosity of gels was also measured as a function of the temperature (5 to 45°C). The gels were stabilized at 5°C for 5 min and submitted to a heating ramp with a rate of 2°C/min and a constant shear rate of 10 $s^{-1}$. For the shear rate, the gels were pre-equilibrated at 37°C for 5 min, and viscosity obtained as a function of the shear rate, from 0.01 to 1000 $s^{-1}$. The effect of pre-shear was also studied by applying a second shear rate cycle on the samples. All analyses were performed for three individual replicates of each sample.

### 3.3.4 Cytocompatibility

The *in vitro* cytocompatibility of the developed gels was evaluated in the chondrogenic cell line ATDC5, by determining the cell metabolic activity through MTS colorimetric assay, in

accordance to ISO 10993-5 [243]. The gel leachables were prepared according to ISO 10993-12 [244], for gel concentrations from 0.6 to 0.075 g/mL, successively diluted in DMEM/F-12 with 0.5% FBS. Cells were cultured in DMEM/F-12 with phenol red, supplemented with 10% FBS and 1% PS (culture media). Media was changed every 2-3 days, until confluency (70-80%) was achieved. For the MTS, cell suspensions of $1.5x10^5$ cells/mL were prepared in culture media and seeded in a 96-well plate (100 µL per well), for 24h. The media was then removed, and the cells submitted to 100 µL of each gel concentration, for 24h. After this period, the cells were washed with PBS, and 100 µL of MTS (diluted 62.5-fold, in DMEM/F-12+0.5% FBS) was added and incubated for 3h. The absorbance at 490 nm was then measured using a VICTOR Nivo™ microplate reader (PerkinElmer, USA). Each sample was analyzed in triplicate, in three independent cell assays. The cell metabolic activity was determined as previously described [245]. All cell incubation periods were performed in a humidified incubator, with 5% $CO_2$, at 37 °C.

### 3.3.5 Drug release

The drug release was performed mimicking two different scenarios, one representing an extreme gel clearance rate and the other a low gel clearance. Briefly, about 0.67 g of the gels (GHA+CEX and GGluS+CEX) or the controls (GS and PBS) were placed in 1.5 mL glass vials closed with a cellulose membrane (0.45 µm, Sartorius, Germany) in one end. These were placed in 15 mL conical tubes, previously filled with 2 mL of PBS, as release media, with the membrane facing down. The schematic setup is represented in Figure 3.1. The conical tubes were then

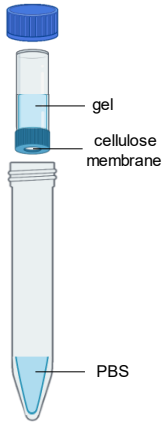


**Figure 3.1** - Schematic representation of the drug release setup.

placed in a thermostatic water bath (Grant, LSB 12 Aqua Pro, UK) at 37°C, with a linear agitation of 60 rpm. At pre-determined time points, aliquots of the released media were collected and replaced by the same volume of fresh PBS. For the extreme gel clearance scenario, all the released media was removed and replaced by 2 mL of fresh PBS, whereas for the setting

mimicking a low gel clearance, 200 µL were collected and replaced by fresh PBS. The amount of celecoxib in the collected aliquots was quantified by HPLC, as previously described in chapter 2, section 2.3.10.1, using linear calibration between 0.05 to 2.7 mg/mL (LOD 0.028 mg/L). Briefly, 20 µL were injected in a Smartline HPLC Series (Knauer, Germany), eluted in acetonitrile:potassium dihydrogen phosphate 50 mM 50:50 (v/v) at pH 4.2, using a Keystone Kromasil C18 column (250 × 4.6 mm 5 µm, Thermo Scientific, USA) with an isocratic flow of 0.6 mL/min, and detected at 220 nm in a Smartline 2500 UV-detector (Knauer, Germany).

### 3.3.6 Nuclear Magnetic Resonance

Proton nuclear magnetic resonance ($^1$H NMR) spectra were recorded on a Bruker Avance III 400 spectrometer (USA) at 400 MHz. About 300 µL of each sample was mixed with 500 µL of DMSO-$d_6$ for analysis. For stability studies, reagents and prepared samples were kept at room temperature. MestReNova software 11.0.4-18998 was used for data analysis and the chemical shifts expressed in ppm.

### 3.3.7 Polarized Optical Microscopy (POM)

A GHA+CEX gel was prepared as described in section 3.3.2, with a celecoxib concentration of 0.04 mg or near 2 mg (excess CEX) per mL of GS:PBS. The obtained mixtures were placed on a microscope glass slide and observed by POM, using a BX-53 polarized optical microscope (Olympus, Japan) in transmission mode. Images were obtained from an equipped camera (Olympus SC50), through the software Olympus Stream Start 2.4.2 (Olympus, Japan). Celecoxib was considered soluble when no crystals or dispersed particles were observed by POM.

### 3.3.8 Statistical analysis

The normality of the results was assessed by the Shapiro–Wilk test. Those presenting a normal distribution were analyzed by One-way ANOVA (metabolic activity profiles and drug release results) or Unpaired t-test with Welch's correction (frequency sweeps, GHA vs GGluS); whereas the ones following a non-normal distribution were analyzed by Mann-Whitney test (viscosity vs temperature, GHA vs GGluS). The results were considered statistically different for p-value ≤ 0.05.

# 3.4 Results and Discussion

## 3.4.1 Rheologic characterization

When developing IA injections, namely viscosupplements, it is critical to study their rheological behavior, to understand how they respond to applied forces. This is highly relevant to assess their manipulability, injectability, and their response to load forces, such as weight-bearing forces, upon injection [246]. Moreover, the ability of healthy synovial fluids to lubricate joints and absorb mechanical shock, is typically compromised in osteoarthritic conditions. Thus, the rheological properties of viscosupplements must mimic healthy synovial fluids, aiming to restore their normal function as bone and cartilage protector, and to allow a normal joint mobility. Herein, the rheological properties of the formulated gels were characterized aiming to assess their ability to be used as viscosupplements for OA.

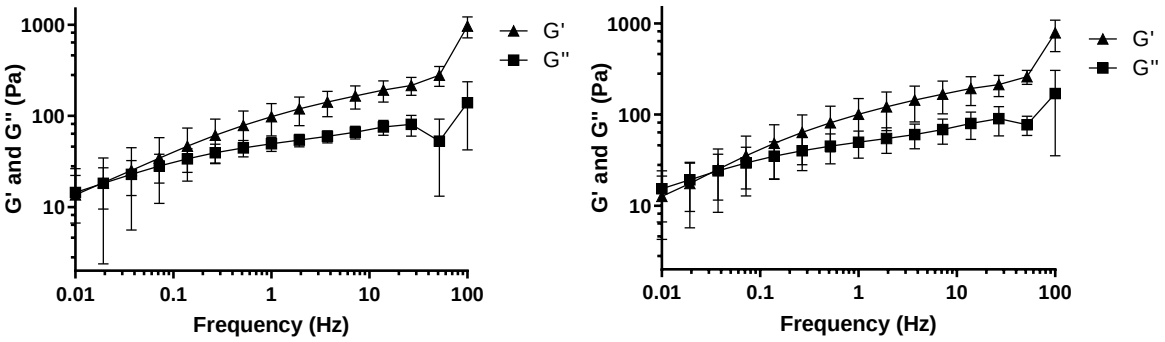


**Figure 3.2** - Frequency sweeps of a) GHA and b) GGluS. Storage (G') and loss (G'') moduli as a function of frequency (Hz).

Figure 3.2 represents the frequency sweep profiles of GHA and GGluS, which were not statistically different. The storage modulus (G') represents the elastic component of the system, while the loss modulus (G'') refers to the viscous component, thus being also referred to as elastic and viscous moduli, respectively [62,242]. As it can be observed, above the crossover frequency (Fc), G' is higher than G''. This indicates a transition from viscous to elastic-fluid behavior. When applied to the synovial joint, this elasticity provides cartilage protection by absorbing mechanical energy [242]. Additionally, G' and G'' values have a close magnitude, mainly for lower frequencies, and both present some frequency-dependent behavior, increasing when frequency increases. These observations support that the formulation possesses some fluidity rather than being a compact-solid-like structure. From these plots, it was possible

to estimate the values of Fc, relaxation time ($t_R$) and the G′ and G′′ at the frequency representative of walking (0.5 Hz) or running activities (2.5Hz). These results are summarized in Table 3.2.

**Table 3.2.** Results of crossover frequency (Fc), relaxation time ($t_R$) and the storage modulus (G′) and loss modulus (G′′) at the frequency representative of walking (0.5 Hz) or running activities (2.5 Hz), at 37°C. G′ and G′′ near 0.5 and 2.5 Hz are represented as mean ± SD. Fc and $t_R$ were estimated from the crossover of G′ and G′ lines, plotted from their mean values (Figure 3.2).

| Sample | Fc (Hz) | $t_R$ (s) | Walking (~ 0.5Hz) | | Running (~ 2.5Hz) | |
|---|---|---|---|---|---|---|
| | | | G′ (Pa) | G′′ (Pa) | G′ (Pa) | G′′ (Pa) |
| GHA | 0.02 | 50 | 78.7 ± 34.6 | 44.6 ± 9.1 | 119.4 ± 41.2 | 54.3 ± 8.6 |
| GGluS | 0.04 | 25 | 81.3 ± 42.3 | 45.0 ± 16.2 | 121.7 ± 55.2 | 54.5 ± 16.9 |

It is reported that commercial viscosupplementations present Fc from under 0.01 to over 10 Hz [62], corresponding to the formulations with highest (crosslinked) and lowest (0.5-0.73 MDa) molecular weight in HA, respectively. In turn, synovial fluids have Fc within 0.13 ± 0.02 to 0.41 ± 0.12 Hz when healthy [247], or 1.8 ± 0.5 Hz for osteoarthritic state [248]. In this context, the range of interest for the formulations herein developed was set for Fc values up to 0.41 Hz, considering as goal to restore or improve the properties of healthy synovial fluids. This was observed for both formulations, with Fc values ranging from <0.01 to 0.14 Hz, for GHA replicates, and from 0.02 to 0.14 Hz for the GGluS. The corresponding mean Fc values obtained from the crossover between G′ and G′′ (Figure 3.2), were 0.02 Hz for GHA and 0.04 Hz for GGluS, with respective relaxation times near 50 and 25 s (Table 3.2).

Furthermore, for weight-bearing joints, such as the knees, it is especially important to characterize the G′ and G′′ under frequencies corresponding to walking (0.5 Hz) or running (2.5 Hz) activities (Table 3.2). Prior research on commercial viscosupplementations, gathered G′(0.5 Hz) values between 2 and 89 Pa, G′′(0.5 Hz) ranging from 3 to 52 Pa, G′(2.5 Hz) from 11 to 129 Pa, and G′′(2.5 Hz) from 5 to 85 Pa [62,248–250]. In Figure 3.3, it is possible to compare the G′ and G′′ values obtained at 0.5 and 2.5 Hz for GHA and GGluS, with the ones reported for several commercial viscosupplementations [62,248–250]. Considering both G′ and G′′, the values obtained for the studied systems were more consistent with the commercial products Monovisc® and Orthovisc®, especially with Orthovisc®. In sum, the properties herein studied are in the range of commercial formulations and healthy synovial fluids.

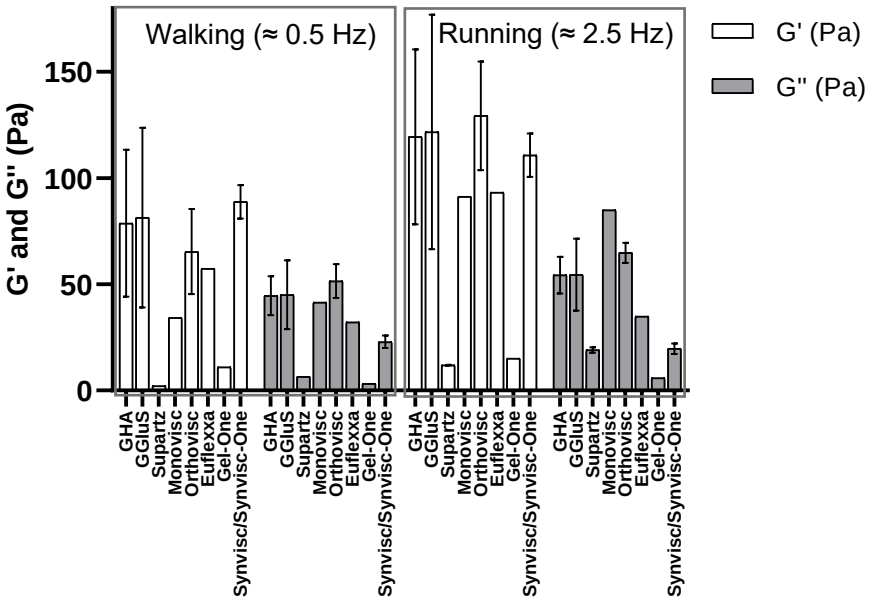


**Figure 3.3** - Storage (G') and loss (G'') moduli of GHA and GGluS gels, in comparison to the ones reported for commercial viscosupplementations [62,248–250].

The gels were also characterized in terms of their viscosity at different temperatures (Figure 3.4), to assess the extent of viscosity variation, especially before injection, at storage or administration conditions (room temperature) in comparison to body temperature. As it can be observed for the GHA, there is a slight decrease of the viscosity profile when temperature increases. Within room temperature and body temperature (20-37°C), the gel has a viscosity between 10-12 Pa.s, with no significant differences. Therefore, no substantial effect on the gel injectability is expected. The system GGluS showed no significant differences from GHA.

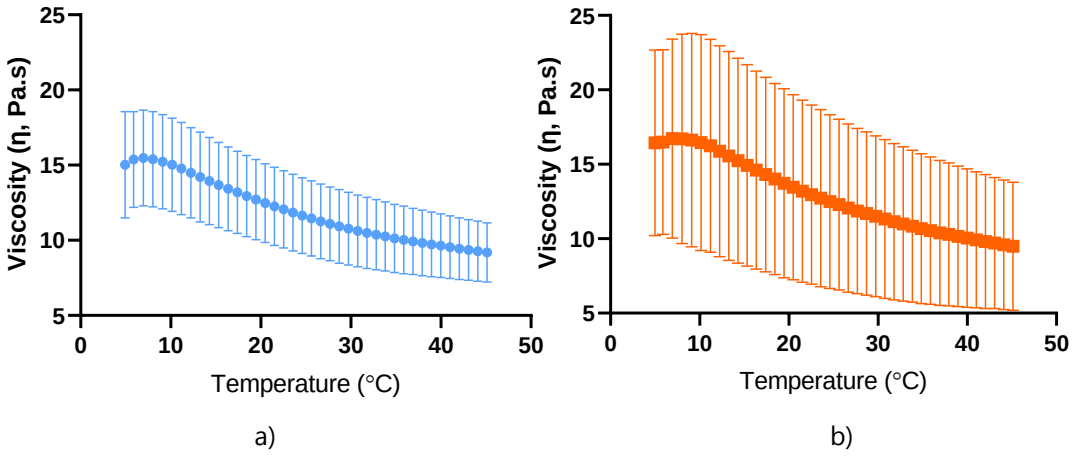


**Figure 3.4** - Viscosity as a function of temperature for a) GHA, and b) GGluS.

Since the rheological properties of GHA and GGluS previously analyzed did not show significant differences, the remaining analysis were only performed for GHA, as representative of both.

Envisioning an intra-articular injection, the gels are expected to be constrained and submitted to compression (or load) forces within the joint, especially in weight-bearing joints. High compression causes the gel to be more restrained (compacted), thus corresponding to low shear rates. Lower loading-forces allow higher gel flow, which corresponds to high shear rates [62]. Therefore, the shear rate profile is an important analysis for intra-articular-intended formulations, to assess the effect of the shear rate in the material properties. Moreover, is it important to consider the conditions upon IA injection, to better mimic the product performance in those conditions. Knee joints were considered as reference since they have the highest volume of synovial fluid. Given that a normal knee joint contains about 6 mL of synovial fluid, this can be totally replaced with the maximum viscosupplementation volume (6 mL) or supplemented with lower volumes, most commonly 2 mL [251]. In this context, upon injection, the viscosupplementation might be in the concentrated form (GHA) or diluted 3-fold (dGHA) in the synovial fluid. Additionally, in OA condition, the synovial fluid is commonly diluted due to effusion. Therefore, the shear rate analysis was performed for both concentrated (GHA) and diluted (dGHA) formulations (Figure 3.5). The 3-fold dilution was performed with PBS to mimic a fictious worst-case scenario where the OA synovial fluid would have a viscosity near the physiological media.

In Figure 3.5 it can be observed that the gels behave as non-Newtonian fluids, presenting shear thinning behavior (viscosity decrease as shear rate increases), a characteristic of healthy synovial fluids and commercial viscosupplementations [249,252], that allows an adjustable and reversible response to loading forces [246]. The effect of pre-shear treatment was further analyzed to study the capacity of the gel to maintain or recover its properties upon exposure to shear rates (from low to high). The results support that the pre-shear treatment influences the viscosity profile of GHA for shear rates < 1 $s^{-1}$. Without pre-shear, the gels presented an almost linear decrease of viscosity with increasing shear rates. In turn, for the pre-sheared gels, lower but constant viscosity values were obtained for shear rates below 1 $s^{-1}$. Above 1 $s^{-1}$, the viscosity profile of the pre-sheared and non pre-sheared gels converged. These occurrences upon pre-shearing are consistent with thixotropic behavior, reinforcing the reversible re-organization of the gels structure.

In comparison to the non pre-sheared GHA, the diluted gel (dGHA) had an equivalent viscosity profile for shear rates ≤ 1 $s^{-1}$; and above those, a deeper viscosity decrease was observed.

The phenomena of shear thinning and thixotropy are also good indicators of injectability, since the injection force increases the shear stress and shear rate, which lowers the gel viscosity, facilitating its administration [246,253]. In this context, injectability was manually tested and confirmed for needle gauges from 21 to 30G.

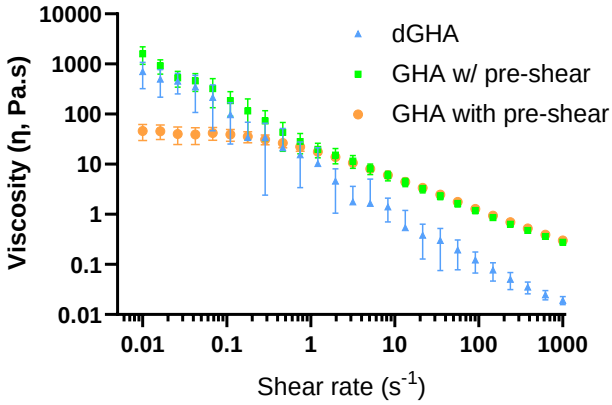


**Figure 3.5.** Viscosity as a function of shear rate (dGHA: GHA diluted 3-fold).

The zero-shear-rate viscosity ($\eta_0$) is an additional parameter, usually used to characterize the viscosity of a material at rest. Commonly, $\eta_0$ is defined as the viscosity measured at the minimum shear rate tested [242]. Here, we considered the $\eta_0$ as $\eta_{0.1}$, to be comparable with the marketed viscosupplementations characterized by Nicholls et al. [62]. The results obtained for the tested formulations are summarized in Table 3.3. All of these formulations have a $\eta_0$ higher than the maximum value reported for OA synovial fluids (0.01-11 Pa.s), and within the range reported for healthy synovial fluids (1-175 Pa.s) [242] and commercial viscosupplementations (0.3-193 Pa.s) [62], which supports their use for the proposed application.

**Table 3.3.** Shear rate properties obtained for the GHA and dGHA formulations.

| Sample | $\eta_{0.1}$ (Pa.s) | $\eta_{240}$ (Pa.s) | $\eta_{0.1}/\eta_{240}$ |
|---|---|---|---|
| GHA with pre-shear | 39 ± 10 | 0.69 ± 0.06 | 56 |
| GHA w/ pre-shear | 185 ± 94 | 0.63 ± 0.07 | 290 |
| dGHA | 97 ± 71 | 0.05 ± 0.02 | 1925 |

Additionally, the ratio between low shear rates (here represented by $\eta_{0.1}$) and high shear rates (here represented by $\eta_{240}$) was previously reported as a quantitative measure of the shear

thinning behavior of synovial fluids ($\eta_{0.1}/\eta_{300}$) [242,252] and commercial viscosupplementations ($\eta_{0.1}/\eta_{250}$) [62]. Here, a shear thinning ratio of $\eta_{0.1}/\eta_{240}$ was used as representative of both. According to Rebenda et al., the shear thinning ratio ranges from 70 to 250 in healthy synovial fluids and from 5 to 40 in osteoarthritic synovial fluids [242]. For commercial viscosupplementations, values between 2 and 651 were reported by Nicholls et al. [62]. As observed for the experimental values of Table 3.3, the GHA based systems presented, once more, rheological properties superior to the ones of OA and within the range reported for normal synovial fluids. In comparison to the shear thinning ratios reported for commercial viscosupplementations, the range values of GHA (56-290) comprehend the magnitude of values stated for Monovisc® (52), Orthovisc® (170), Euflexxa® (237) and Gel-one® (243). Higher values were reported for Synvisc® (651-741), which is due to the use of cross-linked HA instead of the non-crosslinked used in the other products and GHA. Even though crosslinked HA may confer advantage in terms of higher retention in the joints, it may be less biocompatible and cause higher immunogenicity, and therefore, the safety profile of non-crosslinked HA is generally regarded as favorable [254].

In the work of Bhuanantanondh and co-workers [250], they reported the viscosity profiles as a function of shear rate for mixtures of OA-synovial fluid (OA-SF) with three commercial viscosupplementations: Suplasyn® (low molecular weight HA), Orthovisc® (high molecular weight HA) or Synvisc® (cross-linked HA), in a ratio of 1:1 (v/v). In comparison with those, the profile here obtained for GHA (Figure 3.5), presented viscosity values superior to the ones of OA-SF+suplasyn and OA-SF+orthovisc, and equivalent to OA-SF+synvisc. Therefore, although GHA was produced from high molecular weight HA, like orthovisc, the combination OA-SF+orthovisc presented viscosities clearly inferior up to shear rates of 1 $s^{-1}$, after which they converged. Thus, a full replacement of the synovial fluid by the GHA formulation, would be expected to render similar shear-rate properties to OA-SF+synvisc.

Overall, the produced gels share rheological characteristics with some of the commercial viscosupplements, being therefore adequate for viscosupplementation. Moreover, these properties could be further tuned by polymer cross-linking or by changing the molecular weight.

### 3.4.2 Cytocompatibility evaluation

The cytocompatibility of the developed gels was tested in a chondrogenic ATDC5 cell line, representative of joint cells.

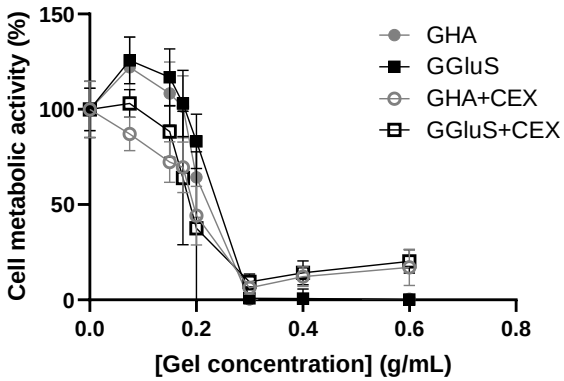


**Figure 3.6.** Cell metabolic activity percentage determined in ATDC5 cells for the developed gels: GHA, GGluS, GHA+CEX, GGluS+CEX.

As it is possible to observe from Figure 3.6, all the gels present a similar metabolic profile and no statistically significant differences were observed between the four formulations tested (p-value > 0.98). Therefore, the results for GHA and GGluS were considered as representative. According to the international standards of ISO 10993-5 [243] and 10993-12 [244], a polymeric leachable in a concentration from 0.18 to 0.22 g/mL with a metabolic activity ≥ 70%, is considered non-cytotoxic. The metabolic activity at 0.2 g/mL was 64±21% for GHA and 83±14% for GGluS, and 100% or higher for lower concentrations of both. Therefore, the non-cytotoxic criteria were met, at least for concentrations ≤ 0.2 g/mL.

For gel concentrations ≥ 0.3 g/mL, the metabolic activity was below 2%. At this higher concentration range, the limiting component(s) might be the glycerol:sorbitol content which had an $IC_{50}$ near 0.09 g/mL in this cell model. As previously reported in chapter 2, section 2.4.4, the glycerol:sorbitol mixture may cause some osmotic stress *in vitro*, mainly induced by sorbitol. However, given the dynamic tendency of cells to achieve homeostasis, this is not expected to occur *in vivo*. In fact, *in vivo*, glycerol can be a potential adjuvant in joint lubrication while its combination with sorbitol results in a more viscous lubricant, which is advantageous for the intended application. Moreover, glycerol and sorbitol are FDA-approved excipients for several human products, and sorbitol is even reported for administration via intra-articular routes up to a maximum unit dose of 45% (w/v) [255], a concentration higher than the formulations herein tested contain.

For gel concentrations ≤ 0.175 g/mL, the cell metabolic activity increased up to 26% compared to the control (100%). This supports that, at certain concentration, the gels are cytocompatible and can even stimulate cell metabolic activity, most probably due to the ECM biopolymers included in the gel [256].

### 3.4.3 Drug release from gels

Mimicking the drug release of the intra-articular environment *in vitro* is not straightforward as this is a very dynamic environment. Osteoarthritic synovial fluids tend to have elevated clearance rates, in comparison to healthy ones. The lower the clearance rate, the higher its retention time and effectiveness, both in terms of action and durability. Some works reported in the literature use high clearance set-ups to analyze their formulations [56,58,257–260], whereas others use conditions to mimic a low clearance environment [261,262]. Herein, we studied both scenarios for a more comprehensive understanding of the developed formulations: Figure 3.7a represents the release profile at an extreme gel clearance scenario, where the released media is totally removed at each time point; and Figure 3.7b represents a low clearance of the gel, where only 10% of the media is removed at each time point. The gel formulations GHA+CEX and GGluS+CEX were compared with the same matrix without polymers (named GS) and with PBS, as reference, to understand how the gel constituents modulate the release of CEX *in vitro*. From the results, there is an increased release of CEX from the gels in comparison to GS or PBS, in both scenarios. However, there is a clear difference between their maximum CEX release and their release profiles.

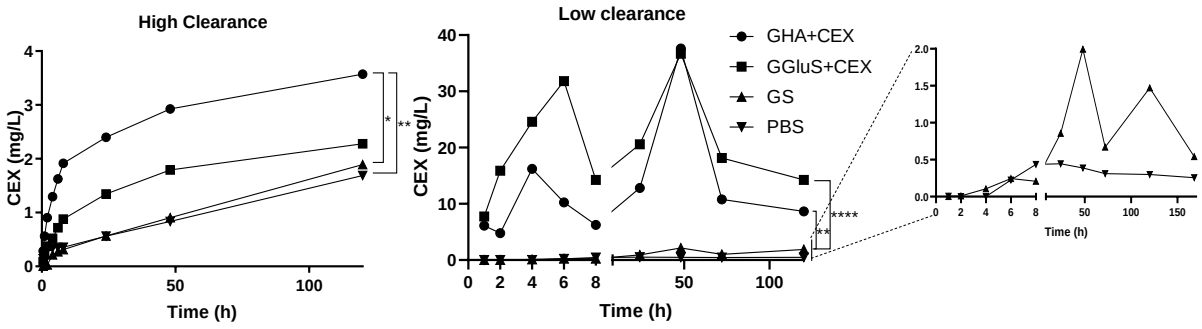


**Figure 3.7.** Representation of the mean values for the cumulative release of celecoxib (mg/L) from GHA+CEX, GGluS+CEX, GS and PBS. The lines are a guide to the eye. a) High clearance rate scenario b) low clearance scenario. *p≤0.05, **p≤0.01, ****p≤0.0001. Full data (Mean ±SD) in Table B.1 and Table B.2, Appendix B.

For the high clearance method (Figure 3.7 a), a higher CEX release rate was achieved in the first 8h, with a CEX concentration up to 6-fold higher in the gel than in GS or PBS. After these first hours, the release reaches a steady state. In turn, for the low clearance path (Figure 3.7 b), a release profile with supersaturation points (e.g: 6h and 48h for GHA+CEX) is observed for all the conditions tested, except for PBS. These are related to the solubility and recrystallization of CEX, which depends on its solvation in each of the formulations and on the gel structure, when

present [263]. In this low clearance set-up, the maximum CEX release was achieved for the gel formulations at 48h, with an increase up to more than 17-fold or 73-fold in comparison to GS or PBS, respectively. Moreover, after 48h release from the gels, the CEX amount retrieved in low clearance was more than 10-times higher than the one obtained at high clearance. This difference reflects the importance of the gel structure in the increment of celecoxib's concentration. In the case of a high clearance scenario, the gel disintegration is faster which translates into a lower and less prolonged CEX release. In a low clearance situation, a fluid gel structure is maintained, confining higher CEX amounts in the polymeric network. From these results, it is expected that the longer the gel structure is maintained upon injection, the more extended will be the release of CEX at higher concentration. Still, even if celecoxib is not retained for more than 48h, it is expected to contribute to the immediate reduction of local inflammation and prevent possible inflammation and subsequent swelling associated with post-intra-articular injection procedures. Reduced inflammation allows to restore or maintain the viscoelasticity of the synovial fluids' or injected viscosupplements', thus reducing the clearance rate of HA and prolonging their protective and therapeutic function.

The gel formulation produced has CEX both dissolved and dispersed. While the dissolved CEX is readily available, the dispersed component is expected to contribute to a controlled release [240,264,265], dependent on drug absorption, drug diffusion from gel and residence time of the gel. Thus, the partial CEX solubilization is expected to provide an immediate release, maintained or extended by the dispersed CEX.

Even though it is difficult to quantitatively determine the maximum CEX soluble in the gel, due to its viscosity, it was qualitatively observed by POM (Figure 3.8), that at least 0.04 mg/mL of CEX appear to be soluble in GHA+CEX, since no CEX crystals or dispersed particles are observed at this concentration (Figure 3.8, top), in contrast to the saturated formulation (Figure 3.8, bottom). This soluble amount is near the maximum CEX concentration obtained from the gels release (Figure 3.7) and it represents improvements above 5-fold and 25-fold than the maximum solubility previously reported for GS-rich media and PBS, respectively [245].

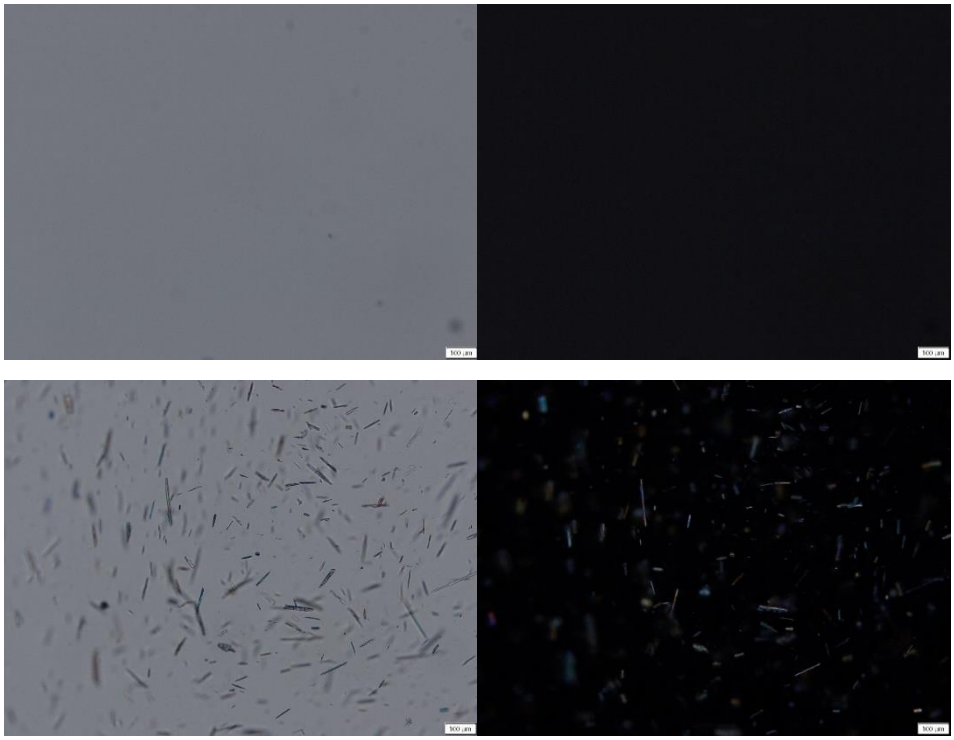

**Figure 3.8.** POM images of GHA+CEX with celecoxib at 0.04 mg/mL$_{GS:PBS}$ (top) and GHA+CEX with excess celecoxib (bottom). Left: Non-polarized images; right: polarized images. Scale bar: 100 µm.

## 3.5 NMR - Long term stability of the gels

Freshly prepared GHA and GGluS presented equivalent results for most of the analysis performed. However, the study of gels' stability over time demonstrated that GGluS gels were not stable for long periods. As it can be observed in the NMR spectra obtained for GGluS with (Figure B.1, left, Appendix B) and without CEX (Figure 3.9, left) at different time points, after 1 month, the signals between δ 4 and 5 ppm converge. This can be justified by the occurrence of Maillard reaction promoted by the presence of glucosamine, therefore modifying the composition and properties of the gel. Thus, for the GGluS gels to be suitable for viscosupplementation or drug delivery system, strategies for the stabilization of glucosamine would have to be studied. In turn, the NMR spectra obtained for the GHA gels with (Figure B.1, right, Appendix B) and without CEX (Figure 3.9, right) did not present alterations up to 1 year, which support chemical stability under this period, at room temperature. No differences between the gels with and without celecoxib were noticed.

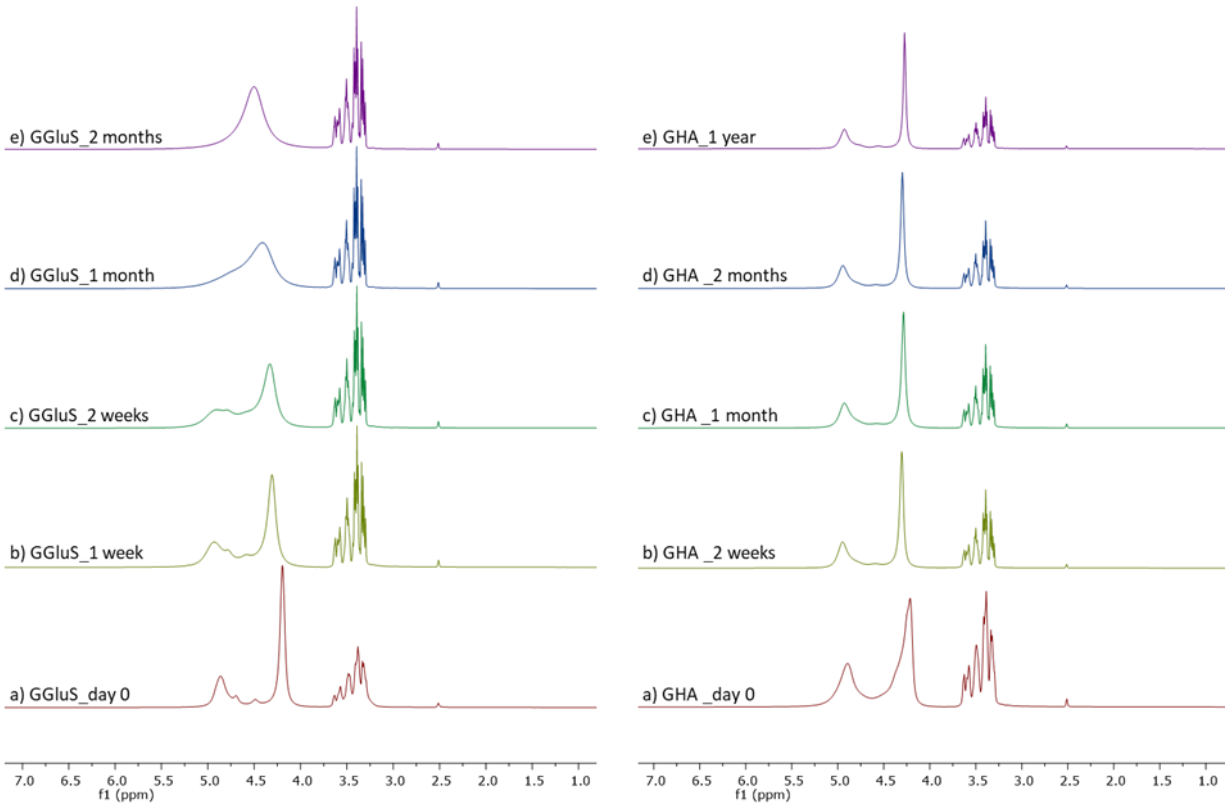


**Figure 3.9** - $^{1}$H NMR spectra over time. Left: GGluS gel at a) day 0, freshly prepared, b) 1 week, c) 2 weeks, d) 1 month, e) 2 months; Right: GHA gels at a) day 0, b) 2weeks, c) 1 month, d) 2 months, e) 1 year. Similar spectra were obtained for gels with celecoxib Figure B.1, Appendix B.

## 3.6 Conclusions

The present chapter focused on the development and characterization of new two-in-one viscosupplements for OA, combining GS+HA+NSAID (GHA+CEX) or GS+HA+NSAID+GluS (GGluS+CEX). These have potentially enhanced therapeutic efficiency, due to the combined delivery of lubricant agents for cartilage protection and shock absorption, biopolymers as source for cartilage regeneration and, celecoxib, for local anti-inflammatory action. The produced formulations were characterized in terms of their rheological properties, cytocompatibility, and drug release. They have rheological properties in the range of commercial formulations and healthy synovial fluids, which supports their potential use for viscosupplemention. Moreover, these gels presented proper cytocompatibility in a mouse chondrogenic cell line (ATDC5) and even exhibited increased metabolic activity, which is a good indicator in a perspective of being used as delayers or disease-modifying agents in OA, in addition to the

symptomatic relief. Regarding drug release from the gels, setups of high and low gel clearance were studied and retrieved a maximum 6-fold and 73-fold increase of CEX released, respectively, in comparison to PBS. This increase showed to be dependent on the gel structure and it may promote a fast and effective local inflammatory action during the first hours upon injection. Despite being equivalent to GHA in most of the analyses performed, the GGluS formulation was not stable after 1 month, whereas GHA presented chemical stability for at least 1 year. The promising results of the properties herein characterized fully support further evaluations of the *in vivo* potential of GHA+CEX as alternative viscosupplement.

# 4

# The effect of an LTTM-based viscosupplement combined with celecoxib in a rat model with post-traumatic knee osteoarthritis

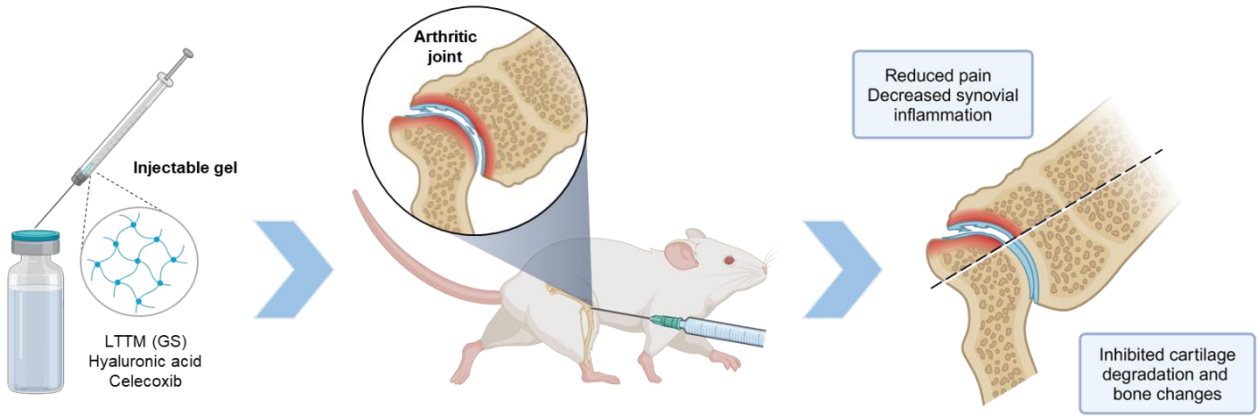

Adapted from the manuscript under preparation: Ana Roda, Jaqueline Lourdes Rios, Yeter Dilek, Kelly Warmink, Remei Escudero, Katrin A. Muenzebrock, Jie Du, Zhiming Wu, Alexandre Paiva, Ana Rita C. Duarte and Laura B. Creemers. A Low Transition Temperature Mixture-based viscosupplementation complemented with celecoxib for osteoarthritis treatment

The author was involved in the conceptualization and design of the developed research and performed all experimental work, except for *in vivo* manipulation, data acquisition and post-mortem harvesting, which was performed in collaboration with Dr. Jaqueline Lourdes Rios and collaborative team, under supervision of Professor Laura B. Creemers from the University Medical Center Utrecht (UMCU), Departments of Orthopedics, and Utrecht Regenerative Medicine Center. The data processing, interpretation, and full preparation of the original manuscript was performed by the author.

## 4.1 Abstract

The work performed in chapters 2 to 3 allowed to develop a formulation as alternative viscosupplement for osteoarthritis treatment: hyaluronic acid (HA) combined with celecoxib (CEX) with enhanced bioavailability by incorporation in a Low Transition Temperature Mixture (LTTM) comprising lubricant properties.

Here, the performance of the developed gel was evaluated *in vivo*. The efficacy of HA+LTTM+CEX versus HA, HA+CEX and saline control was tested (n=6) in a knee post-traumatic OA rat model (female Sprague-Dawley 11-weeks old), induced by unilateral anterior cruciate ligament transection and partial medial meniscectomy (ACLt+pMMx). Knee edema was assessed along dynamic weight bearing evaluation of pain. Systemic CEX release was determined. Bone changes were explored through micro-computed tomography and histological analysis of joint degeneration (Mankin score) and synovitis (Krenn score) was conducted.

The results support that all HA-based formulations effectively reduced synovitis, but only HA and HA+LTTM+CEX alleviated pain-related unloading of the affected paw. HA+LTTM+CEX diminished CEX systemic exposure, and it presented distinctive action on the inhibition of cartilage and subchondral bone degeneration. Overall, these results suggest that the combination of HA+CEX confers an increased therapeutic effect compared to HA alone, especially at the level of inhibiting OA-induced degeneration, but only if combined with the LTTM.

In sum, the treatment with HA+LTTM+CEX showed added value in preventing OA progression: it achieved a therapeutic outcome not found for HA or HA+CEX without LTTM – chondroprotective action, by inhibiting joint degeneration, one of the major criteria considered for disease-modifying-OA-drugs.

**Keywords**: Osteoarthritis, Low Transition Temperature Mixtures, glycerol:sorbitol, hyaluronic acid, celecoxib, non-steroidal anti-inflammatory drugs, chondroprotective

## 4.2 Introduction

Osteoarthritis (OA) causes synovial fluid thinning, cartilage degeneration, bone remodeling, inflammation, pain and, in advanced stages, it may lead to loss of joint mobility [17]. Common therapy includes intra-articular (IA) injections of corticosteroids or hyaluronic acid (HA). The HA injectables, also known as viscosupplementation, intend to restore the physiologic properties of healthy synovial fluids, while corticosteroids are administered to promote a

strong anti-inflammatory action. Both are reported to efficiently reduce pain and improve joint function, but their efficacy is heterogeneous as it depends on several factors such as age and OA stage [25,266]. Some studies report an early stronger effect but less prolonged for corticosteroids in comparison to viscosupplements, while the co-administration of HA and corticosteroids has shown improved therapeutic outcomes [266–268]. Despite the benefits, corticosteroid IA injections have a limited number of applications due to the occurrence of several systemic adverse effects [35]. Locally, it was also reported that prolonged IA exposure to corticosteroids causes extended joint instability and degeneration, triggered by tissue healing inhibition [269]. An alternative to corticosteroids could be the use of non-steroidal anti-inflammatory drugs (NSAIDs), also conventionally used for OA pain management, through oral or topic administration. As described in more detail in chapter 1 (section 1.3.2.1), within NSAIDs, celecoxib (CEX) is a first line option for OA pain relief, with beneficial therapeutic efficiency and safety, attributed partially to its selective COX-2 inhibition. However, NSAIDs' low bioavailability limits the amount reaching the joints and causes adverse systemic side effects [22,23,25,27]. In this context, a local IA injection of CEX could be an option to reduce the dose needed to achieve therapeutic efficiency while reducing systemic adverse effects. In addition to pain relief, CEX is reported to have chondroprotective action [52,270], effective inflammatory inhibition [40,52,53,270] and preventive effect on other changes such as cysts and osteophytes, especially when administered intraarticularly [40,55]. The combined injection of CEX and HA may also present positive outcomes in terms of cartilage protection [271,272], inflammatory reduction [271] and pain control [272]. These studies support a potential synergic or complementary effect of HA and CEX in comparison to either alone [271,272]. Despite promising, the available preclinical data on the topic is insufficient and inconsistent, as it varies with several factors, some of which: dose, delivery type and animal models evaluated [40,52–55]. This might explain why there are no injectable formulations of CEX or HA+CEX in clinical use. Additionally, CEX's low solubility and thus, bioavailability in the physiological environment remains a challenge, possibly limiting further developments. In the previous chapters, Low Transition Temperature Mixtures (LTTMs) were explored as a possible solution to effectively combine CEX and HA. In chapter 2, the use of LTTM-based carriers to improve CEX solubility and its potential to be incorporated in a viscosupplement was studied. The glycerol:sorbitol (GS)-based LTTM presented the highest CEX solubility, it was compatible with the physiological media and suitable for IA injection, given its pH and constituents [245]. Additionally, both glycerol and sorbitol are FDA and EMA-approved for human clinical products [255,273]. Based on these features, a formulation combining GS, CEX and HA was developed in chapter 3, reporting proper

cytocompatibility *in vitro* and rheologic properties within the range of commercial viscosupplements and healthy synovial fluids. Therefore, the produced mixture was considered as suitable to be used for viscosupplementation, aiming to restore the normal lubricant and protective features of joints. Moreover, GS has additional lubricant properties [185,186], that may confer advantage in IA therapy of OA.

Here we tested the effect of HA+GS+CEX versus HA+CEX or HA in an OA rat model, induced by anterior cruciate ligament transection combined with partial medial meniscectomy (ACLt+pMMx). We postulate that the treatment with HA+GS+CEX has a better therapeutic outcome than the formulations without CEX or GS.

## 4.3 Experimental section

### 4.3.1 Materials

Sodium hyaluronate (HA, MW 1.3 MDa, Hyatrue®, HA-EP1.8, pharma grade) was kindly provided by the Bloomage Biotechnology Corporation Limited (China). D-sorbitol (pharma grade, ref. A2222) and glycerol (pharma grade, ref. 141339) were acquired from Panreac AppliChem (USA). Celecoxib (ref. PHR1683), ethylenediaminetetraacetic acid (EDTA, ref. ED2P), Safranin-O (ref. S8884), Fast Green (≥85%, ref. F7252) and acetic acid (ref. 33209) were purchased from Sigma-Aldrich, USA. Carprofen was bought from the veterinarian department of Utrecht University; Enrofloxacin (Baytril®, Bayer, Germany); Buprenorphine (Temgesic®, Eumedica, USA); Isoflurane (Abbott, Green Oaks, USA). Weigert's hematoxylin was prepared by mixing equal parts of Hematoxylin solution A (ref. X906.1) and Hematoxylin solution B (ref. X907.1), acquired from Carl Roth, Germany. Ethanol 70% (ref. 84010059), ethanol 96% (ref. 84045206), and ethanol 100% (ref. 84050065) were purchased from Boom, Netherlands. Remaining reagents were acquired from suppliers as follows: neutral buffered formalin (NBF, ref. 11699408, VWR), eosin Y (ref. 45380, Merck, India), xylene (ref. 4055-9005, Klinipath, Netherlands), Mayer's hemalum solution (ref. 1.09249, Merck, Germany), ammonia solution 32% (ref. 1.05426, Merck, Germany), and hydrochloric acid (37%, ref. 1.00317, Merck, Germany).

### 4.3.2 Preparation of injectables

All the reagents used were pharma grade. Phosphate buffer saline (PBS) was used as recommended by the manufacturer (0.01 M phosphate buffer, 0.0027 M potassium chloride, 0.137 M sodium chloride, pH 7.4, 25 °C, Sigma Aldrich, USA). Glycerol:sorbitol 2:1 (GS, molar ratio)

was prepared by heating and stirring. Four injectables were prepared: PBS for the control group, HA solution in PBS (HA), a solution of HA and celecoxib in PBS (HA+CEX) and a solution of HA and celecoxib in GS:PBS 2:1 (w/w) (GHA +CEX), as reported in chapter 3. Celecoxib was added at 1.82 mg/mL and HA at 1% (w/w).

### 4.3.3 Animal setup and OA model

The *in vivo* experiments were conducted under the guidelines and approval of the Animal Experiments Committee in Utrecht, The Netherlands (project number AVD11500202114837).

Knee osteoarthritis was induced unilaterally by the combination of anterior cruciate ligament transection (ACLt) and partial medial meniscectomy (pMMx) in the right knee (ipsilateral) of 24 rats (Sprague-Dawley female, 12-weeks old, Crl:CD(SD) strain code 001, Charles River, Germany), at day -28. The animals were priorly acclimatized for a period of 7 days, monitored and weighted weekly through all study. Rats were fed *ad libitum* with a regular chow diet ("rat and mouse breeder and grower 801730"; 22 kcal% protein, 9 kcal% from fat, 69 kcal% from carbohydrates of which 8.4% sucrose, SDS Diets, UK). For surgery, the rats were sedated by inhalation with isoflurane (induction 4%, maintenance 1.5-3%). Buprenorphine (0.03 mg/kg) and carprofen (4mg/kg) were subcutaneously administered at least 30 min prior surgery, and buprenorphine reinforced post-surgery, 6 hours after the first administration. The 2 following days (day –27 and –26), the animals also received a daily dose of 4 mg/g of carprofen, for pain management.

Four weeks after OA induction (day 0), the animals were randomized in 4 groups of 6 rats each (sample size calculation from previously reported data [269], using G-Power v3.1.9.7 [274,275]). Each rat received a 25 µL unilateral intra-articular injection (30G needle), through the patellar tendon, in the OA-induced knees. The injectable formulations were administered to the respective groups: HA, HA+CEX, GHA+CEX, and control (PBS). Upon injection, group allocation remained blind during all experiments and data analysis.

Euthanasia was performed at day 56 by aortic excision under anesthesia. 1 rat of PBS and HA+CEX groups were sacrificed at days 1 and 48, respectively, due to lesions external to the experiment. All data collected prior to sacrifice was used since no influence in the parameters analyzed is expected. Upon sacrifice, knees were harvested for further analysis.

### 4.3.4 Caliper measurements

To assess knee swelling, a digital caliper (Kunzer 7EMS01, Germany) was used to measure rat knees' diameter, at predetermined time points, along the study, before and after OA induction and intra-articular injection. A mean value was calculated from three consecutive manual measures for each timepoint. Baseline was considered as the average of three days (day –35 to –33) measured before OA induction. Knee diameters before OA induction (baseline) were subtracted to measurements after OA and presented as mean ± SD.

### 4.3.5 Dynamic weight bearing (DWB)

Pain associated behavior was assessed through DWB analysis. Rats were individually placed in a 22 x 22 x 30 cm plexiglass chamber with floor sensors containing pressure transducers (44 x 44 captors, 10.89 $mm^2$ per captor), and allowed to move freely during all procedure. 5 min videos were recorded using a high-resolution camera (640x480 pixel), coupled to DWB software (Bioseb, module v1.4.2.98, France) that measured, in grams, the average weight exerted by each limb. The zone detection parameters were set as follows: low weight threshold ≥ 1g, weight threshold ≥ 1.5 g, surface threshold ≥ 2. The weight-bearing limbs were validated by a blinded observer, for at least 1.5 min video frames, through association between rat position and sensor activation. 3 day-measurements before OA induction were considered as baseline. Data was expressed as the weight on the contralateral limb as a percentage of total weight distributed by both hind limbs, and represented as mean ± SD.

### 4.3.6 Blood analysis

Systemic celecoxib was analyzed by ELISA (ref. 180719, Neogen, USA), using blood samples drawn via tail end at 2, 4, 6, 8, 24, 48 and 72h after IA injection. Blood was collected in a lithium heparin plasma tube (BD Microtainer, USA). Tubes were put on ice and centrifuged (15 min, 2000g) within 30 min after collection. Plasma aliquots were stored at – 80 °C until analysis.

### 4.3.7 Micro-computed tomography

Micro-computed tomography scans (µCT) were acquired in a Quantum FX CT scanner (PerkinElmer, Massachusetts), one day prior the intra-articular injection (day -1) and post-mortem (endpoint). The *in vivo* measurements were carried under isoflurane anesthesia. The hind legs were extended and scanned for 3 min at an isotropic voxel size of 42 µm, 90 kV voltage, 180 µA current and a field of view of 21 mm. 512 serial slides (2D) were acquired and data

analysis performed using ImageJ software (ImageJ 1.50i, NIH, USA). 8-bit slides were rotated (~ 90° x axis), the brightness/contrast parameter set from 100 to 255, and an autolocal threshold algorithm (v1.16.12, Bernsen method, 5 radius) applied for slide analysis (e.g: Figure C.1 a, Appendix C). Semi-manual segmentation for the tibial subchondral bone plate and trabecular bone was done as previously reported [276], and segmented (polygon selection) regions of interest (ROI) registered (e.g: Figure C.1 b, c, Appendix C). ROI were generated each 5 slides, throughout 70 slides, starting from the union of the medial and lateral side of the tibial epiphysis (back to front joint direction). Interpolation was applied and corrected when necessary. Those stacked ROI were then used to calculate the parameters of thickness (µm) and bone volume fraction (BV/TV, volume of mineralized bone per total volume), using the boneJ plugin (v1.4.1). Changes in the tibial subchondral bone plate (SBP) and trabecular bone (TB) were analyzed by comparing data at the endpoint (day 55) to the obtained pre-injection (day -1). Complementary comparison of group effects was performed upon data normalization by dividing the endpoint by pre-injection data. Results were expressed as mean ± SD. Exceptional cases for which it was not possible to obtain results for at least 5 rats per group were not considered for statistical comparison.

### 4.3.8 Histology

The harvested knees were cleaned (skin, muscle) and then fixated using 10% neutral buffered formalin (NBF) for 5 days, followed by 7 decalcification cycles in EDTA, 7 days each, intercalated with 1 day re-fixation in 10% NBF every week. Fixation and decalcification were performed at room temperature. The decalcified knees were then dehydrated in a tissue processor (Leica biosystems, Netherlands) by sequential immersion in solutions of ethanol 96%, ethanol 100% and xylene, 3 cycles of 5h each, replaced with fresh solution upon each cycle. Then, the knees were infiltrated in series of paraffin wax at 62°C, for a total of 17h, and further embedded in paraffin wax. 5 µm transversal sections were obtained from paraffinized knee sections, using a Leica micrometer (RM2245, China). For staining (Leica autostainer XL, Germany), the sides were deparaffinized by sequential immersion in xylene (2x2 min), ethanol 100% (2x1 min), ethanol 50% (1 min) and demineralized water (≥ 15 s). Safranin-O/Fast Green/Hematoxylin (Saf-O) staining was performed by placing the deparaffinized slides in Weigert's hematoxylin (5 min), running tap water (10 min), 0.4% fast green aqueous solution (4 min), 1% acetic acid (2 x 2.5 min), 0.125% Saf-O solution (5 min), ethanol 96% (15 s), ethanol 100% (2 x 45 s), and xylene (2 x 5 min). In turn, Hematoxylin/Eosin (HE) staining was achieved by immersing deparaffinized slides in Weigert's hematoxylin (4 min), running tap water (5 min), acidified ethanol (EtOH

50%/HCl, 15 s), ethanol 70% (1 min), ammonia ethanol (15 s), ethanol 96% (1 min), eosin (1 min), ethanol 100% (2 x 1 min), and xylene (2 x 1 min). The slides were mounted by placing a thin coat of mounting medium (Pertex™, VWR, USA) and a cover glass on top. Mounted slides were left to dry and imaged using a NanoZoomer 2.0RS (40x resolution, Hamamatsu, Japan). HE slides were used to assess synovitis, by the Krenn score, as previously described [277]. Briefly, the parameters of synovial lining cell layer enlargement, resident cells density and inflammatory infiltrate were scored from 0 to 3, reaching a total of 0-9, where 0-1 means no synovitis; 2-4: low-grade synovitis and 5-9: high-grade synovitis. In turn, joint degeneration was evaluated in Saf-O stained slides through Mankin score, as stated elsewhere [278]. In short, 4 categories were scored as follows: cartilage degradation (0-5), cellularity (0-3), Saf-O staining (0-4), tidemark integrity (0-1). Their sum provides total scores ranging from 0 (healthy) to 14 (severe joint degeneration). Both score systems were randomly attributed by two blind evaluators individually. Averaged scores were used for data representation, plotted as mean ± SD.

### 4.3.9 Statistics

Statistical analysis was performed with GraphPad Prism 8.0.1. Normality was assessed by Shapiro-Wilk tests and Q-Q plots. Knee diameter measurements were assessed by mixed model analysis for group and timepoints comparison. Dynamic weight bearing was analyzed by 2-way-ANOVA for both group and timepoints. Systemic CEX release profiles were analyzed by two-tailed paired t-test, and multiple t-tests for further individual comparisons at each timepoint. µCT analysis was performed using Brown-Forsythe and Welch ANOVA tests for normal data, while non-normal data was assessed by Kruskal-Wallis tests. The histological scoring was analyzed by two-way-ANOVA, to correct for inter-observer variability. P-values $\leq 0.05$ were considered significant. To decrease the chance of discarding false negatives, p-values $< 0.1$ were also reported.

## 4.4 Results and Discussion

### 4.4.1 Assessment of knee edema and pain

Knee edema and pain are common OA symptoms, here evaluated by relation with knee diameter and dynamic weight bearing (DWB) analysis, respectively. The knee diameter measures prior OA induction were subtracted to the diameter of OA knees at each time-point, to assess for knee edema derived from OA progression (Figure 4.1). Even though there was a

slight trend of increased knee edema upon OA surgical induction, it trended to full recovery on the following days (-25 to -1). Thus, no OA-induced knee edema and no significant differences between groups after injection were found throughout all study (Figure 4.1).

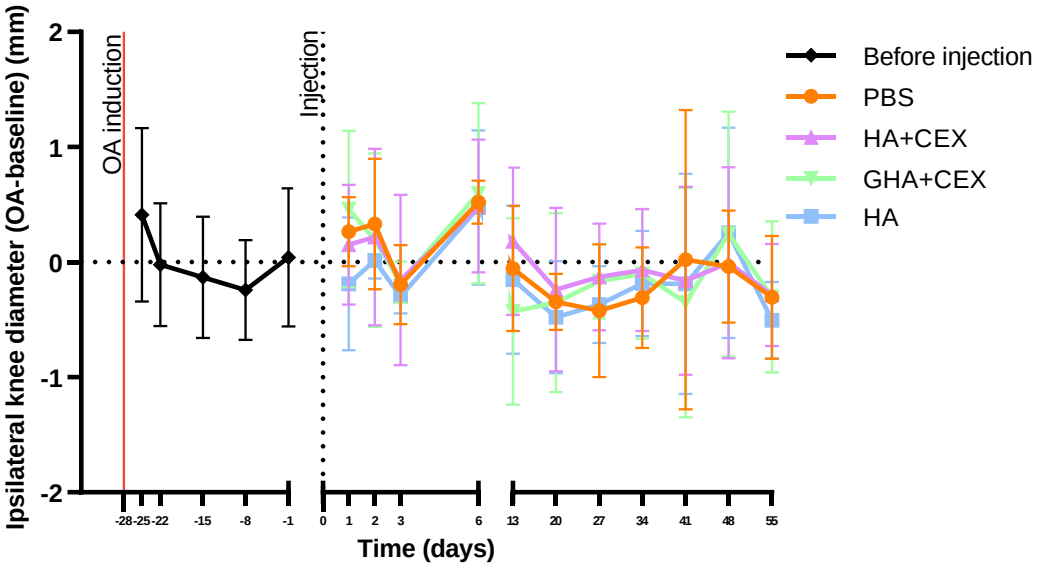


**Figure 4.1** - **Ipsilateral knee diameter** upon OA induction (days -25 to -1) and after IA injection (days 1 to 55), in respect to baseline (healthy, prior OA induction).

Regarding weight bearing analysis, differences between the non-affected limb (contralateral) and OA limb (ipsilateral) were used as pain indicator (Figure 4.2). Pain-induced behavior as measured by weight load transfer from the affected to the non-affected limb was noted. Before OA induction, there was an equivalent weight load on both limbs (50.6 ± 5%). One day prior to injection (3-weeks after OA induction), there was a significant increase of the weight load on the contralateral paw (61.2 ± 6.4%) in comparison to baseline ($p<0.0001$), which indicates unload of the ipsilateral paw as a response to OA-induced pain. Contralateral load reduction was observed for HA in comparison to control (PBS) at all timepoints, which was significant for days 3 ($p=0.0193$) and 6 ($p=0.0074$). GHA+CEX also presented a trend of lower contralateral load in comparison to control, from day 3 to 55, which was statistically significant at day 13 ($p=0.0232$). No significant differences were found between treatments at other timepoints, even though HA was slightly decreased compared to HA+CEX at day 6 ($p=0.0770$).

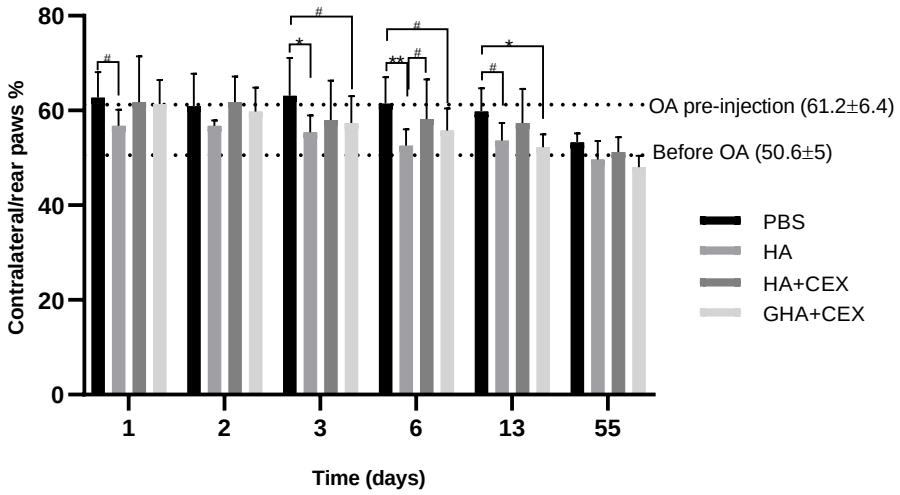


**Figure 4.2** – **Dynamic weight bearing analysis** of OA-induced pain-behavior assessed by the weight on the contralateral limb as a percentage of total weight distributed by both hind limbs. **p ≤ 0.01; *p ≤ 0.05; #p ≤ 0.1.

In terms of time-related differences, all groups presented significant reduction in the contralateral load bearing for the day 55, especially in comparison to the first timepoints. In respect to the contralateral load pre-injection, HA showed increased unloading over time from day 1 ($p=0.0719$, day 2: $p=0.0719$), which was significant from day 3 ($p=0.0188$, day 6: $p=0.0005$, day 13: $p=0.0025$ and day55: $p<0.0001$); GHA+CEX presented significant and successive reduction from day 6 ($p=0.0276$; day 13: $p=0.0003$; day 55: $p<0.0001$). Baseline-equivalent state (before OA) was achieved from day 6 ($p=0.3941$) for HA and from day 13 ($p=0.4781$) for GHA+CEX. The PBS and HA+CEX groups only presented reduced contralateral load and recovery-to-baseline at day 55. This reversion to symmetrical loading at day 55 suggest spontaneous healing, which limits the sensitivity of DWB analysis for pain evaluation in this animal model. Still, it was possible to observe that HA showed the faster analgesic action, from day 1, followed by GHA+CEX, from day 6. Moreover, within the first 13 days, both HA and GHA+CEX presented significant pain reduction in respect to control (PBS), whereas HA+CEX had no analgesic effect during that period.

### 4.4.2 Histological evaluation of synovial inflammation and joint degeneration

The synovial inflammation was scored for the most affected region of the synovium. According to the Krenn score, OA-induced synovial inflammation was significantly decreased for all the HA-based treatments (HA: $p=0.0007$; HA+CEX: $p=0.0456$; GHA+CEX: $p=0.0046$) in comparison to control (PBS) - Figure 4.3 a). The equal effective reduction of HA alone or when

combined with CEX with or without GS, may be related to the intrinsic anti-inflammatory action of HA and the low dose of CEX used, in comparison to other studies previously reported [40,52,55,57,270].

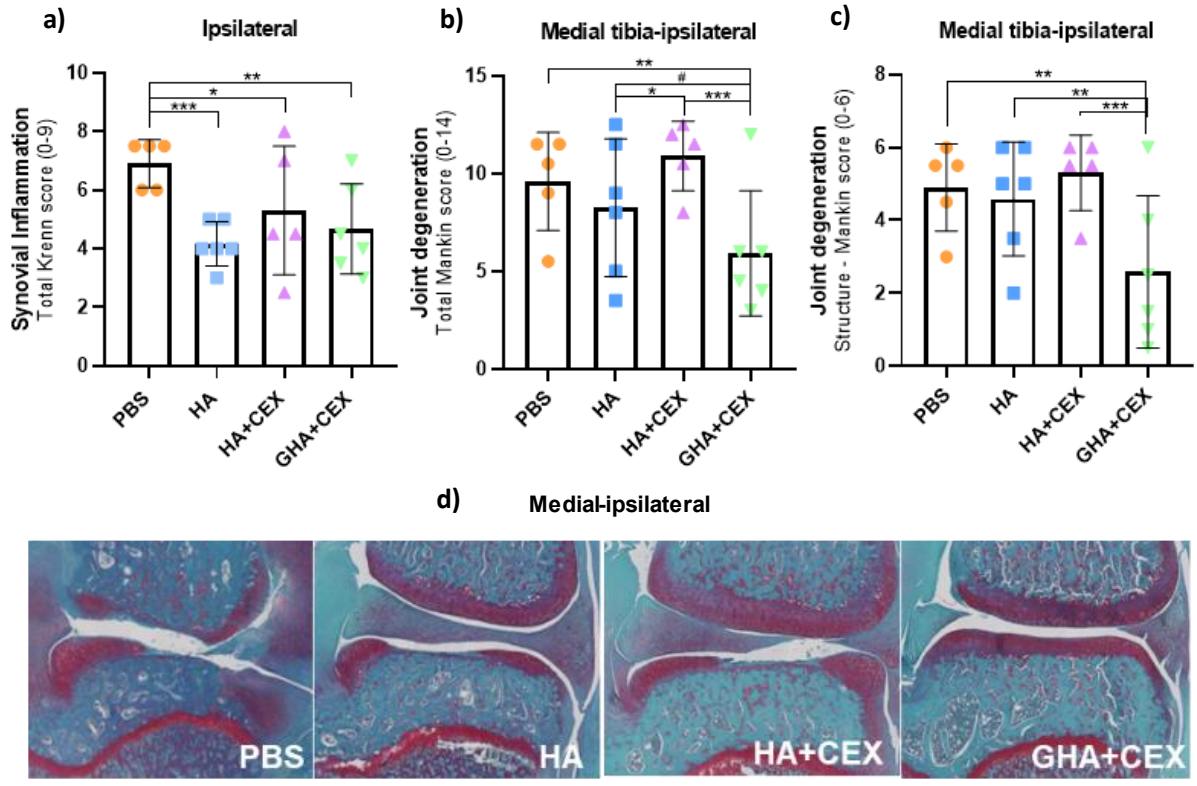


**Figure 4.3** – **Histological evaluation of the injectable effects in OA synovitis and joint degeneration**: **a**) Synovial inflammation as represented by the total Krenn score (0-9). **b**) Joint degeneration as represented by the total Mankin score (0-14). **c**) Degeneration of joint structure denoted by the structure Mankin subscore (0-6), and represented in **d**) Safranin-O/Fast Green-stained medial joint sections. ***$p \leq 0.001$; **$p \leq 0.01$; *$p \leq 0.05$; $^{\#}p \leq 0.1$. Remaining Mankin subscores represented in Figure C.2, Appendix C.

Regarding OA-induced joint degeneration, it was more severe for the medial tibia plateau, for which the histologic results are depicted in Figure 4.3 b-d). GHA+CEX substantially inhibited joint degeneration when compared to the other injectables (Figure 4.3 b, PBS: p=0.0071; HA: p=0.0658 and HA+CEX: p=0.0004), especially in terms of cartilage structure (Figure 4.3 c, d, PBS: p=0.0019; HA: p=0.0046 and HA+CEX: p=0.0004). HA treatment also reduced the total Mankin score in comparison to HA+CEX (p=0.0472), indicating that HA+CEX is only effective in inhibiting joint degeneration when combined with GS. This is consistent with chondroprotective action attributed to GHA+CEX. Only two other studies report a chondroprotective effect upon CEX intra-articular injection [52,270]. The first, in a rabbit OA model induced by anterior and posterior cruciate ligaments transection and medial meniscus excision, a total of 5 weekly CEX injections were administered, corresponding to a 3-fold higher CEX than the used

in the current study. The results were analyzed at the end of a 5-week period, after which the authors found delayed cartilage degeneration for both CEX and HA treatments in comparison to control (saline solution). Their study emphasizes that a continued CEX joint exposure, even at low concentration, may confer chondroprotective effect [52]. However, weekly injections are not a viable option since it is a mildly invasive procedure, and recurrent administration can lead to infection or other complications. Haartmans and colleagues also reported chondroprotective effect upon 12-weeks of CEX IA-injections in an OA rat model (male Lewis) surgically induced by the ACLT/pMMx. In their study, CEX injections were administered on both the affected and non-affected knees, each with 2.05x the amount herein injected [270]. Both studies confirm the chondroprotective potential of CEX intra-articular injections, but their findings are not directly comparable to ours, since different animal models, CEX concentrations and length of study were used, and thus different OA phenotypes and responses to treatment. The OA model herein used showed quite an aggressive OA-phenotype, which can hinder the real potential of the developed formulation [40]. Still, the novel formulation here explored could efficiently inhibit cartilage degeneration, as opposed to other studies using the same OA model, where IA CEX could not reach that effect, even at higher concentrations and prolonged CEX joint exposure [40,54].

### 4.4.3 Microtomography analysis of bone

#### 4.4.3.1 Changes in the subchondral bone plate

When evaluating healthy SBP, bone volume fractions (BV/TV) near 1 are expected as the volume of mineralized bone should match the total volume. To assess the relative effect of the different HA treatments and control (PBS), their comparison was made for normalized data (endpoint/pre-injection) - Figure 4.4. The non-treated joints tended to present reduced BV/TV values with respect to the treated animals. This was more evident for the tibia medial side, for which GHA+CEX significantly inhibited SBP degeneration (Figure 4.4 a), as represented in Figure 4.4 i, j). Complementary analysis was achieved by assessing the endpoint (day 55) results compared to the pre-injection (day -1) ones - Figure 4.5. OA progression as measured by BV/TV could not be prevented by injection of PBS, HA or HA+CEX as demonstrated by a significant reduction, not found upon injection of GHA+CEX (Figure 4.5 a), thus suggesting a protective effect conferred by GHA+CEX but not the other treatments. Even though CEX derived-inhibition of SBP changes, such as sclerosis, have been previously reported, to the best of our knowledge, this is the first study reporting an intra-articular CEX formulation able to inhibit

subchondral bone degeneration, at a single dose, 180x up to 5000x lower than the oral doses required to inhibit bone loss in arthritis rat models [46,279–282]. Whereas subchondral bone defects occur upon deep cartilage deterioration (osteochondral defects), cartilage lesions can occur without disrupting the structural integrity of the subchondral bone (chondral defects) [283]. As such, GHA+CEX not only provided chondroprotective action (section 4.4.2), but it also prevented bone lesions, emphasizing as major novelty the added-value of GS in potentiating those effects, retarding OA-progression. This beneficial action attributed by GS when combined to HA+CEX, may be partially associated to at least 2 routes: enhanced CEX bioavailability conferred by GS, and the intrinsic GS lubricant properties. However, further studies would have

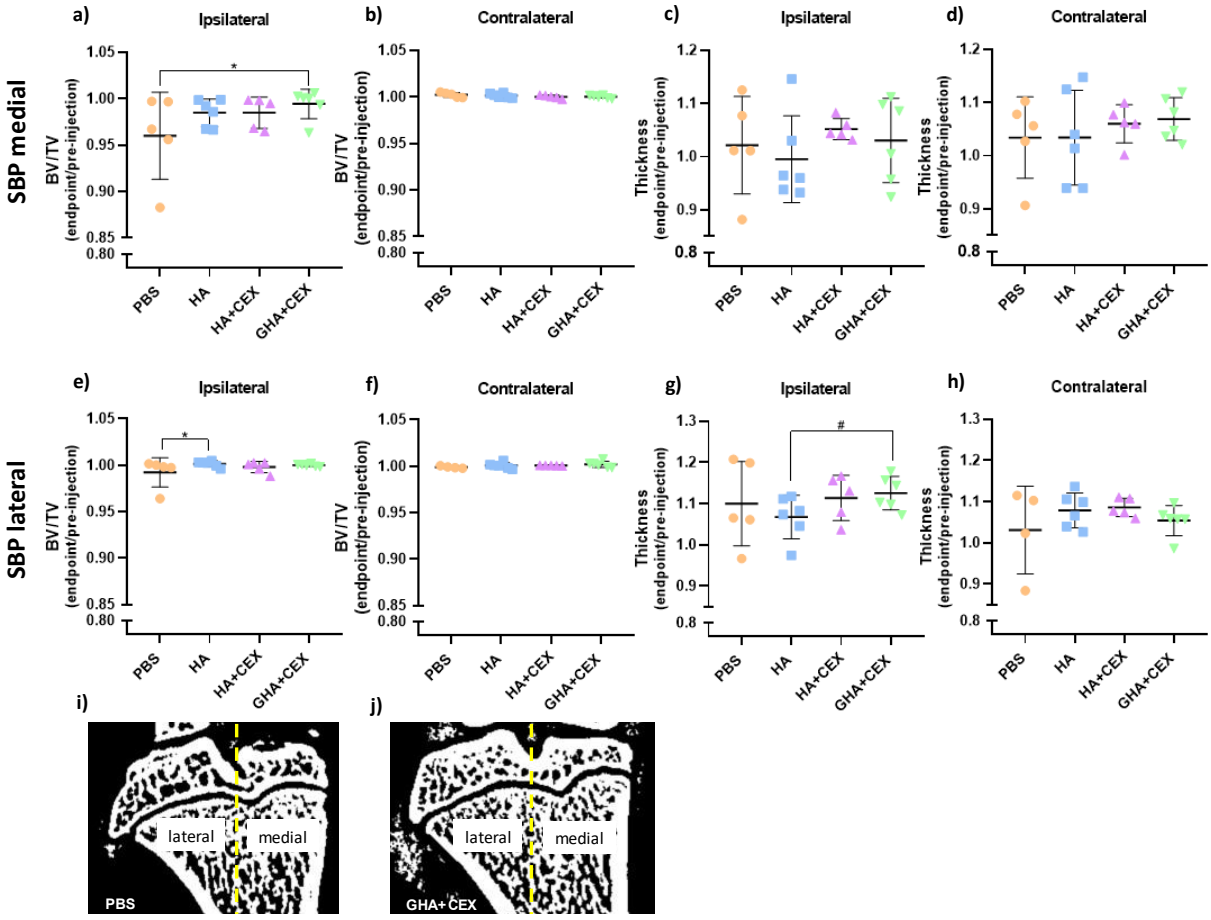


**Figure 4.4** - **Subchondral bone plate (SBP) thickness and bone volume fraction of the tibia plateau.** Micro-computed tomography (μCT) analysis on the differences between groups (data represented as endpoint/pre-injection). Ipsilateral: OA limb; Contralateral: non-OA limb. **a**) Ipsilateral bone volume fraction (BV/TV) significantly reduced for PBS in respect GHA+CEX ($p=0.0252$). **b**) No changes in contralateral BV/TV. **c**) No significant changes in ipsilateral thickness. **d**) No significant changes in contralateral thickness. **e**) Ipsilateral BV/TV slightly reduced for PBS compared to HA ($p=0.0363$). **f**) No changes in contralateral BV/TV (no comparison with control (PBS, n=4). **g**) Trend towards ipsilateral thickness increase for GHA+CEX compared to HA ($p=0.0599$). **h**) No significant changes in contralateral thickness (no comparison with PBS (n=4)). **i**) μCT frame for ipsilateral knee injected with PBS (no treatment), compared to **j**) Ipsilateral μCT of knee injected with GHA+CEX. $^{**}p \leq 0.01$; $^{*}p \leq 0.05$; $^{\#}p \leq 0.1$.

to be conducted to explore the relative extent of these effects, for instance in terms of cause-response, mechanisms, and durability.

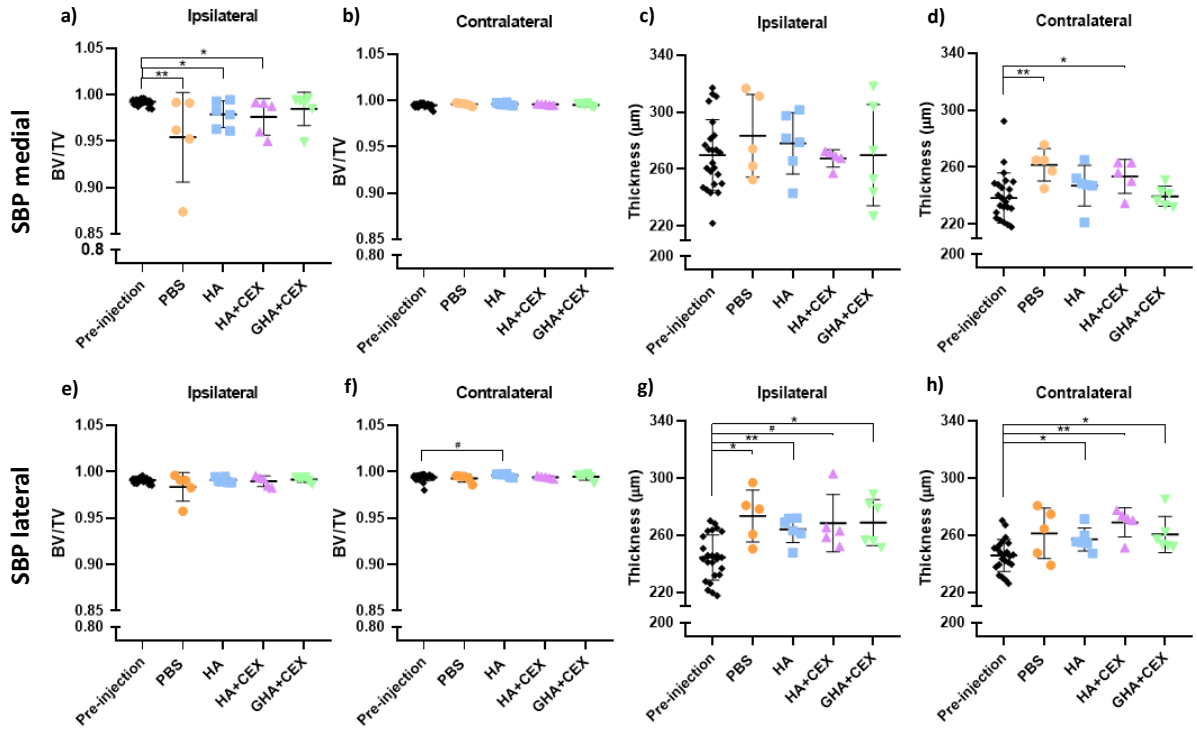


**Figure 4.5 - Subchondral bone plate (SBP) thickness and bone volume fraction of the tibia plateau –** Micro-computed tomography (µCT) changes at day 55 compared to day -1 (OA pre-injection). Ipsilateral: OA limb; Contralateral: non-OA limb. **a**) Ipsilateral BV/TV significantly reduced for PBS (p=0.0064), HA (p=0.0306) and HA+CEX (p=0.0168) compared to OA pre-injection. **b**) No differences in contralateral BV/TV before or after injection. **c**) No significant changes in ipsilateral thickness prior to and upon injection. **d**) Contralateral thickness significantly increased 2 months after injection of PBS (p=0.0051) or HA+CEX (p=0.0463). **e**) No significant differences in ipsilateral BV/TV. **f**) No relevant differences considered for contralateral BV/TV, even though HA vs pre-injection: p=0.0893. **g**) Ipsilateral thickness increased for all groups injected in comparison to OA pre-injection (PBS: p= 0.0189; HA: p=0.0015; HA+CEX: p=0.0520; GHA+CEX: p=0.0110). **h**) Contralateral thickness increase for all groups injected in comparison to OA pre-injection, significant for HA: p=0.0173, HA+CEX: p=0.0037, and GHA+CEX: p=0.0165. **p ≤ 0.01; *p ≤ 0.05; $^{\#}$p ≤ 0.1.

In rat models, SPB thickness may vary along time due to growth, which does not occur in humans. From the µCT analysis, no significant differences in SBP medial thickness between treated or non-treated animals were noted (Figure 4.4 c, d) nor in comparison to pre-injection for the affected limb (Figure 4.5 c). However, there was a significant increase in the medial contralateral subchondral bone thickness for animals injected with PBS or HA+CEX when compared to thickness prior to injection (Figure 4.5 d). This effect is consistent with the DWB data (Figure 4.2), that showed higher and prolonged contralateral load for those groups after

injection, thus supporting SBP thickening as response to higher load on that paw. This is in line with other studies, that also reported subchondral bone changes in the contralateral limb due to compensatory loading, although those may also translate in SBP loss, especially at early stages after OA induction [284,285].

For the lateral SBP, ipsilateral thickness tended to be slightly higher for GHA+CEX compared to HA (Figure 4.4 g), and no injection-related effects were found on the contralateral limb (Figure 4.4 h). In all injected joints, increased thickness at day 55 was noted in comparison to pre-injection Figure 4.5 g, h). However, since this change was observed for both the affected and the contralateral limbs, it is most probably related with rat growth rather than sclerosis, even though it cannot be ruled out.

#### 4.4.3.2 Changes in the trabecular bone

Since in rats the growth plate does not close with adulthood, growth related changes are expected as chondrocytes undergo hypertrophy and calcification along animals growing. On the ipsilateral medial side, GHA+CEX inhibited the increase of BV/TV compared to PBS and HA (Figure 4.6 a), the same groups that presented significant increase compared to OA pre-injection (Figure 4.7 a). A similar trend was observed for the contralateral side; despite no significant differences between injections were found (Figure 4.6 b), when compared to pre-injection, all injectables significantly increased BV/TV, except GHA+CEX (Figure 4.7 b). The trabecular bone volume fraction of the lateral side tended to decrease upon treatments with CEX for both ipsilateral and contralateral limbs (Figure 4.6 e, f), but only significantly for HA+CEX in comparison to HA. Oppositely, HA+CEX increased contralateral trabecular thickness in respect to HA (Figure 4.6 h), thus HA+CEX induced changes do not seem to be related with bone growth inhibition; which is also evidenced by the consistent significant growth-increases on the contralateral limb, after 2 months (Figure 4.7 b, d, f, h). Regarding thickness, the affected limb presented OA-induced increase when compared to the contralateral, more evident for the medial side and tendentially lower for GHA+CEX in respect to the other injections, despite non-significant (Figure 4.6 c, d). In comparison to OA pre-injection, all groups presented significant thickness increase for the medial TB (Figure 4.7 c). GHA+CEX inhibited growth-induced thickness for the contralateral medial side (Figure 4.7 d) and ipsilateral lateral side (Figure 4.7 g).

In sum, GHA+CEX systemically inhibited growth induced increases in thickness and bone volume fraction, in both medial and lateral trabecular bone, more pronounced on the medial

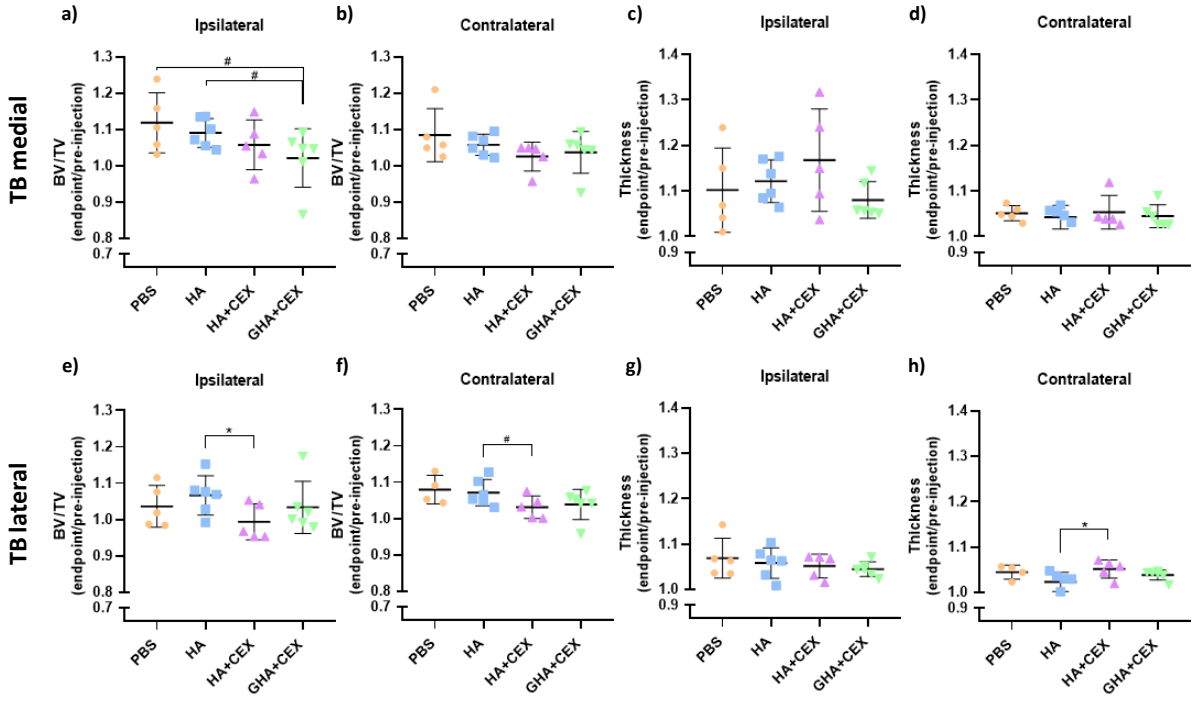


**Figure 4.6** - **Trabecular bone (TB) volume fraction and thickness of the tibia plateau.** Micro-computed tomography (μCT) analysis on the differences between groups**.** Ipsilateral: OA limb; Contralateral: non-OA limb. **a**) Trend towards ipsilateral bone volume fraction (BV/TV) reduction for GHA+CEX in respect PBS (p=0.0831) and HA (p=0.0999). **b**) No significant changes in contralateral BV/TV. **c**) No significant changes in ipsilateral thickness. **d**) No significant changes in contralateral thickness. **e**) Ipsilateral BV/TV significantly reduced for HA+CEX compared to HA (p=0.0445). **f**) Contralateral BV/TV significantly reduced for HA+CEX in respect to HA (p=0.08) (no statistic comparison with PBS, n=4). **g**) No significant changes in ipsilateral thickness. **h**) Contralateral thickness significantly increased for HA+CEX compared to HA (p=0.0495). *p ≤ 0.05; #p ≤ 0.1.

side. As most of these alterations are also observed in the contralateral (non-OA) joint, it is unclear what mechanism would cause such changes, but it might be related to CEX as it has been previously associated to inhibition of bone changes derived from decreased chondrocyte hypertrophic differentiation [40,286]. Chondrocyte hypertrophy is involved in bone ossification and cartilage calcification, a hallmark of osteoarthritis. Thus, in the context of OA, bone growth inhibition is beneficial for hyaline cartilage as it prevents chondrocyte hypertrophy and/or calcification. In turn, cartilage calcification is associated with histological degeneration of the joint [287,288], which was more efficiently inhibited by GHA+CEX in comparison to other treatments, as shown in section 4.4.2. This correlation between the inhibition of cartilage degeneration and bone changes is consistent with inhibited chondrocyte-induced bone formation and thus, further supports the chondroprotective action attributed to GHA+CEX. In adult humans, this would be the only expected effect since the growth plates are closed.

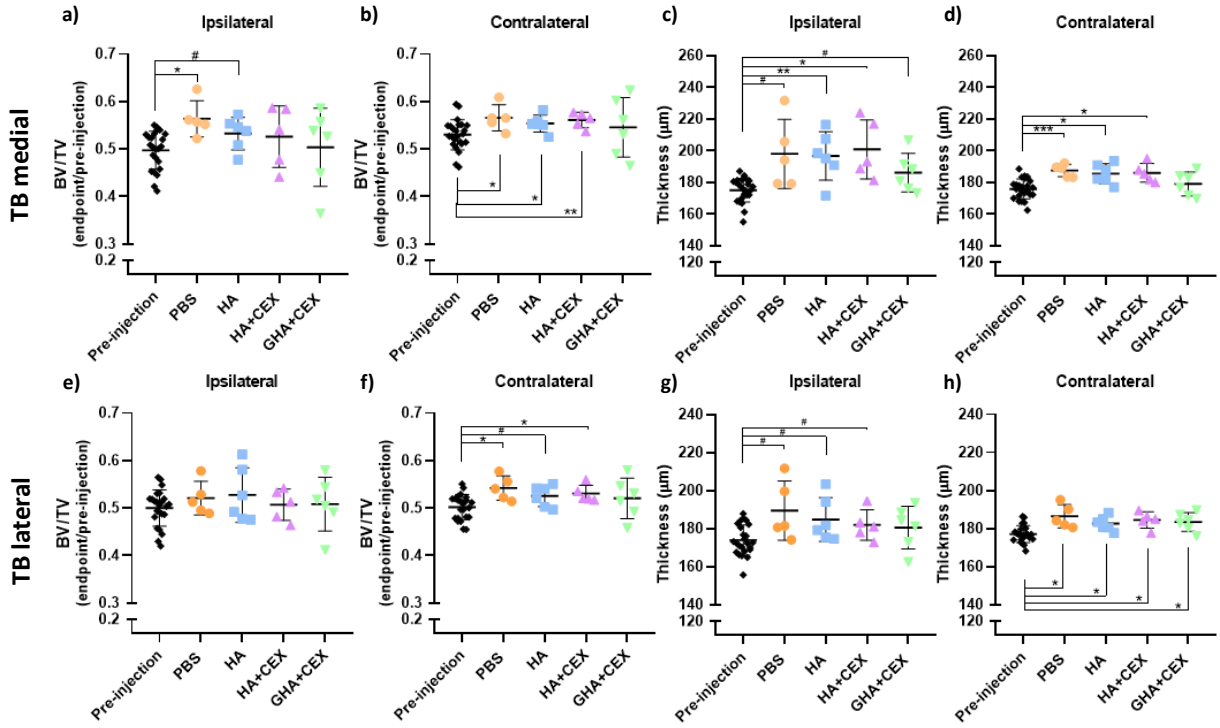


**Figure 4.7 - Trabecular bone (TB) volume fraction and thickness of the tibia plateau.** Micro-computed tomography (µCT) analysis on the differences of OA pre-injection and 2-months upon injections**.** Ipsilateral: OA limb; Contralateral: non-OA limb. **a**) Ipsilateral BV/TV significantly reduced for PBS (p=0.0126) and HA (p=0.0585) compared to OA pre-injection. **b**) Contralateral BV/TV significantly increased 2 months after injection with PBS (p=0.0411), HA (p=0.0307) and HA+CEX (p=0.008), but not GHA+CEX, in comparison to pre-injection. **c**) Ipsilateral thickness increased for all groups injected in comparison to OA pre-injection (PBS: p=0.0784; HA: p=0.0171; HA+CEX: p=0.0351; GHA+CEX: p=0.0780). **d**) Contralateral thickness significantly increased 2 months after injection of PBS (p=0.0005), HA (p=0.0102) or HA+CEX (p=0.0131), but not GHA+CEX, in comparison to pre-injection. **e**) No significant changes in ipsilateral BV/TV before and after injection. **f**) Contralateral BV/TV tendentially increased upon injection with PBS (p=0.0195), HA (p=0.0551) or HA+CEX (p=0.0174). **g**) Ipsilateral thickness tended to increase for groups injected with PBS: p=0.0882; HA: p=0.0709; HA+CEX: p=0.0899, but not for GHA+CEX, in comparison to OA pre-injection. **h**) Contralateral thickness significantly increased for all groups injected in comparison to OA pre-injection (PBS: p=0.0230; HA: p=0.0133; HA+CEX: p=0.0132; GHA+CEX: p=0.0228). ***p ≤ 0.001; **p ≤ 0.01; *p ≤ 0.05; #p ≤ 0.1.

### 4.4.4 Systemic CEX exposure

Given the low amount of synovial fluid in rats, it was not possible to locally monitor CEX concentration. Thus, the systemic CEX levels were taken as indirect measure of intra-articular concentration.

Even though this CEX release is not comparable with the previously performed *in vitro* (Chapter 3, section 3.4.3) as that was made trying to mimic a local release rather than systemic, these *in vivo* release profiles suggest a rapid clearance in the first 24h, despite lower for GHA+CEX than HA+CEX.

When comparing the CEX systemic release (Figure 4.8), the profile of both groups increased in the first 6h and decreased thereafter. Residual CEX was detected from 72h onward. GHA+CEX presented significant lower CEX release than HA+CEX (p=0.0342), especially at 2h (p=0.0184), 4h (p=0.0206), 6h (p=0.0259), 8h (p=0.0154), 24h (p=0.0348) and 48h (p=0.0006).

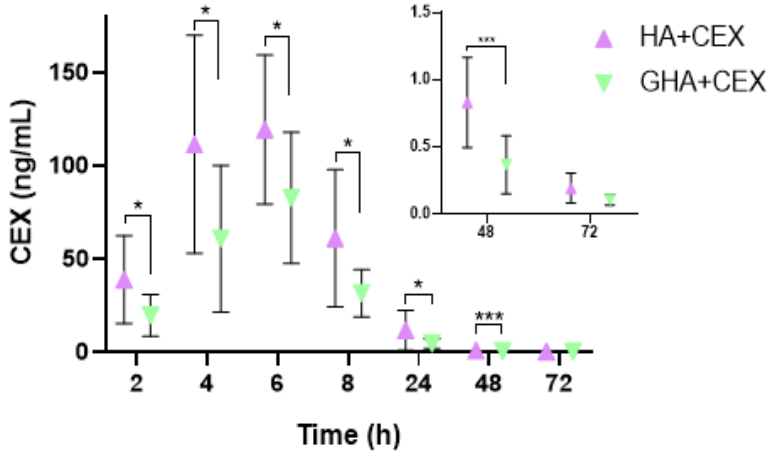


**Figure 4.8 – Celecoxib quantified systemically 2 to 72 h upon intra-articular injection.** HA+CEX and GHA +CEX release profiles with significantly higher CEX released systemically for HA+CEX in comparison to GHA +CEX. ***p ≤ 0.001; **p ≤ 0.01; *p ≤ 0.05.

Therefore, GHA+CEX reduced CEX systemic exposure, expectedly caused by prolonged CEX retention in the joints, and/or slower CEX release in the joints, but at such low levels that these result in undetectable systemic levels. Both hypotheses are consistent with the increased CEX bioavailability conferred by GS, and with longer therapeutic action for GHA+CEX, which may be a suggestive explanation for the analgesic effect observed for GHA+CEX but not for HA+CEX, compared to PBS (section 4.4.1). A CEX improved action may also explain, at least partially, the higher therapeutic potential of GHA+CEX in comparison to HA+CEX in terms of the ability to inhibit bone changes and cartilage degeneration.

## 4.5 Conclusions

Hyaluronic acid and celecoxib have reported advantages for OA treatment, especially in terms of pain, but no intra-articular (IA) injections with CEX, let alone HA+CEX, are yet clinically available, possibly given CEX's low solubility and hence bioavailability. This was improved by incorporating CEX in a formulation combining GS and HA, as designed in the previous chapters. In this chapter, the effect of the designed IA injectable (GHA+CEX) was studied *in vivo*, in a post-traumatic OA rat model, versus HA+CEX and HA. No adverse effects were detected.

The results support that GHA+CEX was safe for IA-administration and effective in reducing pain and synovitis. Thus, it could be an alternative to commercial viscosupplements, while adding improved therapeutic action not conferred by HA or HA+CEX without GS: inhibition of OA-progression, especially in terms of cartilage and bone degeneration, even at low CEX dosage. Follow-up research is necessary to understand the role of GS, further validate GHA+CEX in terms of long-term effect and to explore how these findings translate to other animal models or humans. Still, the evidence here gathered for GHA+CEX showed its potential as alternative OA-therapy.

# 5

# CONCLUDING REMARKS AND OUTLOOK

## 5.1 Work integration and major achievements

The work developed throughout the course of this thesis, makes a valuable contribution for state-of-the-art development, with special emphasis on the limitless potential of LTTMs in the pharmaceutical and biomaterials engineering fields. From LTTM characterization applied to drugs and biopolymers to a particular biomedical application, the work herein developed is on the way to pursue translational research into innovation, namely towards novel osteoarthritis therapies.

Osteoarthritis is the most common form of arthritis and a leading cause of disability worldwide. Given the limitations and drawbacks of current therapies for OA, it is crucial to explore alternatives. In this context, the new formulation herein developed was designed to be an innovative and improved therapeutic using human-approved products combining the following unmet clinical needs:

i. **Combined local administration of hyaluronic acid (HA) and celecoxib (CEX):** increased therapeutic efficiency and convenience (2-in-1). While both are individually approved for viscosupplementation or oral uptake, respectively, no intra-articular injectables are clinically available with CEX or HA+CEX, mostly due to CEX low bioavailability, which leads to the next clinical need;
ii. **Enhanced CEX bioavailability**. CEX oral administration is a first-line treatment option for OA pain, since it selectively inhibits COX-2, reducing inflammation, pain, and the side effects of non-selective COX-1 inhibition. Thus, it has improved safety profile in respect to non-specific NSAIDs. However, its continued use still causes systemic side effects, especially given the high doses needed to reach therapeutic efficacy, due to CEX low

bioavailability. Thus, CEX therapy is time-limited, and its efficiency impaired. For these reasons, a local injectable with enhanced CEX bioavailability, can mitigate systemic exposure and related adverse effects, as it targets the affected region, increasing CEX availability and effective action, while reducing the dose needed for therapeutic efficacy. Here, CEX bioavailability improvement was achieved by local administration and by solubilization and dispersion in the delivery system compared to the physiologic media: the CEX solubility increased 5-fold in a specifically chosen media containing an LTTM of glycerol:sorbitol (GS), and at least 25-fold when combined with GS and HA;

iii. **Improved therapeutic efficiency**. The GS composition was designed to incorporate lubricant properties, thus increasing the injectable power to supplement the synovial fluid (liquid lubricating joints). Both glycerol and sorbitol are FDA and EMA-approved for pharma-applications, and at least one is authorized for intra-articular administration at concentrations higher than the content of HA+GS+CEX. Moreover, GS conferred an alternative media able to incorporate both HA and CEX, combining their therapeutic effect, further enhanced by the increased CEX bioavailability, and thus, efficiency. The *in vivo* studies in an OA rat model supported increased therapeutic action of the injectable with GS in comparison to CEX+HA without it. The obtained results suggest HA+GS+CEX as a strong candidate to disease-modifying-osteoarthritis-drug (DMOAD), given its potential to inhibit cartilage and bone degradation, even in an advanced OA model, and using rather low amounts of CEX.

In sum, HA+GS+CEX provides a novel therapeutic approach combining a 2-in-1 mixture of HA+CEX in a GS carrier for intra-articular injection. It is not only an alternative to common viscosupplements and oral CEX uptake, but also a synergetic cocktail, expected to increase therapeutic outcomes, while bypassing or accelerating validation from regulatory entities, since all constituents are individually approved. To protect the intellectual property rights (IPR) of the developed product, an international patent application was already submitted (PCT/IB2024/056817).

## 5.2 Challenges and Prospects

The current achievements have led to a turning point where market validation is a priority to further research development. In this sense, funding is being pursued towards entrepreneurial science, aiming to study the feasibility of transferring results from the laboratory to the market. Here are some of the envisioned approaches to do so:

i. **Translation from research into innovative therapy.** Even though HA+GS+CEX showed promising therapeutic potential in a post-traumatic OA model, these findings are not

directly relatable to other animal models or even type of OA (e.g: spontaneous vs chemically or surgically induced). Thus, it is important to further explore the extent of the HA+GS+CEX effects to validate trials in OA patients, either animals or humans;

ii. **Market need.** Despite there is scientific evidence on the potential of HA+GS+CEX as alternative OA therapy, before advancing to further product development or optimization, it is crucial to assess its acceptance towards the medical community and potential industry partners;

iii. **Market value and competition.** Even though the scientific study here conducted evidenced the higher therapeutic efficiency of HA+GS+CEX versus HA, as representative of commercial viscosupplements, these findings are not straightforward. A multitude of factors, such as the concentration, molecular weight, origin, type of HA (linear, cross-linked), administration site (e.g: knee, hip), OA stage and other comorbidities, significantly impact their therapeutic efficacy, even though there are no consensus on the best properties or approaches. Thus, HA+GS+CEX may have theoretical advantage, but not proven either against marketed viscosupplements or other competitors such as corticosteroid injections or CINGAL®(HA+corticosteroid). In this context, while it is not yet possible to make those comparisons, it is important to establish the relative market value of HA+GS+CEX and the potential social and economic advantages that justify its market introduction.

iv. **Scale-up design:** it is important to ensure that the scale-up of the product is possible and reproducible, first at pilot and then industrial scale. From the production to the packing and delivery, it is necessary to find and establish strategies that ensure quality control and sterilization.

v. **Industrial production:** it is crucial to find potential partners for human and veterinary products, able to produce the product at industrial scale under the necessary regulatory guidelines.

Overall, the main research goals initially proposed on the scope of the thesis were met, ultimately leading to promising outcomes, that support the translation of the developed product from research into innovation.

# REFERENCES


1. Osteoarthritis Foundation International Available online: https://oafifoundation.com/en (accessed on Dec 5, 2023).
2. NIH Osteoarthritis Available online: https://www.niams.nih.gov/health-topics/osteoarthritis (accessed on Jan 3, 2024).
3. Dai, Y.; van Spronsen, J.; Witkamp, G.-J.; Verpoorte, R.; Choi, Y.H. Ionic Liquids and Deep Eutectic Solvents in Natural Products Research: Mixtures of Solids as Extraction Solvents. *J. Nat. Prod.* **2013**, *76*, 2162–2173; DOI:10.1021/np400051w.
4. Castro, V.I.B.; Mano, F.; Reis, R.L.; Paiva, A.; Duarte, A.R.C. Synthesis and Physical and Thermodynamic Properties of Lactic Acid and Malic Acid-Based Natural Deep Eutectic Solvents. *J. Chem. Eng. Data* **2018**, *63*, 2548–2556; DOI:10.1021/acs.jced.7b01037.
5. Santos, F.; Leitão, M.I.P.S.; Duarte, A.R.C. Properties of Therapeutic Deep Eutectic Solvents of L-Arginine and Ethambutol for Tuberculosis Treatment. *Molecules* **2019**, *24*, 55; DOI:10.3390/molecules24010055.
6. Tuntarawongsa, S.; Phaechamud, T. Polymeric Eutectic System. *Adv. Mater. Res.* **2012**; DOI:10.4028/www.scientific.net/amr.528.180.
7. Tuntarawongsa, S.; Phaechamud, T. Polymeric Eutectic Drug Delivery System. *J. Met. Mater. Miner.* **2012**, *22*, 27–32.
8. Liu, Y.; Zhang, Y.; Chen, S.N.; Friesen, J.B.; Nikolić, D.; Choules, M.P.; McAlpine, J.B.; Lankin, D.C.; Gemeinhart, R.A.; Pauli, G.F. The influence of natural deep eutectic solvents on bioactive natural products: studying interactions between a hydrogel model and Schisandra chinensis metabolites. *Fitoterapia* **2018**, *127*, 212–219; DOI:10.1016/j.fitote.2018.02.024.
9. Mano, F.; Aroso, I.M.; Barreiros, S.; Borges, J.P.; Reis, R.L.; Duarte, A.R.C.; Paiva, A. Production of poly(vinyl alcohol) (PVA) fibers with encapsulated natural deep eutectic solvent (NADES) using electrospinning. *ACS Sustain. Chem. Eng.* **2015**, *3*, 2504–2509; DOI:10.1021/acssuschemeng.5b00613.
10. Mano, F.; Martins, M.; Sá-nogueira, I.; Barreiros, S.; Borges, J.P.; Reis, R.L.; Duarte, A.R.C.; Paiva, A. Production of Electrospun Fast-Dissolving Drug Delivery Systems with Therapeutic Eutectic Systems Encapsulated in Gelatin. *AAPS PharmSciTech* **2017**, *18*, 2579–2585; DOI:10.1208/s12249-016-0703-z.
11. Silva, J.M.; Akkache, S.; Araújo, A.C.; Masmoudi, Y.; Reis, R.L.; Badens, E.; Duarte, A.R.C. Development of innovative medical devices by dispersing fatty acid eutectic blend on gauzes using supercritical particle generation processes. *Mater. Sci. Eng. C* **2019**, *99*,

599–610; DOI:10.1016/j.msec.2019.02.012.
12. Dhandayuthapani, B.; Yoshida, Y.; Maekawa, T.; Kumar, D.S. Polymeric Scaffolds in Tissue Engineering Application: A Review. *Int. J. Polym. Sci.* **2011**, *2011*, 1–19; DOI:10.1155/2011/290602.
13. Ferreira, V.R.A.; Azenha, M.A.; Pinto, A.C.; Santos, P.R.M.; Pereira, C.M.; Silva, A.F. Development of mesoporous polysaccharide/sol-gel composites with two different templating agents: Surfactants and choline chloride-based deep eutectic solvents. *eXPRESS Polym. Lett.* **2019**, *13*, 261–275; DOI:10.3144/expresspolymlett.2019.22.
14. Qin, H.; Owyeung, R.E.; Sonkusale, S.R.; Panzer, M.J. Highly stretchable and nonvolatile gelatin-supported deep eutectic solvent gel electrolyte-based ionic skins for strain and pressure sensing. *J. Mater. Chem. C* **2019**, *7*, 601–608; DOI:10.1039/C8TC05918G.
15. Quinn, M. Structures of a Synovial Joint Available online: https://teachmeanatomy.info/the-basics/joints-basic/synovial-joint/ (accessed on May 13, 2020).
16. Tamer, T.M. Hyaluronan and synovial joint: Function, distribution and healing. *Interdiscip. Toxicol.* **2013**, *6*, 111–125; DOI:10.2478/intox-2013-0019.
17. Kraus, V.B.; Blanco, F.J.; Englund, M.; Karsdal, M.A.; Lohmander, L.S. Call for Standardized Definitions of Osteoarthritis and Risk Stratification for Clinical Trials and Clinical Use. *Osteoarthr. Cartil.* **2015**, *23*, 1233–1241; DOI:10.1016/j.joca.2015.03.036.
18. Mao, L.; Wu, W.; Wang, M.; Guo, J.; Li, H.; Zhang, S.; Xu, J.; Zou, J. Targeted treatment for osteoarthritis: drugs and delivery system. *Drug Deliv.* **2021**, *28*, 1861–1876; DOI:10.1080/10717544.2021.1971798.
19. Vina, E.R.; Kwoh, C.K. Epidemiology of Osteoarthritis: Literature Update. *Curr. Opin. Rheumatol.* **2018**, *30*, 160–167; DOI:10.1097/BOR.0000000000000479.
20. IHME GBD Compare Available online: https://vizhub.healthdata.org/gbd-compare/ (accessed on Jan 9, 2024).
21. Cooper, C.; Dennison, E.; Edwards, M.; Litwic, A. Epidemiology of osteoarthritis. *Medicographia* **2013**, *35*, 145–151.
22. Nelson, A.E. Osteoarthritis year in review 2017: clinical. *Osteoarthr. Cartil.* **2018**, *26*, 319–325; DOI:10.1016/j.joca.2017.11.014.
23. Parker, D.A.; Scholes, C.; Neri, T. Non-operative treatment options for knee osteoarthritis : current concepts Current concepts. *J. ISAKOS* **2018**, *3*, 274–281; DOI:10.1136/jisakos-2016-000094.
24. Roubille, C.; Martel-Pelletier, J.; Pelletier, J.P. Osteoarthritis treatments: where do we stand at the moment? *Medicographia* **2013**, *35*, 172–180.
25. Bannuru, R.R.; Osani, M.C.; Vaysbrot, E.E.; Arden, N.K.; Bennell, K.; Bierma-Zeinstra, S.M.A.; Kraus, V.B.; Lohmander, L.S.; Abbott, J.H.; Bhandari, M.; et al. OARSI guidelines for the non-surgical management of knee, hip, and polyarticular osteoarthritis. *Osteoarthr. Cartil.* **2019**, *27*, 1578–1589; DOI:10.1016/j.joca.2019.06.011.
26. Richard, M.J.; Driban, J.B.; McAlindon, T.E. Pharmaceutical treatment of osteoarthritis. *Osteoarthr. Cartil.* **2023**, *31*, 458–466; DOI:10.1016/j.joca.2022.11.005.
27. Hochberg, M.C. Osteoarthritis: new approaches. *Medicographia* **2013**, *35*, 139–141.
28. McAlindon, T.E.; Bannuru, R.R.; Sullivan, M.C.; Arden, N.K.; Berenbaum, F.; Bierma-Zeinstra, S.M.; Hawker, G.A.; Henrotin, Y.; Hunter, D.J.; Kawaguchi, H.; et al. OARSI guidelines for the non-surgical management of knee osteoarthritis. *Osteoarthr. Cartil.*

**2014**, *22*, 363–388; DOI:10.1016/j.joca.2014.01.003.
29. Pavelka, K.; Bruyère, O.; Cooper, C.; John, A.K.; Leeb, B.F.; Maheu, E.; Martel-Pelletier, J.; Monfort, J.; Pelletier, J.-P.; Reginster, J.-Y. Diacerein: Benefits , Risks and Place in the Management of Osteoarthritis. An Opinion-Based Report from the ESCEO. *Drugs Aging* **2016**, *33*, 75–85; DOI:10.1007/s40266-016-0347-4.
30. Singh, J.A.; Noorbaloochi, S.; Macdonald, R.; Maxwell, L.J. Chondroitin for osteoarthritis. *Cochrane Database Syst. Rev.* **2015**, *2017*; DOI:10.1002/14651858.CD005614.pub2.
31. Gallagher, B.; Tjoumakaris, F.P.; Harwood, M.I.; Good, R.P.; Ciccotti, M.G.; Freedman, K.B. Chondroprotection and the prevention of osteoarthritis progression of the knee: A systematic review of treatment agents. *Am. J. Sports Med.* **2015**, *43*, 734–744; DOI:10.1177/0363546514533777.
32. Barnhill, J.G.; Fye, C.L.; Williams, D.W.; Reda, D.J.; Harris, C.L.; Clegg, D.O. Chondroitin product selection for the Glucosamine/Chondroitin Arthritis Intervention Trial. *J. Am. Pharm. Assoc.* **2006**, *46*, 14–24; DOI:10.1331/154434506775268616.
33. Sawitzke, A.D.; Shi, H.; Finco, M.F.; Dunlop, D.D.; Harris, C.L.; Singer, N.G.; Bradley, J.D.; Silver, D.; Jackson, C.G.; Lane, N.E.; et al. Clinical efficacy and safety over two years use of glucosamine, chondroitin sulfate, their combination, celecoxib or placebo taken to treat osteoarthritis of the knee: a GAIT report. *Ann Rheum Dis* **2010**, *69*, 1459–1464; DOI:10.1136/ard.2009.120469.
34. Kubo, M.; Ando, K.; Mimura, T.; Matsusue, Y.; Mori, K. Chondroitin sulfate for the treatment of hip and knee osteoarthritis: Current status and future trends. *Life Sci.* **2009**, *85*, 477–483; DOI:10.1016/j.lfs.2009.08.005.
35. Malone, M.A.; Kaushik, N.; Waheed, A. Intra-Articular Steroids; How Soon and How Often after the First Injection? *SM J. Community Med.* **2016**, *2*, 1–2.
36. Kamel, S.I.; Rosas, H.G.; Gorbachova, T. Local and Systemic Side Effects of Corticosteroid Injections for Musculoskeletal Indications. *Am. J. Roentgenol.* **2024**, *222*, 1–12; DOI:10.2214/AJR.23.30458.
37. Hunter, D.J. Viscosupplementation for Osteoarthritis of the Knee. *N. Engl. J. Med.* **2015**, *372*, 1040–1047; DOI:10.1056/NEJMct1215534.
38. Rai, M.F.; Christine, T.N. Intra-articular drug delivery systems for joint diseases. *Curr Opin Pharmacol.* **2018**, *40*, 67–73; DOI:10.1016/j.coph.2018.03.013.
39. Wang, P.; Guan, P.P.; Guo, C.; Zhu, F.; Konstantopoulos, K.; Wang, Z.Y. Fluid shear stress-induced osteoarthritis: Roles of cyclooxygenase-2 and its metabolic products in inducing the expression of proinflammatory cytokines and matrix metalloproteinases. *FASEB J.* 2013, *27*.
40. Tellegen, A.R.; Rudnik-Jansen, I.; Pouran, B.; de Visser, H.M.; Weinans, H.H.; Thomas, E.; Kik, M.J.L.; Grinwis, G.C.M.; Thies, J.C.; Woike, N.; et al. Controlled release of celecoxib inhibits inflammation, bone cysts and osteophyte formation in a preclinical model of osteoarthritis. *Drug Deliv.* **2018**, *25*, 1438–1447; DOI:10.1080/10717544.2018.1482971.
41. van den Bosch, M.H.J. Inflammation in osteoarthritis: Is it time to dampen the alarm(in) in this debilitating disease? *Clin. Exp. Immunol.* 2018, *195*, 153–166.
42. Sostres, C.; Gargallo, C.J.; Lanas, A. Nonsteroidal anti-inflammatory drugs and upper and lower gastrointestinal mucosal damage. *Arthritis Res. Ther.* 2013, *15*, 1–8.
43. Nissen, S.E.; Yeomans, N.D.; Solomon, D.H.; Lüscher, T.F.; Libby, P.; Husni, M.E.; Graham, D.Y.; Borer, J.S.; Wisniewski, L.M.; Wolski, K.E.; et al. Cardiovascular Safety of Celecoxib,

Naproxen, or Ibuprofen for Arthritis. *N. Engl. J. Med.* **2016**, *375*, 2519–2529; DOI:10.1056/nejmoa1611593.
44. Cheng, B.R.; Chen, J.Q.; Zhang, X.W.; Gao, Q.Y.; Li, W.H.; Yan, L.J.; Zhang, Y.Q.; Wu, C.J.; Xing, J.L.; Liu, J.P. Cardiovascular safety of celecoxib in rheumatoid arthritis and osteoarthritis patients: A systematic review and meta-analysis. *PLoS One* **2021**, *16*, e0261239; DOI:10.1371/journal.pone.0261239.
45. Gunter, B.R.; Butler, K.A.; Wallace, R.L.; Smith, S.M.; Harirforoosh, S. Non-steroidal anti-inflammatory drug-induced cardiovascular adverse events: a meta-analysis. *J. Clin. Pharm. Ther.* 2017, *42*, 27–38.
46. Zweers, M.C.; de Boer, T.N.; van Roon, J.; Bijlsma, J.W.J.; Lafeber, F.P.J.G.; Mastbergen, S.C. Celecoxib: Considerations regarding its potential disease-modifying properties in osteoarthritis. *Arthritis Res. Ther.* 2011, *13*.
47. Puljak, L.; Marin, A.; Vrdoljak, D.; Markotic, F.; Utrobicic, A.; Tugwell, P. Celecoxib for osteoarthritis. *Cochrane Database Syst. Rev.* **2017**, *2017*, CD009865; DOI:10.1002/14651858.CD009865.pub2.
48. Nakata, K.; Hanai, T.; Take, Y.; Osada, T.; Tsuchiya, T.; Shima, D.; Fujimoto, Y. Disease-modifying effects of COX-2 selective inhibitors and non-selective NSAIDs in osteoarthritis: a systematic review. *Osteoarthr. Cartil.* 2018, *26*, 1263–1273.
49. Zeng, C.; Wei, J.; Li, H.; Wang, Y.L.; Xie, D.X.; Yang, T.; Gao, S.G.; Li, Y.S.; Luo, W.; Lei, G.H. Effectiveness and safety of Glucosamine, chondroitin, the two in combination, or celecoxib in the treatment of osteoarthritis of the knee. *Sci. Rep.* **2015**, *5*, 1–10; DOI:10.1038/srep16827.
50. Panahifar, A.; Jaremko, J.L.; Tessier, A.G.; Lambert, R.G.; Maksymowych, W.P.; Fallone, B.G.; Doschak, M.R. Development and reliability of a multi-modality scoring system for evaluation of disease progression in pre-clinical models of osteoarthritis: celecoxib may possess disease-modifying properties. *Osteoarthr. Cartil.* **2014**, *22*, 1639–1650; DOI:10.1016/j.joca.2014.06.013.
51. Xu, C.; Gu, K.; Yasen, Y.; Hou, Y. Efficacy and Safety of Celecoxib Therapy in Osteoarthritis. *Med. (United States)* 2016, *95*.
52. Jiang, D.; Zou, J.; Huang, L.; Shi, Q.; Zhu, X.; Wang, G.; Yang, H. Efficacy of Intra-Articular Injection of Celecoxib in a Rabbit Model of Osteoarthritis. *Int. J. Mol. Sci.* **2010**, *11*, 4106–4113; DOI:10.3390/ijms11104106.
53. Hurtig, M.; Shive, M.; Kapoor, M.; Grizot, S.; Mahomed, N.; Roberts, G.F.; Marshall, W. Intra-articular injection of a polymer/celecoxib formulation for long-term control of postoperative inflammation. *Osteoarthr. Cartil.* **2016**, *24*, S526–S527; DOI:10.1016/j.joca.2016.01.962.
54. Janssen, M.; Timur, U.T.; Woike, N.; Welting, T.J.M.; Draaisma, G.; Gijbels, M.; van Rhijn, L.W.; Mihov, G.; Thies, J.; Emans, P.J. Celecoxib-loaded PEA microspheres as an auto regulatory drug-delivery system after intra-articular injection. *J. Control. Release* **2016**, *244*, 30–40; DOI:10.1016/j.jconrel.2016.11.003.
55. Tellegen, A.R.; Rudnik-Jansen, I.; Utomo, L.; Versteeg, S.; Beukers, M.; Maarschalkerweerd, R.; van Zuilen, D.; van Klaveren, N.J.; Houben, K.; Teske, E.; et al. Sustained release of locally delivered celecoxib provides pain relief for osteoarthritis: a proof of concept in dog patients. *Osteoarthr. Cartil.* **2023**, *31*, 351–362; DOI:10.1016/j.joca.2022.11.008.
56. Petit, A.; Sandker, M.; Müller, B.; Meyboom, R.; van Midwoud, P.; Bruin, P.; Redout, E.M.;

Versluijs-Helder, M.; van der Lest, C.H.A.; Buwalda, S.J.; et al. Release behavior and intra-articular biocompatibility of celecoxib-loaded acetyl-capped PCLA-PEG-PCLA thermogels. *Biomaterials* **2014**, *35*, 7919–7928; DOI:10.1016/j.biomaterials.2014.05.064.

57. Petit, A.; Redout, E.M.; van de Lest, C.H.; de Grauw, J.C.; Müller, B.; Meyboom, R.; van Midwoud, P.; Vermonden, T.; Hennink, W.E.; René van Weeren, P. Sustained intra-articular release of celecoxib from in situ forming gels made of acetyl-capped PCLA-PEG-PCLA triblock copolymers in horses. *Biomaterials* **2015**, *53*, 426–436; DOI:10.1016/j.biomaterials.2015.02.109.
58. Prince, D.A.; Villamagna, I.J.; Hopkins, C.C.; de Bruyn, J.R.; Gillies, E.R. Effect of drug loading on the properties of temperature-responsive polyester–poly(ethylene glycol)–polyester hydrogels. *Polym. Int.* **2019**, *68*, 1074–1083; DOI:10.1002/pi.5797.
59. Gupta, R.C.; Lall, R.; Srivastava, A.; Sinha, A. Hyaluronic acid: Molecular mechanisms and therapeutic trajectory. *Front. Vet. Sci.* **2019**, *6*, 1–24; DOI:10.3389/fvets.2019.00192.
60. American Academy of Orthopaedic Surgeons *Treatment of Osteoarthritis of the Knee – 2nd EditionEvidence-Based Clinical Practice Guideline*; 2013;
61. American Academy of Orthopaedic Surgeons *Management of Osteoarthritis of the Knee (NonArthroplasty) Evidence-Based Clinical Practice Guideline*; 2021;
62. Nicholls, M.; Manjoo, A.; Shaw, P.; Niazi, F.; Rosen, J. Rheological properties of commercially available hyaluronic acid products in the United States for the treatment of osteoarthritis knee pain. *Clin. Med. Insights Arthritis Musculoskelet. Disord.* **2018**, *11*, 1–5; DOI:10.1177/1179544117751622.
63. Wu, Y.; Huang, H.-T.; Ho, C.-J.; Shih, C.-L.; Chen, C.-H.; Cheng, T.-L.; Wang, Y.-C.; Lin, S.-Y. Molecular Weight of Hyaluronic Acid Has Major Influence on Its Efficacy and Safety for Viscosupplementation in Hip Osteoarthritis: A Systematic Review and Meta-Analysis. *Cartilage* **2021**, *13*, 169S-184S; DOI:10.1177/19476035211021903.
64. Clementi, D.; D'Ambrosi, R.; Bertocco, P.; Bucci, M.S.; Cardile, C.; Ragni, P.; Giaffreda, G.; Ragone, V. Efficacy of a single intra-articular injection of ultra-high molecular weight hyaluronic acid for hip osteoarthritis: a randomized controlled study. *Eur. J. Orthop. Surg. Traumatol.* **2018**, *28*, 915–922; DOI:10.1007/s00590-017-2083-9.
65. Dai, W.L.; Lin, Z.M.; Guo, D.H.; Shi, Z.J.; Wang, J. Efficacy and Safety of Hylan versus Hyaluronic Acid in the Treatment of Knee Osteoarthritis. *J. Knee Surg.* **2018**, *32*, 259–268; DOI:10.1055/s-0038-1641142.
66. Leighton, R.; Fitzpatrick, J.; Smith, H.; Crandall, D.; Flannery, C.R.; Conrozier, T. Systematic clinical evidence review of NASHA (Durolane hyaluronic acid) for the treatment of knee osteoarthritis. *Open Access Rheumatol. Res. Rev.* 2018, *10*, 43–54.
67. Hummer, C.D.; Angst, F.; Ngai, W.; Whittington, C.; Yoon, S.S.; Duarte, L.; Manitt, C.; Schemitsch, E. High molecular weight Intraarticular hyaluronic acid for the treatment of knee osteoarthritis: a network meta-analysis. *BMC Musculoskelet. Disord.* **2020**, *21*, 1–10; DOI:10.1186/s12891-020-03729-w.
68. Phillips, M.; Vannabouathong, C.; Devji, T.; Patel, R.; Gomes, Z.; Patel, A.; Dixon, M.; Bhandari, M. Differentiating factors of intra-articular injectables have a meaningful impact on knee osteoarthritis outcomes: a network meta-analysis. *Knee Surgery, Sport. Traumatol. Arthrosc.* **2020**, *28*, 3031–3039; DOI:10.1007/s00167-019-05763-1.
69. Lee, B.M.; Park, S.J.; Noh, I.; Kim, C.H. The effects of the molecular weights of hyaluronic acid on the immune responses. *Biomater. Res.* **2021**, *25*, 1–13; DOI:10.1186/s40824-021-

00228-4.
70. Altman, R.D.; Bedi, A.; Karlsson, J.; Sancheti, P.; Schemitsch, E. Product Differences in Intra-articular Hyaluronic Acids for Osteoarthritis of the Knee. *Am. J. Sports Med.* **2015**, *44*, 2158–2165; DOI:10.1177/0363546515609599.
71. Abate, M.; Salini, V. Efficacy and safety study on a new compound associating low and high molecular weight hyaluronic acid in the treatment of hip osteoarthritis. *Int. J. Immunopathol. Pharmacol.* **2017**, *30*, 89–93; DOI:10.1177/0394632016689275.
72. Webb, D.; Naidoo, P. Viscosupplementation for knee osteoarthritis: a focus on Hylan G-F 20. *Orthop. Res. Rev.* 2018, *10*, 73–81.
73. Raman, R.; Dutta, A.; Day, N.; Sharma, H.K.; Shaw, C.J.; Johnson, G. V. Efficacy of Hylan G-F 20 and Sodium Hyaluronate in the treatment of osteoarthritis of the knee - A prospective randomized clinical trial. *Knee* **2008**, *15*, 318–324; DOI:10.1016/j.knee.2008.02.012.
74. Dahl, L.B.; Dahl, I.M.S.; Engstrom-Laurent, A.; Granath, K. Concentration and molecular weight of sodium hyaluronate in synovial fluid from patients with rheumatoid arthritis and other arthropathies. *Ann. Rheum. Dis.* **1985**, *44*, 817–822; DOI:10.1136/ard.44.12.817.
75. Wooley, P.H.; Song, Z.; Harrison, A. Hyaluronic acid viscosupplements from avian and non-mammalian sources exhibit biocompatibility profiles with unique, source-specific, antigenic profiles. *J. Biomed. Mater. Res. - Part B Appl. Biomater.* **2012**, *100 B*, 808–816; DOI:10.1002/jbm.b.32514.
76. Larsen, N.E.; Dursema, H.D.; Pollak, C.T.; Skrabut, E.M. Clearance kinetics of a hylan-based viscosupplement after intra-articular and intravenous administration in animal models. *J. Biomed. Mater. Res. - Part B Appl. Biomater.* **2011**, *100*, 457–462; DOI:10.1002/jbm.b.31971.
77. Brandt, K.D.; Smith, G.N.; Simon, L.S. Intraarticular injection of hyaluronan as treatment for knee osteoarthritis: What is the evidence? *Arthritis Rheum.* 2000, *43*, 1192–1203.
78. Lindqvist, U.; Tolmachev, V.; Kairemo, K.; Åström, G.; Jonsson, E.; Lundqvist, H. Elimination of stabilised hyaluronan from the knee joint in healthy men. *Clin. Pharmacokinet.* **2002**, *41*; DOI:10.2165/00003088-200241080-00004.
79. TeachMeSeries TeachMeSurgery Available online: https://teachmesurgery.com/orthopaedic/principles/osteoarthritis/ (accessed on May 5, 2020).
80. Bitton, R. The economic burden of osteoarthritis. *Am. J. Manag. Care* **2009**, *15*.
81. Inacio, M.C.S.; Paxton, E.W.; Graves, S.E.; Namba, R.S.; Nemes, S. Projected increase in total knee arthroplasty in the United States – an alternative projection model. *Osteoarthr. Cartil.* **2017**, *25*, 1797–1803; DOI:10.1016/j.joca.2017.07.022.
82. Oo, W.M.; Little, C.; Duong, V.; Hunter, D.J. The Development of Disease-Modifying Therapies for Osteoarthritis (DMOADs): The Evidence to Date. *Drug Des. Devel. Ther.* 2021, *15*, 2921–2945.
83. Kumar, M.; Dogra, R.; Mandal, U.K. Novel Formulation Approaches used for the Management of Osteoarthritis: A Recent Review. *Curr. Drug Deliv.* **2023**, *20*, 841–856; DOI:10.2174/1567201819666220901092832.
84. Verdict Media Limited Clinical Trials Arena Available online: https://www.clinicaltrialsarena.com/projects/zilretta-triamcinolone-acetonide-

extended-release-injectable-suspension-treatment-osteoarthritis-knee-pain/ (accessed on May 16, 2020).
85. Flexion Therapeutics, I. Zilretta Available online: https://zilretta.com/about-zilretta/the-microspheres/ (accessed on May 16, 2020).
86. Bodick, N.; Lufkin, J.; Willwerth, C.; Kumar, A.; Ballal, R.; Clayman, M.; Bolognese, J.; Schoonmaker, C.; Hunter, D. An intra-articular, extended-release formulation of triamcinolone acetonide prolongs and amplifies analgesic effect in patients with osteoarthritis of the knee: A randomized clinical trial. *J. Bone Jt. Surg. - Am. Vol.* **2015**, *97*, 877–888; DOI:10.2106/JBJS.N.00918.
87. Evans, C.H.; Ghivizzani, S.C.; Robbins, P.D. Gene Delivery to Joints by Intra-Articular Injection. *Hum. Gene Ther.* **2018**, *29*, 2–14; DOI:10.1089/hum.2017.181.
88. Kolon TissueGene Inc. KOLON TISSUEGENE Available online: https://www.tissuegene.com/en_US/technology/invossa (accessed on May 14, 2020).
89. Kolon TissueGene Inc. KOLON TISSUEGENE Available online: https://www.tissuegene.com/en_US/clinical-trials (accessed on May 14, 2020).
90. Cherian, J.J.; Parvizi, J.; Bramlet, D.; Lee, K.H.; Romness, D.W.; Mont, M.A. Preliminary results of a phase II randomized study to determine the efficacy and safety of genetically engineered allogeneic human chondrocytes expressing TGF-β1 in patients with grade 3 chronic degenerative joint disease of the knee. *Osteoarthr. Cartil.* **2015**, *23*, 2109–2118; DOI:10.1016/j.joca.2015.06.019.
91. Guermazi, A.; Kalsi, G.; Niu, J.; Crema, M.D.; Copeland, R.O.; Orlando, A.; Noh, M.J.; Roemer, F.W. Structural effects of intra-articular TGF-β1 in moderate to advanced knee osteoarthritis: MRI-based assessment in a randomized controlled trial. *BMC Musculoskelet. Disord.* 2017, *18*.
92. Chen, Y.; Luo, X.; Kang, R.; Cui, K.; Ou, J.; Zhang, X.; Liang, P. Current therapies for osteoarthritis and prospects of CRISPR-based genome, epigenome, and RNA editing in osteoarthritis treatment. *J. Genet. Genomics* 2023.
93. Li, X.; Shen, L.; Deng, Z.; Huang, Z. New treatment for osteoarthritis: Gene therapy. *Precis. Clin. Med.* 2023, *6*, 1–17.
94. Fuentes-Mera, L.; Camacho, A.; Moncada-Saucedo, N.K.; Víctor, P.-M. Current Applications of Mesenchymal Stem Cells for Cartilage Tissue Engineering. In *Mesenchymal Stem Cells - Isolation, Characterization and Applications*; Pham, P. Van, Ed.; InTech, 2017; pp. 149–183.
95. Tamaddon, M.; Gilja, H.; Wang, L.; Oliveira, J.M.; Sun, X.; Tan, R.; Liu, C. Osteochondral scaffolds for early treatment of cartilage defects in osteoarthritic joints: from bench to clinic. *Biomater. Transl.* 2020, *1*, 3–17.
96. Wasyłeczko, M.; Sikorska, W.; Chwojnowski, A. Review of synthetic and hybrid scaffolds in cartilage tissue engineering. *Membranes (Basel).* 2020, *10*, 1–28.
97. Liang, J.; Liu, P.; Yang, X.; Liu, L.; Zhang, Y.; Wang, Q.; Zhao, H. Biomaterial-based scaffolds in promotion of cartilage regeneration: Recent advances and emerging applications. *J. Orthop. Transl.* 2023, *41*, 54–62.
98. Bistolfi, A.; Ferracini, R.; Galletta, C.; Tosto, F.; Sgarminato, V.; Digo, E.; Vernè, E.; Massè, A. Regeneration of articular cartilage: Scaffold used in orthopedic surgery. A short handbook of available products for regenerative joints surgery. *Clin. Sci. Res. Reports* **2017**, *1*, 1–7; DOI:10.15761/csrr.1000101.

99. Rao, N.V. Hyaluronic acid–based hydrogels for tissue engineering. In *Biomaterials for Organ and Tissue Regeneration New Technologies and Future Prospects*; Vrana, N.E., Knopf-Marques, H., Barthes, J., Eds.; Elsevier, 2020; pp. 551–565.
100. Grieco, M.; Ursini, O.; Palamà, I.E.; Gigli, G.; Moroni, L.; Cortese, B. HYDRHA: Hydrogels of hyaluronic acid. New biomedical approaches in cancer, neurodegenerative diseases, and tissue engineering. *Mater. Today Bio* 2022, *17*, 1–14.
101. Hwang, H.S.; Lee, C.S. Recent Progress in Hyaluronic-Acid-Based Hydrogels for Bone Tissue Engineering. *Gels* 2023, *9*, 588.
102. Amann, E.; Wolff, P.; Breel, E.; van Griensven, M.; Balmayor, E.R. Hyaluronic acid facilitates chondrogenesis and matrix deposition of human adipose derived mesenchymal stem cells and human chondrocytes co-cultures. *Acta Biomater.* **2017**, *52*, 130–144; DOI:10.1016/j.actbio.2017.01.064.
103. Muran, A.C.; Schaffler, B.C.; Wong, A.; Neufeld, E.; Swami, P.; Pianka, M.; Grande, D. Effect of increasing hyaluronic acid content in collagen scaffolds on the maintenance of chondrogenic phenotype in chondrocytes and mesenchymal stem cells. *J. Cartil. Jt. Preserv.* **2023**, *3*, 1–8; DOI:10.1016/j.jcjp.2023.100099.
104. Vinatier, C.; Guicheux, J. Cartilage tissue engineering: From biomaterials and stem cells to osteoarthritis treatments. *Ann. Phys. Rehabil. Med.* 2016, *59*, 139–144.
105. Zhao, X.; Hu, D.A.; Wu, D.; He, F.; Wang, H.; Huang, L.; Shi, D.; Liu, Q.; Ni, N.; Pakvasa, M.; et al. Applications of Biocompatible Scaffold Materials in Stem Cell-Based Cartilage Tissue Engineering. *Front. Bioeng. Biotechnol.* 2021, *9*, 1–23.
106. Benthien, J.P.; Behrens, P. Autologous matrix-induced chondrogenesis (AMIC): Combining microfracturing and a collagen I/III matrix for articular cartilage resurfacing. *Cartilage* **2010**, *1*, 65–68; DOI:10.1177/1947603509360044.
107. Nazempour, A.; Van Wie, B.J. Chondrocytes, Mesenchymal Stem Cells, and Their Combination in Articular Cartilage Regenerative Medicine. *Ann. Biomed. Eng.* **2016**, *44*, 1325–1354; DOI:10.1007/s10439-016-1575-9.
108. Urbanek, O.; Kołbuk, D.; Wróbel, M. Articular cartilage: New directions and barriers of scaffolds development–review. *Int. J. Polym. Mater. Polym. Biomater.* **2019**, *68*, 396–410; DOI:10.1080/00914037.2018.1452224.
109. Huang, B.J.; Hu, J.C.; Athanasiou, K.A. Cell-based tissue engineering strategies used in the clinical repair of articular cartilage. *Biomaterials* 2016, *98*, 1–22.
110. Jeuken, R.M.; Roth, A.K.; Peters, R.J.R.W.; van Donkelaar, C.C.; Thies, J.C.; van Rhijn, L.W.; Emans, P.J. Polymers in cartilage defect repair of the knee: Current status and future prospects. *Polymers (Basel).* 2016, *8*, 219.
111. Irawan, V.; Sung, T.C.; Higuchi, A.; Ikoma, T. Collagen Scaffolds in Cartilage Tissue Engineering and Relevant Approaches for Future Development. *Tissue Eng. Regen. Med.* 2018, *15*, 673–697.
112. Park, Y.-B.; Ha, C.-W.; Lee, C.-H.; Yoon, Y.C.; Park, Y.-G. Cartilage Regeneration in Osteoarthritic Patients by a Composite of Allogeneic Umbilical Cord Blood-Derived Mesenchymal Stem Cells and Hyaluronate Hydrogel: Results from a Clinical Trial for Safety and Proof-of-Concept with 7 Years of Extended Follow-Up. *Stem Cells Transl. Med.* **2017**, *6*, 613–621; DOI:10.5966/sctm.2016-0157.
113. Negoro, T.; Takagaki, Y.; Okura, H.; Matsuyama, A. Trends in clinical trials for articular cartilage repair by cell therapy. *npj Regen. Med.* **2018**, *3*, 1–10; DOI:10.1038/s41536-018-

0055-2.
114. Lam, A.T.L.; Reuveny, S.; Oh, S.K.W. Human mesenchymal stem cell therapy for cartilage repair: Review on isolation, expansion, and constructs. *Stem Cell Res.* **2020**, *44*, 1–14; DOI:10.1016/j.scr.2020.101738.
115. Martins, M.A.R.; Pinho, S.P.; Coutinho, J.A.P. Insights into the Nature of Eutectic and Deep Eutectic Mixtures. *J. Solution Chem.* **2018**; DOI:10.1007/s10953-018-0793-1.
116. Passos, H.; Tavares, D.J.P.; Ferreira, A.M.; Freire, M.G.; Coutinho, J.A.P. Are Aqueous Biphasic Systems Composed of Deep Eutectic Solvents Ternary or Quaternary Systems? *ACS Sustain. Chem. Eng.* **2016**, *4*, 2881–2886; DOI:10.1021/acssuschemeng.6b00485.
117. Abranches, D.O.; Coutinho, J.A.P. Everything You Wanted to Know about Deep Eutectic Solvents but Were Afraid to Be Told. *Annu. Rev. Chem. Biomol. Eng.* **2023**, *14*, 141–163; DOI:10.1146/annurev-chembioeng-101121-085323.
118. Roda, A.; Santos, F.; Chua, Y.Z.; Kumar, A.; Do, H.T.; Paiva, A.; Duarte, A.R.C.; Held, C. Unravelling the nature of citric acid:L-arginine:water mixtures: The bifunctional role of water. *Phys. Chem. Chem. Phys.* **2021**, *23*, 1706–1717; DOI:10.1039/d0cp04992a.
119. Fajar, A.T.N.; Hanada, T.; Hartono, A.D.; Goto, M. Estimating the phase diagrams of deep eutectic solvents within an extensive chemical space. *Commun. Chem.* **2024**, *7*, 27; DOI:10.1038/s42004-024-01116-3.
120. Smith, E.L.; Abbott, A.P.; Ryder, K.S. Deep Eutectic Solvents (DESs) and Their Applications. *Chem. Rev.* **2014**, *114*, 11060–11082; DOI:10.1021/cr300162p.
121. Guthrie, F. On eutexia. *Proc. Phys. Soc. London* **1884**, *6*, 124–146; DOI:10.1088/1478-7814/6/1/312.
122. Abbott, A.P.; Capper, G.; Davies, D.L.; Rasheed, R.K.; Tambyrajah, V. Novel solvent properties of choline chloride/urea mixtures. *Chem. Commun.* **2003**, 70–71; DOI:10.1039/b210714g.
123. Abranches, D.O.; Coutinho, J.A.P. Type V deep eutectic solvents: Design and applications. *Curr. Opin. Green Sustain. Chem.* 2022, *35*.
124. Abranches, D.O.; Silva, L.P.; Martins, M.A.R.; Pinho, S.P.; Coutinho, J.A.P. Understanding the Formation of Deep Eutectic Solvents: Betaine as a Universal Hydrogen Bond Acceptor. *ChemSusChem* **2020**, *13*; DOI:10.1002/cssc.202001331.
125. Kollau, L.J.B.M.; Vis, M.; Van Den Bruinhorst, A.; Esteves, A.C.C.; Tuinier, R. Quantification of the liquid window of deep eutectic solvents. *Chem. Commun.* **2018**, *54*; DOI:10.1039/c8cc05815f.
126. Abranches, D.O.; Martins, R.O.; Silva, L.P.; Martins, M.A.R.; Pinho, S.P.; Coutinho, J.A.P. Liquefying Compounds by Forming Deep Eutectic Solvents: A Case Study for Organic Acids and Alcohols. *J. Phys. Chem. B* **2020**, *124*, 4174–4184; DOI:10.1021/acs.jpcb.0c02386.
127. Andruch, V.; Makoś-Chełstowska, P.; Płotka-Wasylka, J. Remarks on use of the term "deep eutectic solvent" in analytical chemistry. *Microchem. J.* 2022, *179*, 107498.
128. van den Bruinhorst, A.; Costa Gomes, M. Is there depth to eutectic solvents? *Curr. Opin. Green Sustain. Chem.* 2022, *37*.
129. Zdanowicz, M.; Wilpiszewska, K.; Spychaj, T. Deep eutectic solvents for polysaccharides processing. A review. *Carbohydr. Polym.* **2018**, *200*, 361–380; DOI:10.1016/j.carbpol.2018.07.078.
130. Francisco, M.; van den Bruinhorst, A.; Zubeir, L.F.; Peters, C.J.; Kroon, M.C. A new low

transition temperature mixture (LTTM) formed by choline chloride+lactic acid: Characterization as solvent for CO2 capture. *Fluid Phase Equilib.* **2013**, *340*, 77–84; DOI:10.1016/j.fluid.2012.12.001.
131. Zahn, S.; Kirchner, B.; Mollenhauer, D. Charge Spreading in Deep Eutectic Solvents. *ChemPhysChem* **2016**, *17*, 3354–3358; DOI:10.1002/cphc.201600348.
132. Ashworth, C.R.; Matthews, R.P.; Welton, T.; Hunt, P.A. Doubly ionic hydrogen bond interactions within the choline chloride–urea deep eutectic solvent. *Phys.Chem.Chem.Phys.* **2016**, *18*, 18145–18160; DOI:10.1039/c6cp02815b.
133. Stefanovic, R.; Ludwig, M.; Webber, G.B.; Atkin, R.; Page, A.J. Nanostructure, hydrogen bonding and rheology in choline chloride deep eutectic solvents as a function of the hydrogen bond donor. *Phys. Chem. Chem. Phys.* **2017**, *19*, 3297–3306; DOI:10.1039/c6cp07932f.
134. Achkar, T. El; Fourmentin, S.; Greige-Gerges, H. Deep eutectic solvents: An overview on their interactions with water and biochemical compounds. *J. Mol. Liq.* **2019**, *288*, 111028; DOI:10.1016/j.molliq.2019.111028.
135. Hammond, O.S.; Bowron, D.T.; Edler, K.J. Effect of Water upon Deep Eutectic Solvent Nanostructure: An Unusual Transition from Ionic Mixture to Aqueous Solution. *Angew. Chemie - Int. Ed.* **2017**, *56*, 9782–9785; DOI:10.1002/anie.201702486.
136. López-Salas, N.; Vicent-Luna, J.M.; Imberti, S.; Posada, E.; Roldán, M.J.; Anta, J.A.; Balestra, S.R.G.; Castro, R.M.M.; Calero, S.; Jiménez-Riobóo, R.J.; et al. Looking at the "Water-in-Deep-Eutectic-Solvent" System: A Dilution Range for High Performance Eutectics. *ACS Sustain. Chem. Eng.* **2019**, *7*, 17565–17573; DOI:10.1021/acssuschemeng.9b05096.
137. Martins, M.A.R.; Crespo, E.A.; Pontes, P.V.A.; Silva, L.P.; Bülow, M.; Maximo, G.J.; Batista, E.A.C.; Held, C.; Pinho, S.P.; Coutinho, J.A.P. Tunable Hydrophobic Eutectic Solvents Based on Terpenes and Monocarboxylic Acids. *ACS Sustain. Chem. Eng.* **2018**, *6*, 8836–8846; DOI:10.1021/acssuschemeng.8b01203.
138. Francisco, M.; Van Den Bruinhorst, A.; Kroon, M.C. Low-transition-temperature mixtures (LTTMs): A new generation of designer solvents. *Angew. Chemie - Int. Ed.* **2013**, *52*, 3074–3085; DOI:10.1002/anie.201207548.
139. del Monte, F.; Carriazo, D.; Serrano, M.C.; Gutiérrez, M.C.; Ferrer, M.L. Deep eutectic solvents in polymerizations: A greener alternative to conventional syntheses. *ChemSusChem* **2014**, *7*, 999–1009; DOI:10.1002/cssc.201300864.
140. Anastas, P.T.; Warner, J.C. Green chemistry: theory and practice. *Oxford Univ. Press. New York* **1998**, 30.
141. Choi, Y.H.; van Spronsen, J.; Dai, Y.; Verberne, M.; Hollmann, F.; Arends, I.W.C.E.; Witkamp, G.-J.; Verpoorte, R. Are Natural Deep Eutectic Solvents the Missing Link in Understanding Cellular Metabolism and Physiology? *Plant Physiol.* **2011**, *156*, 1701–1705; DOI:10.1104/pp.111.178426.
142. Paiva, A.; Craveiro, R.; Aroso, I.; Martins, M.; Reis, R.L.; Duarte, A.R.C. Natural deep eutectic solvents - Solvents for the 21st century. *ACS Sustain. Chem. Eng.* **2014**, *2*, 1063–1071; DOI:10.1021/sc500096j.
143. Vanda, H.; Dai, Y.; Wilson, E.G.; Verpoorte, R.; Choi, Y.H. Green solvents from ionic liquids and deep eutectic solvents to natural deep eutectic solvents. *Comptes Rendus Chim.* **2018**, *21*, 628–638; DOI:10.1016/j.crci.2018.04.002.
144. Web of Science Available online: https://www.webofscience.com/wos/woscc/advanced-

search (accessed on Jan 9, 2024).
145. García-Álvarez, J. Deep Eutectic Mixtures: Promising Sustainable Solvents for Metal-Catalysed and Metal-Mediated Organic Reactions. *Eur. J. Inorg. Chem.* **2015**, *2015*, 5147–5157; DOI:10.1002/ejic.201500892.
146. Alonso, D.A.; Baeza, A.; Chinchilla, R.; Guillena, G.; Pastor, I.M.; Ramón, D.J. Deep Eutectic Solvents: The Organic Reaction Medium of the Century. *European J. Org. Chem.* **2016**, *2016*, 612–632; DOI:10.1002/ejoc.201501197.
147. Duarte, A.R.C.; Ferreira, A.S.D.; Barreiros, S.; Cabrita, E.; Reis, R.L.; Paiva, A. A comparison between pure active pharmaceutical ingredients and therapeutic deep eutectic solvents: Solubility and permeability studies. *Eur. J. Pharm. Biopharm.* **2017**, *114*, 296–304; DOI:10.1016/j.ejpb.2017.02.003.
148. Aroso, I.M.; Craveiro, R.; Rocha, Â.; Dionísio, M.; Barreiros, S.; Reis, R.L.; Paiva, A.; Duarte, A.R.C. Design of controlled release systems for THEDES - Therapeutic deep eutectic solvents, using supercritical fluid technology. *Int. J. Pharm.* **2015**, *492*, 73–79; DOI:10.1016/j.ijpharm.2015.06.038.
149. Hyun, S.-M.; Lee, B.J.; Abuzar, S.M.; Lee, S.; Joo, Y.; Hong, S.-H.; Kang, H.; Kwon, K.-A.; Velaga, S.; Hwang, S.-J. Preparation , characterization , and evaluation of celecoxib eutectic mixtures with adipic acid / saccharin for improvement of wettability and dissolution rate. *Int. J. Pharm.* **2019**, *554*, 61–71; DOI:10.1016/j.ijpharm.2018.10.044.
150. Mokhtarpour, M.; Shekaari, H.; Zafarani-Moattar, M.T.; Golgoun, S. Solubility and solvation behavior of some drugs in choline based deep eutectic solvents at different temperatures. *J. Mol. Liq.* **2020**, *297*, 1–11; DOI:10.1016/j.molliq.2019.111799.
151. Palmelund, H.; Andersson, M.P.; Asgreen, C.J.; Boyd, B.J.; Rantanen, J.; Korbinian, L. Tailor-made solvents for pharmaceutical use? Experimental and computational approach for determining solubility in deep eutectic solvents (DES). *Int. J. Pharm. X* **2019**, *1*, 1–9; DOI:10.1016/j.ijpx.2019.100034.
152. Lu, C.; Cao, J.; Wang, N.; Su, E. Significantly improving the solubility of non-steroidal anti-inflammatory drugs in deep eutectic solvents for potential non-aqueous liquid administration. *Medchemcomm* **2016**, *7*, 955–959; DOI:10.1039/c5md00551e.
153. Wen, Q.; Chen, J.-X.; Tang, Y.-L.; Wang, J.; Yang, Z. Assessing the toxicity and biodegradability of deep eutectic solvents. *Chemosphere* **2015**, *132*, 63–69; DOI:10.1016/j.chemosphere.2015.02.061.
154. Ahmadi, R.; Hemmateenejad, B.; Safavi, A.; Shojaeifard, Z.; Mohabbati, M.; Firuzi, O. Assessment of cytotoxicity of choline chloride-based natural deep eutectic solvents against human HEK-293 cells: A QSAR analysis. *Chemosphere* **2018**, *209*, 831–838; DOI:10.1016/j.chemosphere.2018.06.103.
155. Benlebna, M.; Ruesgas-Ramón, M.; Bonafos, B.; Fouret, G.; Coudray, C.; Durand, E.; Figueroa-Espinoza, M.C.; Feillet-Coudray, C. Toxicity of Natural Deep Eutectic Solvent Betaine:Glycerol in Rats. *J. Agric. Food Chem.* **2018**, *66*, 6205–6212; DOI:10.1021/acs.jafc.8b01746.
156. Roda, A.; Matias, A.A.; Paiva, A.; Duarte, A.R.C. Polymer Science and Engineering Using Deep Eutectic Solvents. *Polymers (Basel).* **2019**, *11*, 22; DOI:10.3390/polym11050912.
157. Tuntarawongsa, S.; Phaechamud, T. Polymeric Eutectic System. *Adv. Mater. Res.* **2012**, *528*, 180–183; DOI:10.4028/www.scientific.net/amr.528.180.
158. Xiao, S.; Wang, L.; Han, W.; Gu, L.; Cui, X.; Wang, C. Novel Deep Eutectic Solvent–Hydrogel

Systems for Synergistic Transdermal Delivery of Chinese Herb Medicine and Local Treatments for Rheumatoid Arthritis. *Pharm. Res.* **2022**, *39*, 2431–2446; DOI:10.1007/s11095-022-03239-5.

159. Pedro, S.N.; Mendes, M.S.M.; Neves, B.M.; Almeida, I.F.; Costa, P.; Correia-Sá, I.; Vilela, C.; Freire, M.G.; Silvestre, A.J.D.; Freire, C.S.R. Deep Eutectic Solvent Formulations and Alginate-Based Hydrogels as a New Partnership for the Transdermal Administration of Anti-Inflammatory Drugs. *Pharmaceutics* **2022**, *14*, 827; DOI:10.3390/pharmaceutics14040827.
160. Li, M.; Cui, H.; Cao, Y.; Lin, Y.; Yang, Y.; Gao, M.; Zhang, W.; Wang, C. Deep eutectic solvents—Hydrogels for the topical management of rheumatoid arthritis. *J. Control. Release* **2023**, *354*, 664–679; DOI:10.1016/j.jconrel.2023.01.050.
161. Panbachi, S.; Beranek, J.; Kuentz, M. Polymer-embedded deep eutectic solvents (PEDES) as a novel bio-enabling formulation approach. *Eur. J. Pharm. Sci.* **2023**, *186*, 1–10; DOI:10.1016/j.ejps.2023.106463.
162. Ghlichloo, I.; Gerriets, V. *Nonsteroidal Anti-inflammatory Drugs (NSAIDs)*; StatPearls Publishing, 2020;
163. Markowicz-Piasecka, M.; Mikiciuk-Olasik, E. 2.3.1 Non-steroidal anti-inflammatory drugs (NSAIDs). In *Nanobiomaterials in Drug Delivery. Applications of Nanobiomaterials Volume 9*; Grumezescu, A.M., Ed.; William Andrew, 2016; p. 44.
164. Scarpignato, C.; Lanas, A.; Blandizzi, C.; Lems, W.F.; Hermann, M.; Hunt, R.H. Safe prescribing of non-steroidal anti-inflammatory drugs in patients with osteoarthritis - an expert consensus addressing benefits as well as gastrointestinal and cardiovascular risks. *BMC Med.* **2015**, *13*, 55; DOI:10.1186/s12916-015-0285-8.
165. Aroso, I.M.; Silva, J.C.; Mano, F.; Ferreira, A.S.D.; Dionísio, M.; Sá-Nogueira, I.; Barreiros, S.; Reis, R.L.; Paiva, A.; Duarte, A.R.C. Dissolution enhancement of active pharmaceutical ingredients by therapeutic deep eutectic systems. *Eur. J. Pharm. Biopharm.* **2016**, *98*, 57–66; DOI:10.1016/j.ejpb.2015.11.002.
166. Faggian, M.; Sut, S.; Perissutti, B.; Baldan, V.; Grabnar, I.; Dall'Acqua, S. Natural Deep Eutectic Solvents (NADES) as a tool for bioavailability improvement: Pharmacokinetics of rutin dissolved in proline/glycine after oral administration in rats: Possible application in nutraceuticals. *Molecules* **2016**, *21*, 1531; DOI:10.3390/molecules21111531.
167. Sut, S.; Faggian, M.; Baldan, V.; Poloniato, G.; Castagliuolo, I.; Grabnar, I.; Perissutti, B.; Brun, P.; Maggi, F.; Voinovich, D.; et al. Natural Deep Eutectic Solvents (NADES) to enhance berberine absorption: An in vivo pharmacokinetic study. *Molecules* **2017**, *22*, 1921; DOI:10.3390/molecules22111921.
168. Shamseddin, A.; Crauste, C.; Durand, E.; Villeneuve, P.; Dubois, G.; Durand, T.; Vercauteren, J.; Veas, F. Resveratrol formulated with a natural deep eutectic solvent inhibits active matrix metalloprotease-9 in hormetic conditions. *Eur. J. Lipid Sci. Technol.* **2017**, *119*, 1700171; DOI:10.1002/ejlt.201700171.
169. Durand, E.; Lecomte, J.; Upasani, R.; Chabi, B.; Bayrasy, C.; Baréa, B.; Jublanc, E.; Clarke, M.J.; Moore, D.J.; Crowther, J.; et al. Evaluation of the ROS Inhibiting Activity and Mitochondrial Targeting of Phenolic Compounds in Fibroblast Cells Model System and Enhancement of Efficiency by Natural Deep Eutectic Solvent (NADES) Formulation. *Pharm. Res.* **2017**, *34*, 1134–1146; DOI:10.1007/s11095-017-2124-4.
170. Pereira, C. V.; Silva, J.M.; Rodrigues, L.; Reis, R.L.; Paiva, A.; Duarte, A.R.C.; Matias, A. Unveil

the Anticancer Potential of Limomene Based Therapeutic Deep Eutectic Solvents. *Sci. Rep.* **2019**, *9*, 1–11; DOI:10.1038/s41598-019-51472-7.
171. Silva, E.; Oliveira, F.; Silva, J.M.; Matias, A.; Reis, R.L.; Duarte, A.R.C. Optimal design of THEDES based on perillyl alcohol and ibuprofen. *Pharmaceutics* **2020**, *12*, 1121; DOI:10.3390/pharmaceutics12111121.
172. Silva, J.M.; Pereira, C. V.; Mano, F.; Silva, E.; Castro, V.I.B.; Sá-Nogueira, I.; Reis, R.L.; Paiva, A.; Matias, A.A.; Duarte, A.R.C. Therapeutic Role of Deep Eutectic Solvents Based on Menthol and Saturated Fatty Acids on Wound Healing. *ACS Appl. Bio Mater.* **2019**, *2*, 4346–4355; DOI:10.1021/acsabm.9b00598.
173. Nguyen, C.-H.; Augis, L.; Fourmentin, Sophie Barratt, G.; Legrand, F.-X. Deep Eutectic Solvents for Innovative Pharmaceutical Formulations. In *Deep Eutectic Solvents for Medicine, Gas Solubilization and Extraction of Natural Substances*; Fourmentin, S., Gomes, M.C., Lichtfouse, E., Eds.; Springer Nature, 2020; pp. 41–102.
174. Silva, J.M.M.; Reis, R.L.; Paiva, A.; Duarte, A.R.C. Design of functional therapeutic deep eutectic solvents based on choline chloride and ascorbic acid. *ACS Sustain. Chem. Eng.* **2018**, *6*, 10355–10363; DOI:10.1021/acssuschemeng.8b01687.
175. Santos, F.; Duarte, A.R.C. Therapeutic Deep Eutectic Systems for the Enhancement of Drug Bioavailability. In *Deep Eutectic Solvents for Medicine, Gas Solubilization and Extraction of Natural Substances*; Fourmentin, S., Gomes, M.C., Lichtfouse, E., Eds.; Springer Nature, 2020; pp. 103–129.
176. Drexler, H.G.; Dirks, W.; MacLeod, R.A.F.; Quentmeier, H.; Steube, K.G.; Uphoff, C.C. *DSMZ catalogue of human and animal cell lines*; DSMZ.; Braunschweig, 2001;
177. International Organization for Standardization *ISO 10993-5 Biological evaluation of medical devices - Part 5: Tests for in vitro cytotoxicity*, 2009;
178. Reichardt, C. Empirical Parameters of Solvent Polarity as Linear Free-Energy Relationships. *Angew. Chemie Int. Ed. English* **1979**, *18*, 98–110; DOI:10.1002/anie.197900981.
179. Machado, C.; Machado, V.G. An easy and versatile experiment to demonstrate solvent polarity using solvatochromic dyes. *J. Chem. Educ.* **2001**, *78*, 649–651; DOI:10.1021/ed078p649.
180. Nováková, L.; Matysová, L.; Havlíková, L.; Solich, P. Development and validation of HPLC method for determination of indomethacin and its two degradation products in topical gel. *J. Pharm. Biomed. Anal.* **2005**, *37*, 899–905; DOI:10.1016/j.jpba.2004.09.012.
181. Ascar, L.; Ahumada, I.; López, A.; Quintanilla, F.; Leiva, K. Nonsteroidal anti-inflammatory drug determination in water samples by HPLC-DAD under isocratic conditions. *J. Braz. Chem. Soc.* **2013**, *24*, 1160–1166; DOI:10.5935/0103-5053.20130150.
182. Fox, M.R.S.; Mickelsen, O. Salt Mixtures for Purified-Type Diets: II. Effect of Salts on the Maillard Browning Reaction. *J. Nutr.* **1959**, *68*, 289–295; DOI:10.1093/jn/68.2.289.
183. Li, J.; Zhang, Z.; Huang, X. L-Arginine and allopurinol supplementation attenuates inflammatory mediators in human osteoblasts–osteoarthritis cells. *Int. J. Biol. Macromol.* **2018**, *118*, 716–721; DOI:10.1016/j.ijbiomac.2018.06.047.
184. Shi, H.P.; Wang, S.M.; Zhang, G.X.; Zhang, Y.J.; Barbul, A. Supplemental L-arginine enhances wound healing following trauma/hemorrhagic shock. *Wound Repair Regen.* **2007**, *15*, 66–70; DOI:10.1111/j.1524-475X.2006.00186.x.
185. Pagliaro, M.; Rossi, M. Glycerol: Properties and Production. In *The Future of Glycerol*; The

Royal Society of Chemistry, 2010; pp. 1–28.
186. Azelee, N.I.W.; Ramli, A.N.M.; Manas, N.H.A.; Salamun, N.; Man, R.C.; El Enshasy, H. Glycerol in food, cosmetics and pharmaceutical industries: Basics and new applications. *Int. J. Sci. Technol. Res.* **2019**, *8*, 553–558.
187. D'souza, A.A.; Shegokar, R. Polyethylene glycol (PEG): a versatile polymer for pharmaceutical applications. *Expert Opin. Drug Deliv.* 2016, *13*, 1257–1275.
188. Hoffman, G.S.; Schumacher, H.R.; Paul, H.; Cherian, V.; Reed, R.; Ramsay, A.G.; Franck, W.A. Calcium oxalate microcrystalline-associated arthritis in end-stage renal disease. *Ann. Intern. Med.* **1982**, *97*, 36–42; DOI:10.7326/0003-4819-97-1-36.
189. Lorenz, E.C.; Michet, C.J.; Milliner, D.S.; Lieske, J.C. Update on oxalate crystal disease. *Curr. Rheumatol. Rep.* **2013**, *15*, 340; DOI:10.1007/s11926-013-0340-4.
190. Katona, G.; Szalontai, B.; Budai-Szűcs, M.; Csányi, E.; Szabó-Révész, P.; Jójárt-Laczkovich, O. Formulation of paracetamol-containing pastilles with in situ coating technology. *Eur. J. Pharm. Sci.* **2016**, *95*, 54–61; DOI:10.1016/j.ejps.2016.08.006.
191. Dezena, R.M.B.; Junior, J. dos S.M. Preformulation comparative study between two samples of sorbitol used as excipient in the direct compression process. *Brazilian J. Anal. Chem.* **2017**, *4*, 19–26.
192. Rodrigues, L.A.; Pereira, C. V; Leonardo, I.C.; Fernández, N.; Gaspar, F.B.; Silva, J.M.; Reis, R.L.; Duarte, A.R.C.; Paiva, A.; Matias, A.A. Terpene-Based Natural Deep Eutectic Systems as Efficient Solvents To Recover Astaxanthin from Brown Crab Shell Residues. *Sustain. Chem. Eng.* **2020**, *8*, 2246–2259; DOI:10.1021/acssuschemeng.9b06283.
193. Zondervan, R.; Kulzer, F.; Berkhout, G.C.G.; Orrit, M. Local viscosity of supercooled glycerol near Tg probed by rotational diffusion of ensembles and single dye molecules. *Proc. Natl. Acad. Sci. U. S. A.* **2007**, *104*, 12628–12633; DOI:10.1073/pnas.0610521104.
194. Linstrom, P. NIST Chemistry WebBook, NIST Standard Reference Database 69. **1997**; DOI:10.18434/T4D303.
195. Merck IR Spectrum Table & Chart Available online: https://www.sigmaaldrich.com/technical-documents/articles/biology/ir-spectrum-table.html (accessed on Jul 23, 2020).
196. Mallik, T.; Kar, T. Growth and characterization of nonlinear optical L-arginine dihydrate single crystals. *J. Cryst. Growth* **2005**, *285*, 178–182; DOI:10.1016/j.jcrysgro.2005.08.025.
197. Gowri, S.; Sathiyabama, J.; Rajendran, S. Corrosion inhibition effect of carbon steel in sea water by L-Arginine-Zn2+ system. *Int. J. Chem. Eng.* **2014**, *11*, 1–9; DOI:10.1155/2014/607209.
198. Petrosyan, A.M.; Sukiasyan, R.P. Vibrational spectra of L-arginine nitrates. *J. Mol. Struct.* **2008**, *874*, 51–56; DOI:10.1016/j.molstruc.2007.03.032.
199. Mikes, P.; Brož, A.; Sinica, A.; Asatiani, N.; Bacakova, L. In vitro and in vivo testing of nanofibrous membranes doped with alaptide and L-arginine for wound treatment. *Biomed. Mater.* **2020**, 1–26; DOI:10.1088/1748-605X/ab950f.
200. Pimpang, P.; Sumang, R.; Choopun, S. Effect of concentration of citric acid on size and optical properties of fluorescence graphene quantum dots prepared by tuning carbonization degree. *Chiang Mai J. Sci.* **2018**, *45*, 2005–2014.
201. Bichara, L.C.; Lans, H.E.; Ferrer, E.G.; Gramajo, M.B.; Brandán, S.A. Vibrational study and force field of the citric acid dimer based on the SQM methodology. *Adv. Phys. Chem.* **2011**, *2011*, 1–10; DOI:10.1155/2011/347072.

202. Thuy, N.T.; Minh, D. Le Size effect on the structural and magnetic properties of nanosized perovskite LaFeO3 prepared by different methods. *Adv. Mater. Sci. Eng.* **2012**, *2012*, 1–6; DOI:10.1155/2012/380306.
203. Danish, M.; Mumtaz, M.W.; Fakhar, M.; Rashid, U. Response surface methodology based optimized purification of the residual glycerol from biodiesel production process. *Chiang Mai J. Sci.* **2017**, *44*, 1570–1582.
204. Database of ATR-FT-IR spectra of various materials Available online: https://spectra.cs.ut.ee/paint/binders/glycerine/ (accessed on Feb 9, 2021).
205. de Castro, E. da S.G.; Cassella, R.J. Direct determination of sorbitol and sodium glutamate by attenuated total reflectance Fourier transform infrared spectroscopy (ATR-FTIR) in the thermostabilizer employed in the production of yellow-fever vaccine. *Talanta* **2016**, *152*, 33–38; DOI:10.1016/j.talanta.2016.01.054.
206. Wang, Y.; Gao, J.; Yin, Q.; Hao, H. Isolation and characterization of a new polymorph of D-sorbitol. *Cryst. Res. Technol.* **2012**, *47*, 409–414; DOI:10.1002/crat.201100565.
207. Stokes, G.G. *Volume the Ninth*; Trans. Cambridge Philos. Soc., 1856;
208. Einstein, A. Zur Theorie der Brownschen Bewegung. *Ann. Phys.* **1906**, *324*, 371–381; DOI:10.1002/andp.19063240208.
209. Debye, P. *Polar Molecules*; Dover Publications: New York, USA, 1929;
210. Koenderink, G.H.; Zhang, H.; Aarts, D.G.A.L.; Lettinga, M.P.; Philipse, A.P.; Nägele, G. On the validity of Stokes–Einstein–Debye relations for rotational diffusion in colloidal suspensions. *Faraday Discuss.* **2003**, *123*, 335–354; DOI:10.1039/b204668g.
211. Dote, J.L.; Kivelson, D.; Schwartz, R.N. A molecular quasi-hydrodynamic free-space model for molecular rotational relaxation in liquids. *J. Phys. Chem.* **1981**, *85*, 2169–2180; DOI:10.1021/j150615a007.
212. Zhang, L.; Greenfield, M.L. Rotational relaxation times of individual compounds within simulations of molecular asphalt models. *J. Chem. Phys.* **2010**, *132*, 184502; DOI:10.1063/1.3416913.
213. Mann, S.K.; Pham, T.N.; McQueen, L.L.; Lewandowski, J.R.; Brown, S.P. Revealing Intermolecular Hydrogen Bonding Structure and Dynamics in a Deep Eutectic Pharmaceutical by Magic-Angle Spinning NMR Spectroscopy. *Mol. Pharm.* **2020**, *17*, 622–631; DOI:10.1021/acs.molpharmaceut.9b01075.
214. Silva, R.A.; Palladino, M. V.; Cavalheiro, R.P.; Machado, D.; Cruz, B.L.G.; Paredes-Gamero, E.J.; Gomes-Marcondes, M.C.C.; Zambuzzi, W.F.; Vasques, L.; Nader, H.B.; et al. Activation of the low molecular weight protein tyrosine phosphatase in keratinocytes exposed to hyperosmotic stress. *PLoS One* **2015**, *10*, e0119020; DOI:10.1371/journal.pone.0119020.
215. Dai, Y.; Witkamp, G.-J.; Verpoorte, R.; Choi, Y.H. Tailoring properties of natural deep eutectic solvents with water to facilitate their applications. *Food Chem.* **2015**, *187*, 14–19; DOI:10.1016/j.foodchem.2015.03.123.
216. Braun, R.J.; Parrott, E.L. Influence of Viscosity and Solubilization on Dissolution Rate. *J. Pharm. Sci.* **1972**, *61*, 175–178; DOI:10.1002/jps.2600610206.
217. Cayman Product Information (±)-Ibuprofen Item Number 70280.
218. Levis, K.A.; Lane, M.E.; Corrigan, O.I. Effect of buffer media composition on the solubility and effective permeability coefficient of ibuprofen. *Int. J. Pharm.* **2003**, *253*, 49–59; DOI:10.1016/S0378-5173(02)00645-2.
219. Felton, L.A.; Popescu, C.; Wiley, C.; Esposito, E.X.; Lefevre, P.; Hopfinger, A.J. Experimental

and computational studies of physicochemical properties influence NSAID-cyclodextrin complexation. *AAPS PharmSciTech* **2014**, *15*, 872–881; DOI:10.1208/s12249-014-0110-2.
220. Chatani, H.; Goto, S.; Kataoka, H.; Fujita, M.; Otsuka, Y.; Shimada, Y.; Terada, H. Effects of phosphate on drug solubility behavior of mixture ibuprofen and lidocaine. *Chem. Phys.* **2019**, *525*, 110415; DOI:10.1016/j.chemphys.2019.110415.
221. Ivanova, N.; Stefanova, T.S.; Iliev, I.R.; Stoyanov, G.S.; Bratoeva, K.Z. Kinetic Modeling on Amide Hydrolysis, Drug Release and Mucosal Permeation of Indomethacin in the Composition of Selected Semisolid Vehicles. *J. IMAB - Annu. Proceeding (Scientific Pap.* **2018**, *24*, 2303–2312; DOI:10.5272/jimab.2018244.2303.
222. Cayman Product Information Indomethacin Item Number 70270.
223. Cayman Product Information (±)-Ketoprofen Item Number 10006661.
224. Shohin, I.E.; Kulinich, J.I.; Ramenskaya, G. V.; Abrahamsson, B.; Kopp, S.; Langguth, P.; Polli, J.E.; Shah, V.P.; Groot, D.W.; Barends, D.M.; et al. Biowaiver Monographs for Immediate-Release Solid Oral Dosage Forms: Ketoprofen. *J. Pharm. Sci.* **2012**, *101*, 3593–3603; DOI:10.1002/jps.23233.
225. Sadik, M.J.; Khan, A. Formulation and Evaluation of Flurbiprofen Solid Dispersions using Novel Carriers for Enhancement of Solubility. *Asian J. Pharm.* **2020**, *14*, 475–482; DOI:10.22377/ajp.v14i03.3765.
226. Daravath, B.; Naveen, C.; Vemula, S.K.; Tadikonda, R.R. Solubility and dissolution enhancement of flurbiprofen by solid dispersion using hydrophilic carriers. *Brazilian J. Pharm. Sci.* **2017**, *53*, 1–10; DOI:10.1590/s2175-97902017000400010.
227. Park, K.M.; Kim, C.K. Preparation and evaluation of flurbiprofen-loaded microemulsion for parenteral delivery. *Int. J. Pharm.* **1999**, *181*, 173–179; DOI:10.1016/S0378-5173(99)00029-0.
228. Cayman Product Information (±)-Flurbiprofen Item Number 70250.
229. Machado, V.G.; Stock, R.I.; Reichardt, C. Pyridinium N-Phenolate Betaine Dyes. *Chem. Rev.* **2014**, *114*, 10429–10475; DOI:10.1021/cr5001157.
230. Nigam, S.; Rutan, S. Principles and Applications of Solvatochromism. *Appl. Spectrosc.* **2001**, *55*, 362A-370A; DOI:10.1366/0003702011953702.
231. Meloun, M.; Bordovská, S.; Galla, L. The thermodynamic dissociation constants of four non-steroidal anti-inflammatory drugs by the least-squares nonlinear regression of multiwavelength spectrophotometric pH-titration data. *J. Pharm. Biomed. Anal.* **2007**, *45*, 552–564; DOI:10.1016/j.jpba.2007.07.029.
232. National Center for Biotechnology Information. PubChem Compound Summary for CID 156391, Naproxen Available online: https://pubchem.ncbi.nlm.nih.gov/compound/Naproxen (accessed on Feb 24, 2021).
233. National Center for Biotechnology Information. PubChem Compound Summary for CID 3715, Indomethacin Available online: https://pubchem.ncbi.nlm.nih.gov/compound/Indomethacin (accessed on Feb 24, 2021).
234. National Center for Biotechnology Information. PubChem Compound Summary for CID 2662, Celecoxib Available online: https://pubchem.ncbi.nlm.nih.gov/compound/Celecoxib (accessed on Feb 24, 2021).
235. Goldie, I.; Nachemson, A. Synovial pH in rheumatoid knee joints: II. The effect of local

corticosteroid treatment. *Acta Orthop.* **1970**, *41*, 354–362; DOI:10.3109/17453677008991521.
236. Pedro, S.N.; Freire, C.S.R.; Silvestre, A.J.D.; Freire, M.G. Deep Eutectic Solvents and Pharmaceuticals. *Encyclopedia* **2021**, *1*, 942–963; DOI:10.3390/encyclopedia1030072.
237. Mustafa, N.R.; Spelbos, V.S.; Witkamp, G.; Verpoorte, R.; Choi, Y.H. Solubility and Stability of Some Pharmaceuticals in Natural Deep Eutectic Solvents-Based Formulations. *Molecules* **2021**, *6*, 2645; DOI:10.3390/molecules26092645.
238. Bazzo, G.C.; Pezzini, B.R.; Stulzer, H.K. Eutectic mixtures as an approach to enhance solubility, dissolution rate and oral bioavailability of poorly water-soluble drugs. *Int. J. Pharm.* **2020**, *588*, 119741; DOI:10.1016/j.ijpharm.2020.119741.
239. Chakraborty, S.; Chormale, J.H.; Bansal, A.K. Deep eutectic systems: An overview of fundamental aspects, current understanding and drug delivery applications. *Int. J. Pharm.* **2021**, *610*, 121203; DOI:10.1016/j.ijpharm.2021.121203.
240. Terezinha, M.T.; Martins, T.M.; Costa, P.F.A.; Carolina, G.C.; Pereira, R.N.; Gerola, A.P.; Stulzer, H.K. Eutectic mixture and amorphous solid dispersion: Two different supersaturating drug delivery system strategies to improve griseofulvin release using saccharin. *Int. J. Pharm.* **2022**, *615*, 121498; DOI:10.1016/j.ijpharm.2022.121498.
241. Lu, W.; Chen, H. Application of deep eutectic solvents (DESs) as trace level drug extractants and drug solubility enhancers: State-of-the-art, prospects and challenges. *J. Mol. Liq.* **2022**, *349*, 118105; DOI:10.1016/j.molliq.2021.118105.
242. Rebenda, D.; Vrbka, M.; Čípek, P.; Toropitsyn, E.; Nečas, D.; Pravda, M.; Hartl, M. On the Dependence of Rheology of Hyaluronic Acid Solutions and Frictional Behavior of Articular Cartilage. *Materials (Basel).* **2020**, *13*, 2659; DOI:10.3390/ma13112659.
243. ISO International Standard ISO 10993-5 Biological evaluation of medical devices - Part 5: Tests for cytotoxicity: in vitro methods. In *Biological evaluation of medical devices*; 2009.
244. International Organization for Standardization *ISO 10993-12 Biological evaluation of medical devices — Part 12: Sample preparation and reference materials*; 2012;
245. Roda, A.; Paiva, A.; Duarte, A.R.C. Therapeutic Liquid Formulations Based on Low Transition Temperature Mixtures for the Incorporation of Anti-Inflammatory Drugs. *Pharmaceutics* **2021**, *13*, 1620; DOI:10.3390/pharmaceutics13101620.
246. Chen, M.H.; Wang, L.L.; Chung, J.J.; Kim, Y.-H.; Atluri, P.; Burdick, J.A. Methods to Assess Shear-Thinning Hydrogels for Application As Injectable Biomaterials. *ACS Biomater. Sci. Eng.* **2017**, *3*, 3146–3160; DOI:10.1021/acsbiomaterials.7b00734.
247. Balazs, E.A. The physical properties of synovial fluid and the special role of hyaluronic acid. In *Disorders of the Knee*; Helfet, A.-, Ed.; T. B. Lippincott Company: Philadelphia, 1974; pp. 63–75 ISBN 0397503229.
248. Mazzucco, D.; McKinley, G.; Scott, R.D.; Spector, M. Rheology of joint fluid in total knee arthroplasty patients. *J. Orthop. Res.* **2002**, *20*, 1157–1163; DOI:10.1016/S0736-0266(02)00050-5.
249. Bhuanantanondh, P.; Grecov, D.; Kwok, E. Rheological study of viscosupplements and synovial fluid in patients with osteoarthritis. *J. Med. Biol. Eng.* **2012**, *32*, 12; DOI:10.5405/jmbe.834.
250. Bhuanantanondh, P.; Grecov, D.; Kwok, E.; Guy, P. Rheology of osteoarthritic synovial fluid mixed with viscosupplements: A pilot study. *Biomed. Eng. Lett.* **2011**, *1*, 213–219;

DOI:10.1007/s13534-011-0034-7.
251. Heilmann, H.-H.; Lindenhayn, K.; Walther, H.-U. Das Synovia-Volumen gesunder und arthrotischer menschlicher Kniegelenke. *Z. Orthop. Unfall.* **2008**, *134*, 144–148; DOI:10.1055/s-2008-1039786.
252. Schurz, J.; Ribitsch, V. Rheology of synovial fluid. *Biorheology* **1987**, *24*, 385–399; DOI:10.3233/BIR-1987-24404.
253. Guvendiren, M.; Lu, H.D.; Burdick, J.A. Shear-thinning hydrogels for biomedical applications. *Soft Matter* **2012**, *8*, 260–272; DOI:10.1039/c1sm06513k.
254. Ishikawa, M.; Yoshioka, K.; Urano, K.; Tanaka, Y.; Hatanaka, T.; Nii, A. Biocompatibility of cross-linked hyaluronate (Gel-200) for the treatment of knee osteoarthritis. *Osteoarthr. Cartil.* **2014**, *22*, 1902–1909; DOI:10.1016/j.joca.2014.08.002.
255. FDA Inactive Ingredient Search for Approved Drug Products Available online: https://www.accessdata.fda.gov/scripts/cder/iig/index.cfm (accessed on Dec 12, 2023).
256. Strecanska, M.; Danisovic, L.; Ziaran, S.; Cehakova, M. The Role of Extracellular Matrix and Hydrogels in Mesenchymal Stem Cell Chondrogenesis and Cartilage Regeneration. *Life* **2022**, *12*, 2066; DOI:10.3390/life12122066.
257. Eladawy, N.O.; Morsi, N.M.; Shamma, R.N. Diacerein-loaded hyaluosomes as a dual-function platform for osteoarthritis management via intra-articular injection: In vitro characterization and in vivo assessment in a rat model. *Pharmaceutics* **2021**, *13*, 1–19; DOI:10.3390/pharmaceutics13060765.
258. Kang, M.L.; Jeong, S.Y.; Im, G. Il Hyaluronic Acid Hydrogel Functionalized with Self-Assembled Micelles of Amphiphilic PEGylated Kartogenin for the Treatment of Osteoarthritis. *Tissue Eng. - Part A* **2017**, *23*, 630–639; DOI:10.1089/ten.tea.2016.0524.
259. Miao, B.; Song, C.; Ma, G. Injectable thermosensitive hydrogels for intra-articular delivery of methotrexate. *J. Appl. Polym. Sci.* **2011**, *122*, 2139–2145; DOI:10.1002/app.34332.
260. Li, P.; Li, H.; Shu, X.; Wu, M.; Liu, J.; Hao, T.; Cui, H.; Zheng, L. Intra-articular delivery of flurbiprofen sustained release thermogel: improved therapeutic outcome of collagenase II-induced rat knee osteoarthritis. *Drug Deliv.* **2020**, *27*, 1034–1043; DOI:10.1080/10717544.2020.1787555.
261. Joshi, N.; Yan, J.; Levy, S.; Bhagchandani, S.; Slaughter, K. V.; Sherman, N.E.; Amirault, J.; Wang, Y.; Riegel, L.; He, X.; et al. Towards an arthritis flare-responsive drug delivery system. *Nat. Commun.* **2018**, *9*, 1–11; DOI:10.1038/s41467-018-03691-1.
262. Han, Y.; Yang, J.; Zhao, W.; Wang, H.; Sun, Y.; Chen, Y.; Luo, J.; Deng, L.; Xu, X.; Cui, W.; et al. Biomimetic injectable hydrogel microspheres with enhanced lubrication and controllable drug release for the treatment of osteoarthritis. *Bioact. Mater.* **2021**, *6*, 3596–3607; DOI:10.1016/j.bioactmat.2021.03.022.
263. Patel, D.D.; Anderson, B.D. Maintenance of Supersaturation II: Indomethacin Crystal Growth Kinetics Versus Degree of Supersaturation. *J. Pharm. Sci.* **2013**, *102*, 1544–1553; DOI:10.1002/jps.23498.
264. Giri, T.K.; Kumar, K.; Alexander, A.; Ajazuddin; Badwaik, H.; Tripathi, D.K. A novel and alternative approach to controlled release drug delivery system based on solid dispersion technique. *Bull. Fac. Pharmacy, Cairo Univ.* **2012**, *50*, 147; DOI:10.1016/j.bfopcu.2012.07.002.
265. Pandi, P.; Bulusu, R.; Kommineni, N.; Khan, W.; Singh, M. Amorphous solid dispersions: An update for preparation, characterization, mechanism on bioavailability, stability,

regulatory considerations and marketed products. *Int. J. Pharm.* 2020, *586*, 1–28.
266. Peck, J.; Slovek, A.; Miro, P.; Vij, N.; Traube, B.; Lee, C.; Berger, A.A.; Kassem, H.; Kaye, A.D.; Sherman, W.F.; et al. A Comprehensive Review of Viscosupplementation in Osteoarthritis of the Knee. *Orthop. Rev. (Pavia).* **2021**, *13*, 1–11; DOI:10.52965/001C.25549.
267. Hangody, L.; Szody, R.; Lukasik, P.; Zgadzaj, W.; Lénárt, E.; Dokoupilova, E.; Bichovsk, D.; Berta, A.; Vasarhelyi, G.; Ficzere, A.; et al. Intraarticular Injection of a Cross-Linked Sodium Hyaluronate Combined with Triamcinolone Hexacetonide (Cingal) to Provide Symptomatic Relief of Osteoarthritis of the Knee: A Randomized, Double-Blind, Placebo-Controlled Multicenter Clinical Trial. *Cartilage* **2018**, *9*, 276–283; DOI:10.1177/1947603517703732.
268. Mccormack, R.; Lamontagne, M.; Vannabouathong, C.; Deakon, R.T.; Belzile, E.L. Comparison of the 3 Different Injection Techniques Used in a Randomized Controlled Study Evaluating a Cross-Linked Sodium Hyaluronate Combined With Triamcinolone Hexacetonide (Cingal) for Osteoarthritis of the Knee : A Subgroup Analysis. *SAGE* **2017**, *10*, 1–8; DOI:10.1177/1179544117725026.
269. Rudnik-Jansen, I.; Tellegen, A.R.; Pouran, B.; Schrijver, K.; Meij, B.P.; Emans, P.J.; de Gendt, E.; Thomas, R.E.; Kik, M.J.L.; de Visser, H.M.; et al. Local controlled release of corticosteroids extends surgically induced joint instability by inhibiting tissue healing. *Br. J. Pharmacol.* **2019**, *176*, 4050–4064; DOI:10.1111/bph.14817.
270. Haartmans, M.J.J.; Timur, U.T.; Emanuel, K.S.; Caron, M.M.J.; Jeuken, R.M.; Welting, T.J.M.; van Osch, G.J.V.M.; Heeren, R.M.A.; Cillero-Pastor, B.; Emans, P.J. Evaluation of the Anti-Inflammatory and Chondroprotective Effect of Celecoxib on Cartilage Ex Vivo and in a Rat Osteoarthritis Model. *Cartilage* **2022**, *13*, 1–12; DOI:10.1177/19476035221115541.
271. El-Gogary, R.I.; Khattab, M.A.; Abd-Allah, H. Intra-articular multifunctional celecoxib loaded hyaluronan nanocapsules for the suppression of inflammation in an osteoarthritic rat model. *Int. J. Pharm.* **2020**, *583*, 1–10; DOI:10.1016/j.ijpharm.2020.119378.
272. Dong, J.; Jiang, D.; Wang, Z.; Wu, G.; Miao, L.; Huang, L. Intra-articular delivery of liposomal celecoxib-hyaluronate combination for the treatment of osteoarthritis in rabbit model. *Int. J. Pharm.* **2013**, *441*, 285–290; DOI:10.1016/j.ijpharm.2012.11.031.
273. Committee for Human Medicinal Products (CHMP) Annex to the European Commission guideline on "Excipients in the labelling and package leaflet of medicinal products for human use" (SANTE-2017-11668) Excipients and information for the package leaflet. *EMA* **2017**.
274. Faul, F.; Erdfelder, E.; Buchner, A.; Lang, A.G. Statistical power analyses using G*Power 3.1: Tests for correlation and regression analyses. *Behav. Res. Methods* **2009**, *41*, 1149–1160; DOI:10.3758/BRM.41.4.1149.
275. Faul, F.; Erdfelder, E.; Lang, A.-G.; Buchner, A. G*Power 3:A flexible statistical power analysis program for the social, behavioral, and biomedical sciences. *Behav. Res. Methods* **2007**, *39*, 175–191.
276. Waarsing, J.H.; Day, J.S.; Weinans, H. An improved segmentation method for in vivo µCT imaging. *J. Bone Miner. Res.* **2004**, *19*, 1640–1650; DOI:10.1359/JBMR.040705.
277. Krenn, V.; Morawietz, L.; Burmester, G.-R.; Kinne, R.W.; Mueller-Ladner, U.; Muller, B.; Haupl, T. Synovitis score: discrimination between chronic low-grade and high-grade synovitis. *Histopathology* **2006**, *49*, 358–364; DOI:10.1111/j.1365-2559.2006.02508.x.

278. Mankin, H.J.; Dorfman, H.; Lippiello, L.; Zarins, A. Biochemical and metabolic abnormalities in articular cartilage from osteo-arthritic human hips. II. Correlation of morphology with biochemical and metabolic data. *J. Bone Joint Surg. Am.* **1971**, *53*, 523–37.
279. Katagiri, M.; Ogasawara, T.; Hoshi, K.; Chikazu, D.; Kimoto, A.; Noguchi, M.; Sasamata, M.; Harada, S.I.; Akama, H.; Tazaki, H.; et al. Suppression of adjuvant-induced arthritic bone destruction by cyclooxygenase-2 selective agents with and without inhibitory potency against carbonic anhydrase II. *J. Bone Miner. Res.* **2006**, *21*, 219–227; DOI:10.1359/JBMR.051025.
280. Noguchi, M.; Kimoto, A.; Sasamata, M.; Miyata, K. Micro-CT imaging analysis for the effect of celecoxib, a cyclooxygenase-2 inhibitor, on inflammatory bone destruction in adjuvant arthritis rats. *J. Bone Miner. Metab.* **2008**, *26*, 461–468; DOI:10.1007/s00774-008-0855-3.
281. Tsuboi, H.; Nampei, A.; Matsui, Y.; Hashimoto, J.; Kawai, S.; Ochi, T.; Yoshikawa, H. Celecoxib prevents juxta-articular osteopenia and growth plate destruction adjacent to inflamed joints in rats with collagen-induced arthritis. *Mod. Rheumatol.* **2007**, *17*; DOI:10.1007/s10165-007-0552-4.
282. Costela-Ruiz, V.J.; Melguizo-Rodríguez, L.; Illescas-Montes, R.; Ramos-Torrecillas, J.; Manzano-Moreno, F.J.; Ruiz, C.; De Luna-Bertos, E. Effects of therapeutic doses of celecoxib on several physiological parameters of cultured human osteoblasts. *Int. J. Med. Sci.* **2019**, *16*, 1466–1472; DOI:10.7150/ijms.37857.
283. Madry, H.; van Dijk, C.N.; Mueller-Gerbl, M. The basic science of the subchondral bone. *Knee Surgery, Sport. Traumatol. Arthrosc.* **2010**, *18*, 419–433; DOI:10.1007/s00167-010-1054-z.
284. Zhang, K.Y.; Kedgley, A.E.; Donoghue, C.R.; Rueckert, D.; Bull, A.M.J. The relationship between lateral meniscus shape and joint contact parameters in the knee: A study using data from the Osteoarthritis Initiative. *Arthritis Res. Ther.* **2014**, *16*, 1–9; DOI:10.1186/ar4455.
285. Poulet, B.; de Souza, R.; Kent, A. V.; Saxon, L.; Barker, O.; Wilson, A.; Chang, Y.M.; Cake, M.; Pitsillides, A.A. Intermittent applied mechanical loading induces subchondral bone thickening that may be intensified locally by contiguous articular cartilage lesions. *Osteoarthr. Cartil.* **2015**, *23*, 940–948; DOI:10.1016/j.joca.2015.01.012.
286. Welting, T.; Caron, M.; Emans, P.; Janssen, M.; Sanen, K.; Coolsen, M.; Voss, L.; Surtel, D.; Cremers, A.; Voncken, J.; et al. Inhibition of cyclooxygenase-2 impacts chondrocyte hypertrophic differentiation during endochondral ossification. *Eur. Cells Mater.* **2011**, *22*, 420–437; DOI:10.22203/eCM.v022a31.
287. Hubert, J.; Beil, F.T.; Rolvien, T.; Butscheidt, S.; Hischke, S.; Püschel, K.; Frosch, S.; Mussawy, H.; Ries, C.; Hawellek, T. Cartilage calcification is associated with histological degeneration of the knee joint: a highly prevalent, age-independent systemic process. *Osteoarthr. Cartil.* **2020**, *28*, 1351–1361; DOI:10.1016/j.joca.2020.04.020.
288. Bernabei, I.; So, A.; Busso, N.; Nasi, S. Cartilage calcification in osteoarthritis: mechanisms and clinical relevance. *Nat. Rev. Rheumatol.* **2023**, *19*, 10–27; DOI:10.1038/s41584-022-00875-4.
289. Sundararajan, S.; Samui, A.B.; Kulkarni, P.S. Versatility of polyethylene glycol (PEG) in designing solid-solid phase change materials (PCMs) for thermal management and their

application to innovative technologies. *J. Mater. Chem. A* **2017**, *5*, 18379–18396; DOI:10.1039/c7ta04968d.
290. Cilurzo, F.; Alberti, E.; Minghetti, P.; Gennari, C.G.M.; Casiraghi, A.; Montanari, L. Effect of drug chirality on the skin permeability of ibuprofen. *Int. J. Pharm.* **2010**, *386*, 71–76; DOI:10.1016/j.ijpharm.2009.10.053.
291. Hong, J.; Hua, D.; Wang, X.; Wang, H.; Li, J. Solid-liquid-gas equilibrium of the ternaries ibuprofen + myristic acid + CO2 and ibuprofen + tripalmitin + CO2. *J. Chem. Eng. Data* **2010**, *55*, 297–302; DOI:10.1021/je900342a.
292. Wassvik, C.M.; Holmén, A.G.; Bergström, C.A.S.; Zamora, I.; Artursson, P. Contribution of solid-state properties to the aqueous solubility of drugs. *Eur. J. Pharm. Sci.* **2006**, *29*, 294–305; DOI:10.1016/j.ejps.2006.05.013.
293. Gracin, S.; Rasmuson, Å.C. Solubility of phenylacetic acid, p-hydroxyphenylacetic acid, p-aminophenylacetic acid, p-hydroxybenzoic acid, and ibuprofen in pure solvents. *J. Chem. Eng. Data* **2002**, *47*, 1379–1383; DOI:10.1021/je0255170.
294. Li, Z.J.; Zell, M.T.; Munson, E.J.; Grant, D.J.W. Characterization of racemic species of chiral drugs using thermal analysis, thermodynamic calculation, and structural studies. *J. Pharm. Sci.* **1999**, *88*, 337–346; DOI:10.1021/js980205u.
295. Gutz, I.G.R. CurTiPot – pH and Acid–Base Titration Curves: Analysis and Simulation freeware, version 4.2 Available online: http://www.iq.usp.br/gutz/Curtipot_.html.

# A

# APPENDIX OF CHAPTER 2

## A.1 Screening of PEG-based mixtures

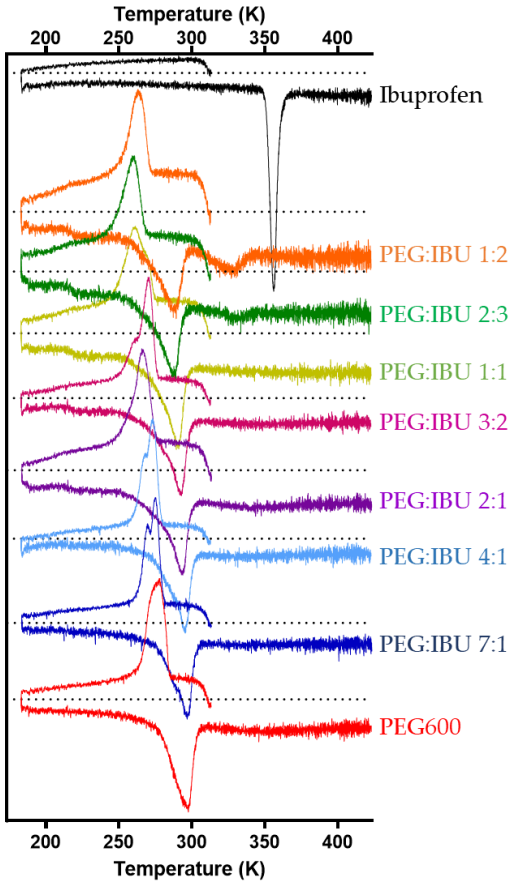


**Figure A.1** - DSC scans performed for PEG600, ibuprofen and their mixtures at several molar ratios (PEG:IBU). Thermal events registered in Table A.2.

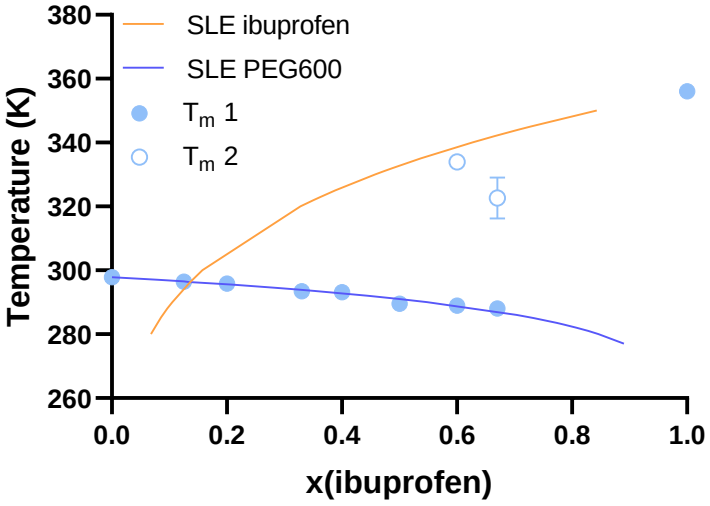


$$\textbf{Eq 3: } x_i^L = \frac{1}{\gamma_i^L} \cdot \exp\left\{-\frac{\Delta_m H}{RT}\left(1 - \frac{T}{T_m}\right)\right\}$$

**Figure A.2 - Solid-Liquid Equilibrium (SLE).** Lines represent SLE based on the simplified thermodynamic equation (Eq 3), expressing solubility of the component i in the liquid phase $x_i^L$ at specified temperature T, considering its activity coefficient $\gamma_i^L$, its melting enthalpy $\Delta_m H$, its melting temperature $T_m$ and the universal gas constant R (8.314 J/mol·K). Theoric SLE estimated assuming an ideal mixture ($\gamma_i^L$=1) and using the parameters of Table A.1. Symbols represent the experimental $T_m$ obtained for ibuprofen, PEG600 and their mixtures at several molar fractions (Table A.2, Figure A.1).

**Table A.1** - Melting temperature ($T_m$) and enthalpy ($\Delta_m H$) of the pure components: PEG600 and ibuprofen. $T_m$ retrieved experimentally from DSC (Figure A.1). Melting enthalpy used from literature, respectively listed.

| Compounds | $T_m$ (K) | $\Delta_m H$ (J/mol) |
|---|---|---|
| PEG600 | 297.85 | 72660 [289] |
| Ibuprofen | 356.05 | 29278 [194,290–294] |

**Table A.2** - Thermal events acquired from DSC for PEG600, ibuprofen their mixtures (PEG:IBU) at several molar ratios, and respective molar fractions. Namely, melting temperatures ($T_m$) and crystallization temperatures ($T_c$) were obtained from the DSC scans represented in Figure A.1.

| Sample | Molar fraction | | Temperature (K) | | |
|---|---|---|---|---|---|
| | χ(ibuprofen) | χ(PEG600) | $T_{m(1)}$ | $T_{m(2)}$ | $T_c$ |
| Ibuprofen | 1 | 0 | 356.05 | - | - |
| PEG:IBU 1:2 | 0.67 | 0.33 | 288.05±2.12 | 322.7±6.43 | 259.8±5.02 |
| PEG:IBU 2:3 | 0.6 | 0.4 | 288.95 | 333.95 | 260.05 |
| PEG:IBU 1:1 | 0.5 | 0.5 | 289.55 | - | 261.55 |
| PEG:IBU 3:2 | 0.4 | 0.6 | 293.15 | - | 270.85 |
| PEG:IBU 2:1 | 0.33 | 0.67 | 293.45 | - | 265.35 |
| PEG:IBU 4:1 | 0.2 | 0.8 | 295.85 | - | 273.15 |
| PEG:IBU 7:1 | 0.125 | 0.875 | 296.45 | - | 274.65 |
| PEG600 | 0 | 1 | 297.85 | - | 277.85 |

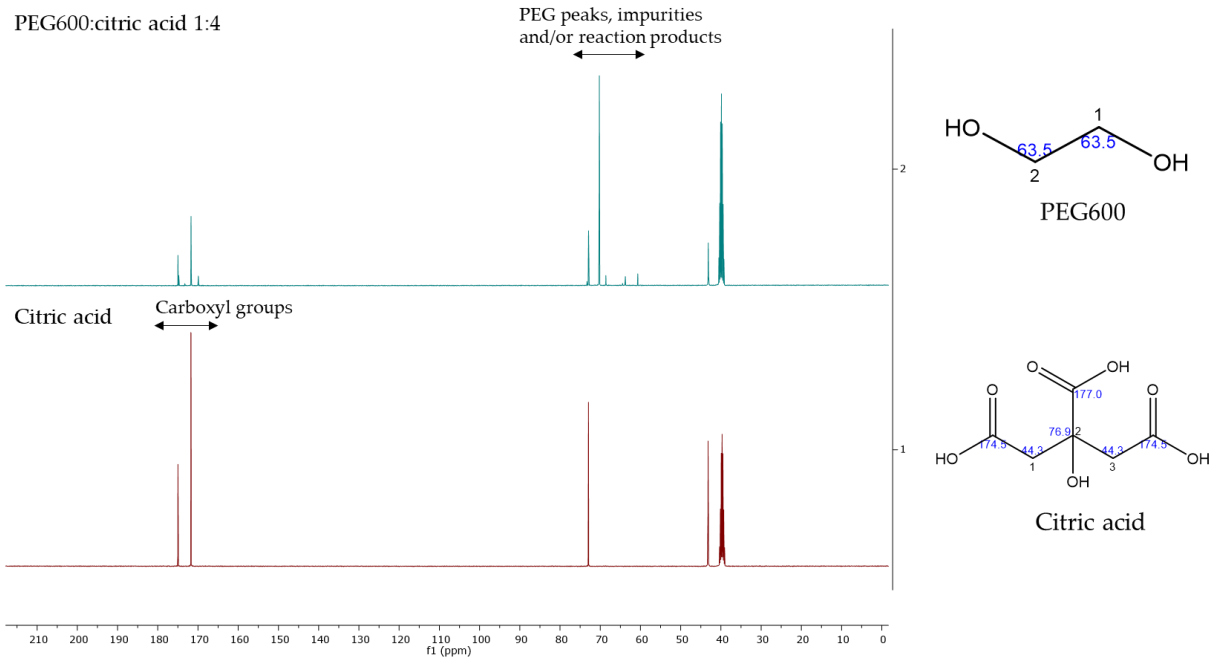


**Figure A.3 - Derivatizations of the carboxyl groups in the $^{13}$C NMR spectra of the mixture PEG600:citric acid 1:4 (top) in respect to pure citric acid (bottom), indicate the presence of reaction products, such as esters (esterification).** The PEG600:citric acid mixtures were therefore excluded as LTTM, since their liquefaction resulted from chemical reaction instead of physical interactions. Structures of pure components and respective $^{13}$C signals (right) retrieved from ChemDraw 18.0.

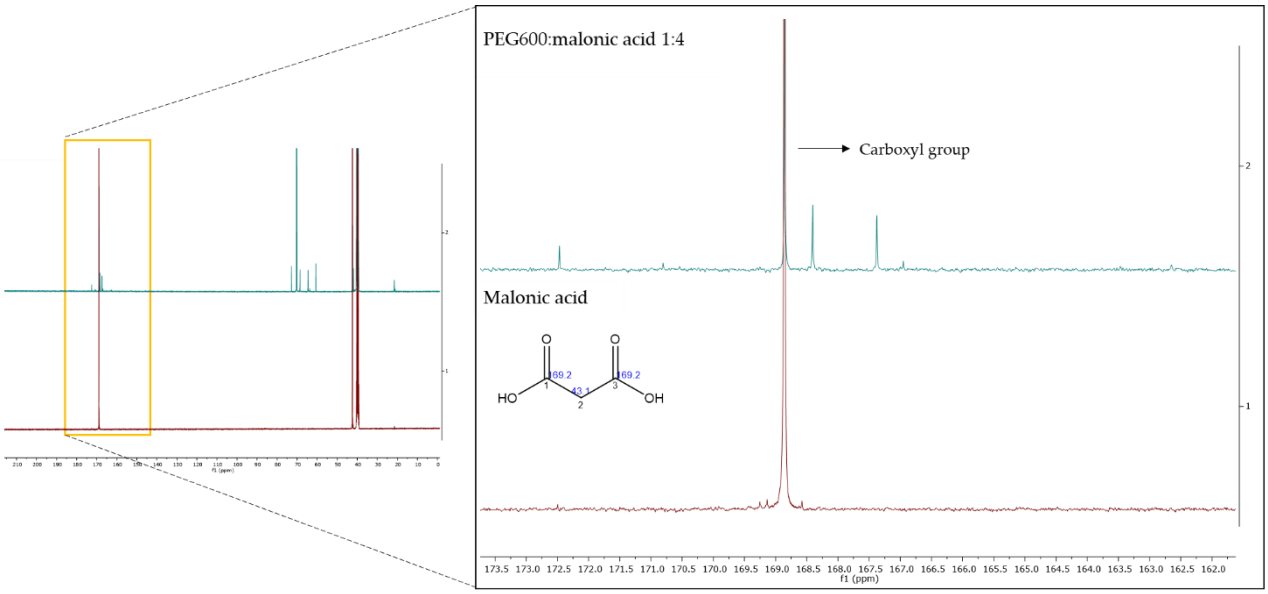


**Figure A.4 - Derivatizations of the carboxyl groups in the $^{13}$C NMR spectra of the mixture PEG600:malonic acid 1:4 (top) in respect to pure malonic acid (bottom), indicate the presence of reaction products, such as esters (esterification).** The PEG600:malonic acid mixtures were therefore excluded as LTTM, since their liquefaction resulted from chemical reaction instead of physical interactions. Structure of malonic acid and respective $^{13}$C signals (right) retrieved from ChemDraw 18.0 (PEG structure in Figure A.3).

## A.2 Physicochemical characterization of citric acid:L-arginine:water mixtures

**Table A.3** - Summary of the mixtures prepared with citric acid, L-arginine and $H_2O$, their ratio, physical state and pH.

| Mixture | Molar ratio | Physical state | pH |
|---|---|---|---|
| Citric acid:L-arginine:$H_2O$ (CAW) | 1:1:7 | Translucid liquid | 3.58 ±0.15 |
| Citric acid:$H_2O$ | 1:7 | Translucid liquid | 0.46 |
| Citric acid:$H_2O$ pH 3.5 | 1:7 | White solid paste | - |
| Citric acid:$H_2O$ pH 3.5 | - [a] | Translucid liquid | 3.62 |
| L-arginine:$H_2O$ | 1:7 | White solid paste | - |
| L-arginine:$H_2O$ pH 3.5 | - [b] | Translucid liquid | 3.43 |

[a]Diluted with $H_2O$ until a translucid liquid was obtained; [b]Diluted with $H_2O$ and HCl until a translucid liquid at pH around 3.5 was obtained.

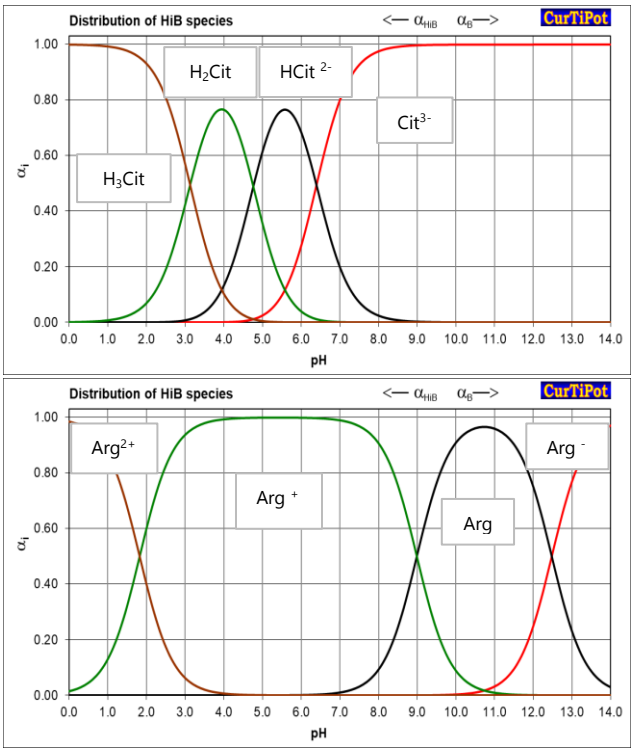


**Figure A.5** - Diagram of the relative distribution of species ($\alpha_i$) depending on pH, for citric acid (up) and L-arginine (down). Cit: citric acid; Arg: L-arginine. Calculated by CurTiPot [295] using pKa's from Table A.4.

**Table A.4** - pKa's of citric acid and L-arginine. Functional group numbers' according to Figure A.6.

| | Citric acid | L-arginine |
|---|---|---|
| pKa | 2.9 (COOH 4) | 2.5 (OH 1) |
| | 4.8 (COOH 6) | 9 ($NH_2$ 4) |
| | 6.4 (COOH 1) | 12.5 (guanidine 8, 10, 11) |

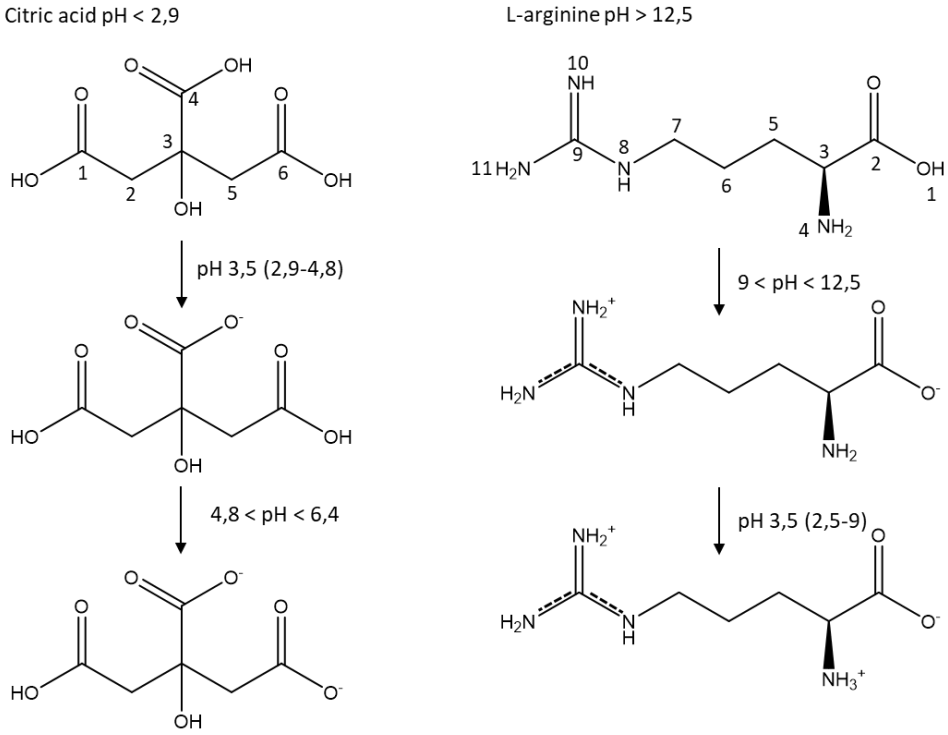


**Figure A.6** - Chemical structure of citric acid (left) and L-arginine (right) at different pH's, according to pKa's from Table A.4.

**Table A.5** - Assignment of L-arginine functional groups to the respective FTIR wavenumber. Functional group numbers' according to Figure A.6, right.

| Wavenumber ($cm^{-1}$) | Assignment | Reference |
|---|---|---|
| 3358 | s N-H 4 | [195–198] |
| 3302 | s N-H 6 (guanidine) | [195–198] |
| 3057 | s OH (COOH) 1 | [195] |
| 2946<br>2863 | s CH 5,6,7 | [195,198] |
| 1722 | - | - |

| | | |
|---|---|---|
| 1676 | s C=O (COOH) 1 | [195,197–199] |
| 1612 | s C=N 9 | [195,196] |
| 1553 | b NH | [195,196,198] |
| 1472 | | |
| 1422 | b CH +/ b OH | [195,198,199] |
| 1374 | | |
| 1330 | | |
| 1279 | - | - |
| 1180 | s C-N 3 | [195–198] |
| 1137 | s C-N 9 (guanidine) +/ b NH | |
| 979 | b OH | [198] |
| 766 | b NH | [196] |
| 701 | - | - |
| 607 | | |
| 551 | b COO- 1 | [196,198] |
| 495 | | |

**Table A.6** - Assignment of citric acid functional groups to the respective FTIR wavenumber. Functional group numbers' according Figure A.6, left.

| Wavenumber ($cm^{-1}$) | Assignment | Reference |
|---|---|---|
| 3499 | s OH 4 | - |
| 3370 | | |
| 3290 | s OH(COOH) 1,4,6 | [195,200–202] |
| 3242 | | |
| 3000 | s CH 2,5 | [200,201] |
| 2993 | | |
| 2640 | OH(COOH) 4 | - |
| 2531 | | |
| 1750 | | |
| 1719 | s C=O 1,4,6 | [195,200,201] |
| 1681 | | |
| 1421 | b CH | [201] |
| 1394 | b OH | [195,201] |
| 1351 | b CH | [201] |
| 1314 | b COH + b CH | [201] |
| 1292 | b CH | [201] |
| 1207 | b CH + s COH | [201] |

| | | |
|---|---|---|
| 1171 | b C-OH | [201] |
| 1103 | s CC | [201] |
| 1055 | s CC(COOH) | [201] |
| 1025 | - | - |
| 944 | s C-O | [201] |
| 904 | s CC | [201] |
| 775 | b CH/s CC | [195,200]/[201] |
| 725 | - | - |
| 687 | - | - |
| 635 | - | - |
| 599 | b OH | [201] |
| 505 | b COOH | [201] |
| 441 | - | - |
| 404 | - | - |

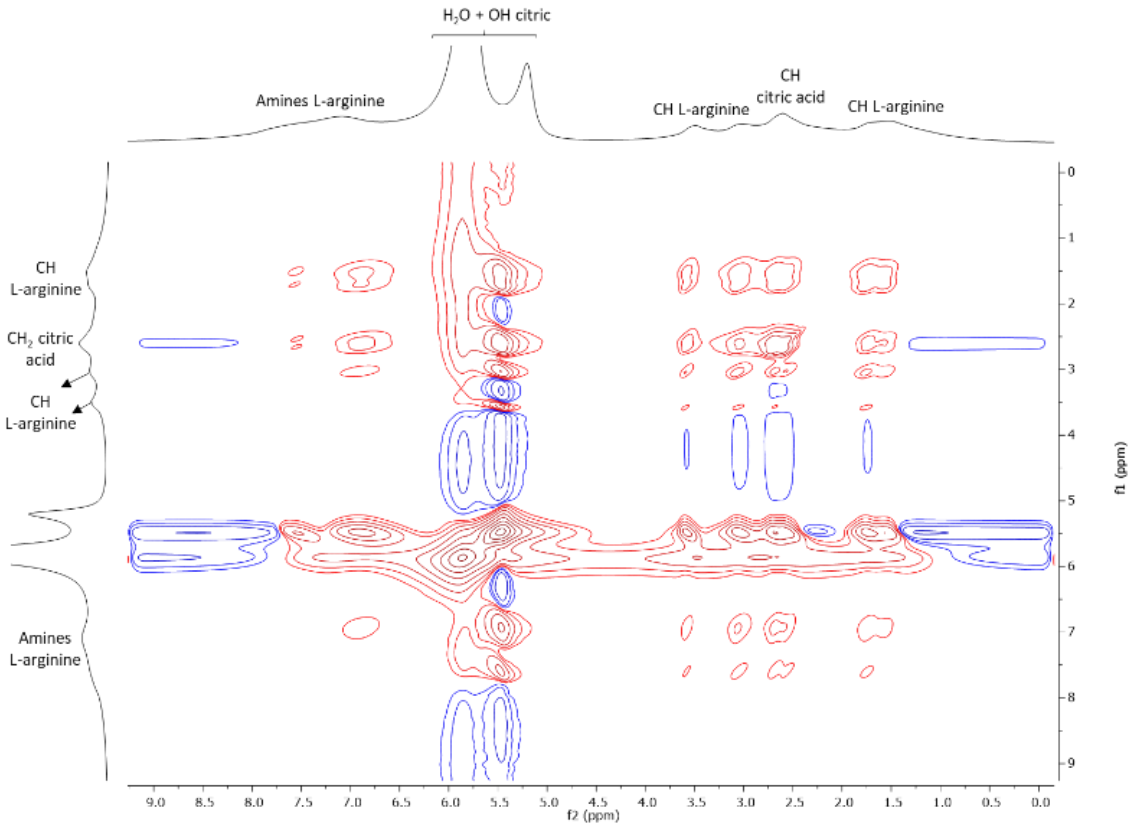


**Figure A.7** - 2D NOESY spectra of the mixture citric acid:L-arginine:$H_2O$ 1:1:7 (molar ratio). The functional groups of the protons identified are aligned with the respective peaks.

# B

# APPENDIX OF CHAPTER 3

## B.1 Celecoxib release

**Table B.1** - Cumulative release of celecoxib (mg/L) from GHA+CEX, GGluS+CEX, GS and PBS, in a high clearance setup.

| | Celecoxib cumulative release – high clearance (mg/L, mean ± SD) | | | |
|---|---|---|---|---|
| Time (h) | GHA+CEX | GGluS+CEX | GS | PBS |
| 0.5 | 0.285 ± 0.247 | 0.087 ± 0.151 | 0.006 ± 0.009 | 0.142 ± 0.246 |
| 1 | 0.562 ± 0.487 | 0.241 ± 0.417 | 0.025 ± 0.013 | 0.2 ± 0.346 |
| 2 | 0.906 ± 0.787 | 0.374 ± 0.647 | 0.028 ± 0.009 | 0.333 ± 0.577 |
| 4 | 1.295 ± 1.055 | 0.522 ± 0.899 | 0.215 ± 0.148 | 0.340 ± 0.589 |
| 6 | 1.624 ± 1.29 | 0.717 ± 1.175 | 0.27 ± 0.146 | 0.351 ± 0.59 |
| 8 | 1.917 ± 1.49 | 0.878 ± 1.426 | 0.311 ± 0.135 | 0.354 ± 0.588 |
| 24 | 2.397 ± 1.551 | 1.344 ± 1.598 | 0.564 ±0.095 | 0.563 ± 0.63 |
| 48 | 2.924 ± 1.612 | 1.792 ± 1.726 | 0.905 ± 0.113 | 0.836 ± 0.654 |
| 120 | 3.57 ± 1.72 | 2.278 ± 1.907 | 1.89 ± 0.9 | 1.687 ± 0.437 |

**Table B.2** - Cumulative release of celecoxib (mg/L) from GHA+CEX, GGluS+CEX, GS and PBS, in a low clearance setup.

| | Celecoxib cumulative release – low clearance (mg/L, mean ± SD) | | | |
|---|---|---|---|---|
| Time (h) | GHA+CEX | GGluS+CEX | GS | PBS |
| 1 | 6.11 ± 6.152 | 7.741 ± 10.902 | 0 ± 0 | 0.005 ± 0.009 |
| 2 | 4.78 ± 5.277 | 15.875 ± 11.435 | 0.009 ± 0.015 | 0.001 ± 0.001 |
| 4 | 16.207 ± 20.96 | 24.577 ± 27.240 | 0.107 ± 0.051 | 0.001 ± 0.001 |
| 6 | 10.239 ± 8.28 | 31.821 ± 27.866 | 0.255 ± 0.073 | 0.225 ± 0.261 |
| 8 | 6.267 ± 5.756 | 14.234 ± 18.702 | 0.243 ± 0.047 | 0.458 ± 0.569 |
| 24 | 12.814 ± 6.115 | 20.597 ± 16.774 | 0.912 ± 0.579 | 0.511 ± 0.251 |
| 48 | 37.618 ± 51.615 | 36.695 ± 31.336 | 2.136 ± 0.707 | 0.498 ± 0.212 |
| 72 | 10.787 ± 7.056 | 18.157 ± 16.790 | 1.011 ± 0.305 | 0.461 ± 0.203 |
| 120 | 8.664 ± 8.115 | 14.241 ± 11.811 | 1.879 ± 1.389 | 0.48 ± 0.114 |

## B.2 NMR of gels with celecoxib

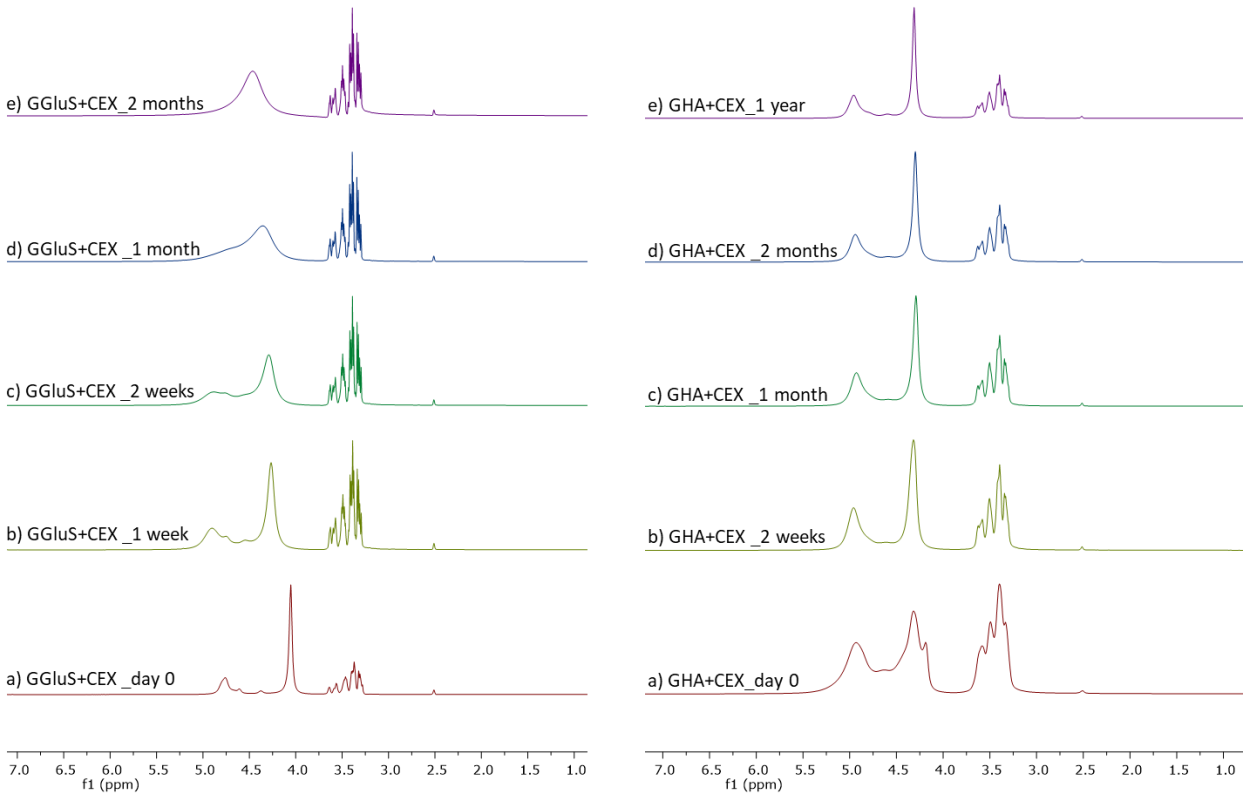


**Figure B.1** - $^{1}H$ NMR spectra over time. Left: GGluS+CEX gel at a) day 0, freshly prepared, b) 1 week, c) 2 weeks, d) 1 month, e) 2 months; Right: GHA+CEX gels at a) day 0, b) 2weeks, c) 1 month, d) 2 months, e) 1 year.

# C

# APPENDIX OF CHAPTER 4

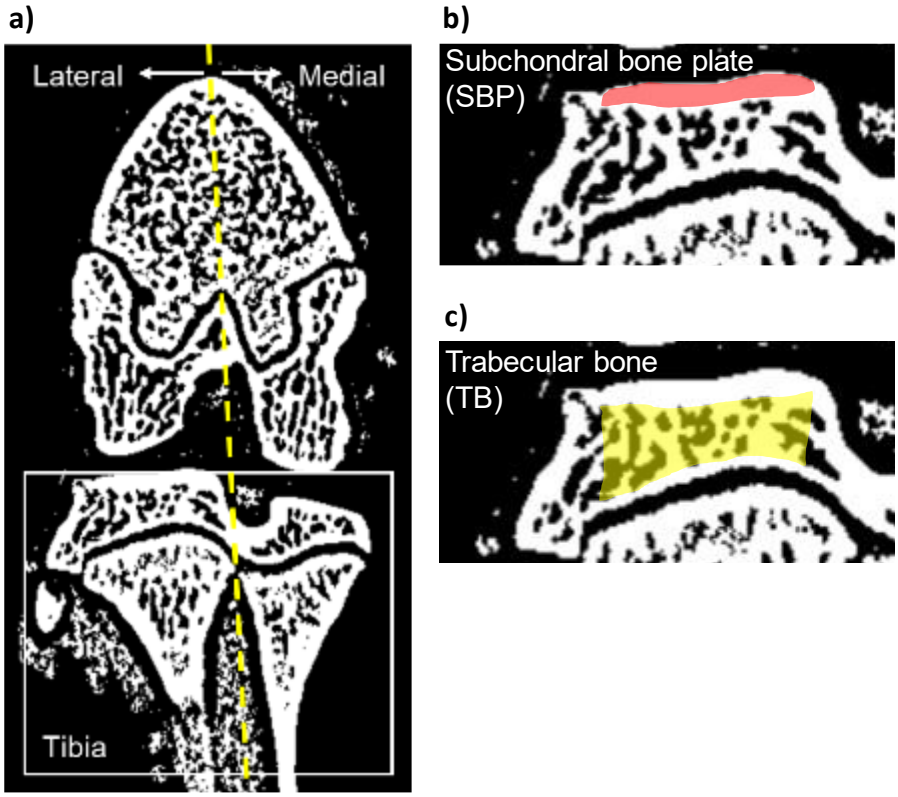


**Figure C.1** - **a**) Knee joint structure represented by means of 2D micro-computed tomography (μCT), and respective example of the regions of interest (ROI) selected for μCT analysis: **b**) Subchondral bone plate (SBP) denoted by the selected region (red); **c**) Trabecular bone (TB) - depicted by the selected region (yellow).

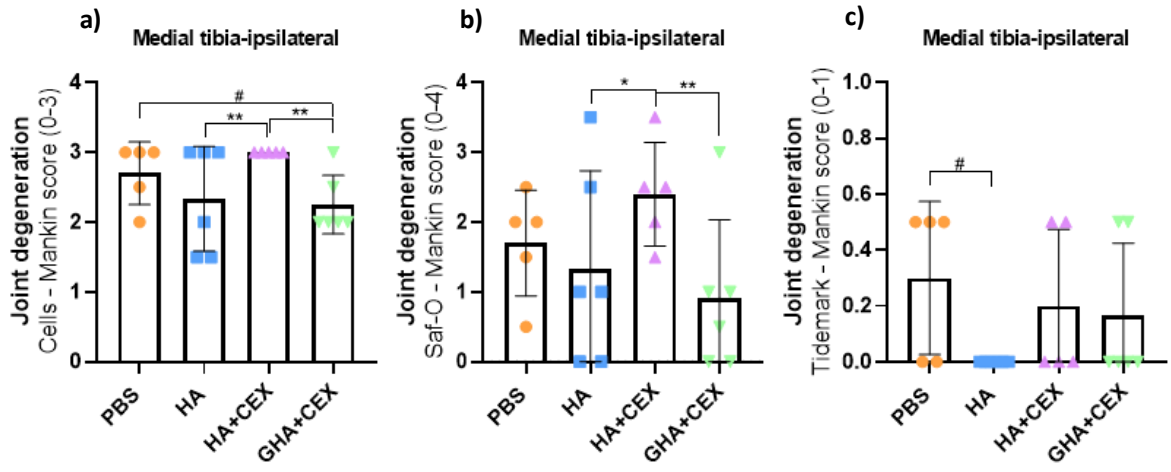


**Figure C.2 - Mankin subscores used for the histological evaluation of joint degeneration**: **a**) Cells Mankin subscore (0-3). **b**) Safranin-O Mankin subscore (0-4), and **c**) Tidemark Mankin subscore (0-1). $^{**}p \leq 0.01$; $^{*}p \leq 0.05$; $^{\#}p \leq 0.1$. Total Mankin score and structure Mankin subscore represented in Figure 4.3, chapter 4, section 4.4.2.

ANA SOFIA MARTINS RODA

# ENGINEERING AN LTTM-POLYMERIC-DRUG FORMULATION FOR OSTEOARTHRITIS TREATMENT

⟨2024⟩